TILLAGE TRANSLOCATION AND TILLAGE EROSION:

MEASUREMENT, MODELING, APPLICATION AND VALIDATION

BY

SHENG LI

A Thesis
Submitted to the Faculty of Graduate Studies
in Partial Fulfillment of the Requirements
for the Degree of

DOCTOR OF PHILOSOPHY

Department of Soil Science
University of Manitoba
Winnipeg, Manitoba

ABSTRACT

Li, Sheng. Ph.D., The University of Manitoba, July, 2006. Tillage translocation and tillage erosion: measurement, modeling, application and validation. Advisor; David A. Lobb.

Tillage erosion is a major contributor to the total soil erosion in cultivated topographically complex lands. No study has been carried out on tillage erosion associated with cereal-based production systems in the Canadian Prairies, and there is a need to examine tillage erosivity of secondary tillage and seeding implements and the effect of slope curvature on tillage translocation. With both tillage and water erosion occurring in a cultivated topographically complex landscape, it is valuable to investigate the relative contributions of and the possible linkage and interactions between these two erosion processes. Tillage translocation causes the mixture of subsoil into the till-layer, which may considerably affect soil properties and therefore the related biophysical processes.

In this study, using plot tracers, we examined tillage translocation caused by four tillage implements: air-seeder, spring-tooth-harrow, light-cultivator and deep-tiller in southern Manitoba, Canada. We determined that secondary tillage and seeding

implements could be as erosive as primary tillage implements in a cereal-based production system. In the majority of cases, tillage translocation could be explained by slope gradient alone; however, slope curvature also significantly affected tillage translocation.

In two field sites in the North America Great Plains (NAGP), measured ^{137}Cs inventories were converted into total soil erosion rates. Tillage and water erosion rates were estimated using models. The comparisons of the model estimates to ^{137}Cs estimates showed that both tillage and water erosion significantly contributed to the total soil erosion in undulating slopes while tillage erosion was the predominant erosion process in hummocky hilltops. The contributions of and the linkage and interactions between water and tillage erosion showed predictable patterns in different landform elements, with the knowledge of which, landscape segmentation could be used to assess the potential of soil erosion.

Further investigation of tillage translocation was demonstrated with four hypothetic landscapes: plane slope, symmetric hill, asymmetric hill and irregular hill, and is tested against field data. A Visual Basic coded program (TillTM) was developed to simulate the redistribution of soil constituents and soil mass. We determined that the pattern of soil mass redistribution was dependent on topography, while the pattern of soil constituent redistribution was affect by topographic features, tillage patterns and temporal scales.

ACKNOWLEDGEMENTS

I would like to acknowledge Natural Sciences and Engineering Research Council of Canada (NSERC) and the Graduate Studies of the University of Manitoba for funding.

I would like to thank my Advisory Committee members, Dr. Annemieke Farenhorst, Dr. Ying Chen and in particular, my supervisor, Dr. David Lobb, for their encouragement, support and thoughtful advices for the duration of my studies at the University of Manitoba. Dr. David Lobb not only guided me in science and set me on the right path in research but also helped me to immerge into Canadian culture.

I would like to thank Bill Turner, Clay Sawka, Aaron Jeninga, Kristin Archibald, Shaan Tsai and Harmony Koiter for their help with the field experiments and/or lab analyses. I would also like to thank all my fellow graduate students, in particular, Kevin Tiessen, Pascal Cyr, Michelle Erb, Jeanette Gaultier and Janna Shymko, and the faculty and staff in the Department of Soil Science, in particular, Barb Finkelman and Terry Ramm. You all made the past about four years a wonderful experience of my life.

I would also like to thank my wife, Mei Yu, my baby girl, Felicia Li and my parents and parents in-law back in China for their tremendous moral support.

THE UNIVERSITY OF MANITOBA

FACULTY OF GRADUATE STUDIES

*****

COPYRIGHT PERMISSION

Tillage Translocation and Tillage Erosion: Measurement, Modeling, Application and Validation

By

Sheng Li

A Thesis/Practicum submitted to the Faculty of Graduate Studies of The University of Manitoba in partial fulfillment of the requirement of the degree of Doctor of Philosophy

(c) 2006 year

TABLE OF CONTENTS

LIST OF TABLES

Table **Page**

LIST OF FIGURES

Figure **Page**

1. INTRODUCTION

1.1 General Background on Soil Erosion and Tillage Erosion

Soil erosion causes the loss of topsoil and soil degradation. The redistribution of soil within landscapes due to soil erosion also changes soil properties at a given point, which has implications on other biophysical processes such as nutrients and pesticides movement and greenhouse gas emission. In agricultural land, soil erosion is accelerated due to human activities. Based on the force driving the process, soil erosion is classified as water, wind and tillage erosion. The studies of water and wind erosion started in the 1930s, with the establishments of Universal Soil Loss Equation (USLE) (Wischmeier and Smith, 1965) and Wind Erosion Prediction Equation (WEQ) (Chepil et al., 1962) as the respective milestones. The recognition of tillage erosion can be dated back to 1920s (Aufrère, 1929). Mech and Free (1942) measured the displacement of soil by tillage and concluded that significant amount of soil was moved downslope by tillage. However, for decades, water and wind erosion was assumed to be the major forms of soil erosion on

cultivated land. Tillage was considered as an important factor that influences soil erodibility but the direct movement of soil by tillage was ignored (Govers et al., 1999).

Different soil erosion processes have different spatial signatures in the landscape. Water erosion primarily causes soil loss in mid-slopes or troughs (where water flows are concentrated); wind erosion is relatively uniform at the field scale; and tillage erosion primarily causes soil loss on hilltops (convexities) and soil accumulation in footslopes and depressions (concavities). Typical field evidence of soil erosion in cultivated land is eroded hilltops. Techniques such as ^{137}Cs have provided strong definitive evidence of high soil losses on hilltops and accumulations in hill bottoms, which can not be fully explained by water and/or wind erosion (e.g. de Jong et al., 1983; Kachanoski, 1987). In the early 1990s, researchers from different parts of the world carried out field experiments to examine soil movement by tillage and suggested that tillage erosion is a major cause of these observed patterns of soil redistribution in cultivated field (e.g. Lindstrom et al., 1990, 1992; Lobb et al., 1991,1995; Govers et al., 1994).

Tillage erosion is the redistribution of soil that occurs within a landscape as a direct result of tillage. Tillage erosion is caused by the variation in the amount of soil that is displaced by tillage. The displacement of soil by tillage is called tillage translocation. Tillage translocation is primarily determined by local slope gradient and, therefore, tillage erosion is dependent on the change of slope gradient. Typically, tillage results in the progressive downslope movement of soil, causing severe soil loss on convexities and the upslope field boundaries and soil accumulation in concavities and downslope field boundaries (Govers et al., 1999). There are more convexities and concavities on topographically complex landscapes than on topographically simple landscapes, so that

tillage erosion is more intensive on topographically complex landscapes than on topographically simple landscapes.

Due to the geological youth of the landscape and the relatively short cultivation history, soil-landscapes in the northern region of the North American Great Plains (northern NAGP) are generally more topographically and pedologically complex than those in Europe and Asia. More than 75 percent of the agricultural land in this region is classified as hilly (rolling, undulating and hummocky) landscapes. Tillage erosion likely is a major contributor to the total soil erosion in this region. There is a need to examine tillage translocation and tillage erosion in this region for the purposes of soil and water quality, environment and crop productivity enhancements.

1.2 Tillage Translocation and Tillage Erosion Modeling

Lindstrom et al. (1990, 1992) were among the first who carried out systematic experimental studies on tillage translocation and tillage erosion. These researchers established a simple model to simulate tillage translocation. This model has been adopted and further developed by several other researchers and is generally referred to as a diffusion (e.g. Govers et al., 1994) or dispersion model (e.g. Lobb, 1991). The original version of this model was simply a linear function between tillage translocation and slope gradient. A single parameter, the tillage transport coefficient, was used to characterize the erosivity of the examined tillage operation. Later on, other factors such as slope

curvature, tillage speed and soil conditions were introduced into this model (e.g. Lobb et al., 1995; Van Muysen et al., 1999, 2002). Lobb and Kachanoski (1999) summarized these factors and described tillage translocation as a function of tillage erosivity and landscape erodibility. Tillage erosivity is determined by the type and design of the tillage implement and how the tillage is operated. Landscape is determined by topographic features, i.e. slope gradient and slope curvature, and soil properties. These researchers proposed to include slope curvature as a second variable in the model.

Any implement that disturbs soil has the potential to cause tillage erosion. The diffusion/dispersion model needs to be calibrated with field experiments for different types of tillage operations. Currently, tillage translocation studies have focused on primary tillage implements with the assumption that tillage translocation associated with secondary tillage is minor and that associated with seeding operations is negligible. In addition, no study has been carried out to examine tillage erosion associated with cereal-based production systems, which are the predominant form of crop production in the Canadian Prairies.

In the first data chapter of this thesis, field data of tillage translocation experiments carried out in a field site located near Deerwood, Manitoba, Canada are presented. Tillage translocation caused by four implements, which forms a typical conventional tillage sequence for cereal-based production in Canadian Prairies, was investigated individually or in combination. Tillage translocation caused by individual tillage implements and, in particular, that of secondary tillage and seeding implements was compared. In addition, the effect of one tillage operation on subsequent operations and the effect of slope curvature on tillage translocation were also examined.

1.3 Validation of Soil Erosion Models Using ^{137}Cs Measurements

Cesium-137 (^{137}Cs) is an artificial ridionuclide that comes from the thermonuclear weapons testing in the 1950s and 1960s. ^{137}Cs falls out onto the ground during precipitation and is then adsorbed tightly by soil particles, especially by clay particles. Like a tag attached on soil particles, ^{137}Cs can be used as a tracer to assess soil redistribution. The basic principle of the ^{137}Cs technique is to compare the ^{137}Cs inventory at a given sample point to that at a reference point where soil erosion is considered to be negligible. Lower or higher ^{137}Cs inventory at the given sample point than that at the reference point indicates soil loss or accumulation, respectively, at this sample point. The amount of loss or gain of ^{137}Cs, when compared to the reference level, can be converted into the mass of soil loss or gain by using a conversion model (e.g. Lobb et al., 1999; Walling et al., 2001). The ^{137}Cs technique has proved to be an effective tool to estimate total soil erosion rates at given point-locations and has been widely used to validate water and tillage erosion models (e.g. de Jong et al., 1983; Pennock, 2003).

Observed total soil erosion on agricultural land, especially in topographically complex landscapes, is an integrated result of all forms of soil erosion, i.e. water, wind and tillage erosion. In addition to the contributions of individual erosion processes, the pattern of total erosion is further complicated due to the linkages and interactions between different erosion processes (Lobb et al., 2003). The validation of tillage or water erosion model has to involve modeling or assumptions of other erosion processes (e.g. Walling et al., 2001). Water and tillage erosion are both topography driven processes. In

topographically complex landscapes, for a given type of landscape element, different erosion processes have characterized patterns (spatial signatures) (Lobb et al. 2003). Landscape segmentation summarizes the topographic features. Landform information, which can be used for landscape segmentation, is available in some nationwide soil databases (e.g. Canada and China). Therefore, it is valuable to investigate the possibility of using landscape segmentation procedure as a simple tool to assess the general patterns of water, tillage and total erosion.

In the second data chapter of this thesis, two field sites, characterized by undulating slopes and hummocky knolls, respectively, located in the northern region of the North American Great Plains were examined. Tillage erosion is estimated using TillEM, a computer program developed based on a diffusion/dispersion type tillage erosion model. Tillage erosion estimates were coupled with water erosion estimates, which were estimated using established water erosion models. The model estimates were compared to ^{137}Cs-estimated total soil erosion to examine the relative contributions of and linkage and interactions between these two erosion processes. The landscapes were segmented using the LandMapR program. The patterns of tillage and water erosion in different landscape elements were examined and the possibility of using landscape segmentation to assess the pattern of tillage, water and total erosion was evaluated.

1.4 Modeling the Redistribution of Soil Constituents

During tillage, soil constituents (e.g. soil organic carbon) are translocated together with soil mass. The concentrations of soil constituents vary with depth in soil profiles. On soil loss positions the subsoil is brought up into the till-layer and on soil accumulation positions, the surface soil is buried under the till-layer, which causes the mixing (transfer) of subsoil and surface soil (Kachanoski et al., 1984; Lobb, 1997; Lobb and Kachanoski., 1999b). The pattern of soil constituent redistribution, therefore, is not determined by the redistribution pattern of soil mass alone.

The simple diffusion/dispersion type tillage erosion models estimates the average translocation but do not account the mixture of soil from different layers and they do not describe the extent of tillage translocated soil so that can not be directly used to simulate the redistribution of soil constituents. Van Oost et al. (2000, 2003a, b) proposed the use of a convoluting procedure to simulate the translocation process. However, the convoluting procedure requires more input data than the simple diffusion/dispersion model.

The redistribution of soil constituents determines the variation of soil properties over landscapes. However, the studies of tillage-induced soil constituent redistribution were rare. No study has been carried out to examine the redistribution of soil constituents under the context of different topographic features, different tillage patterns and different temporal scales.

In the third data chapter of this thesis, a computer program, TillTM, was developed to simulate the tillage translocation process. Soil mass and soil constituent redistributions on four hypothetical landscapes were estimated using TillTM. The effects of different tillage patterns and temporal scales were examined. And the similarity between the redistribution patterns of soil mass and soil constituents was evaluated. The model was validated using field data collected in a site located near the town of Cyrus, Minnesota, USA.

1.5 References

Aufrère, L., 1929. Les rideaux, étude topographique. Annales de Géographie 38, 529-560.

Chepil, W.S., Siddoway, F.H., Armbrust Dean V., 1962. Climatic factor for estimating wind erodibility of farm fields. J. Soil Water Conservation 17, 162-165.

de Jong, E., Begg, C.B.M., Kachanoski, R.G., 1983. Estimates of soil erosion and deposition for some Saskatchewan soils. Can. J. Soil Science 63, 607–617.

Govers, G., Vandaele, K., Desmet, P.J.J., Poesen, J., Bunte, K., 1994. The role of tillage in soil redistribution on hillslopes. Eur. J. Soil Science 45, 469-478.

Govers, G., Lobb, D.A., Quine, T.A., 1999. Tillage erosion and translocation emergence of a new paradigm in soil erosion research. Soil Tillage Research 51, 167-174.

Kachanoski, R.G., de Jong, E., 1984. Predicting the temporal relationship between soil Cesium-137 and erosion rate. J. Environmental Quality 13, 301-304.

Mech, S.J., Free, G.A., 1942. Movement of soil during tillage operations. Agricultural Engineering 23, 379-382.

Lindstrom, M.J., Nelson, W.W., Schumacher, T.E., Lemme, G.D., 1990. Soil movement by tillage as affected by slope. Soil Tillage Research 17, 255-264.

Lindstrom, M.J., Nelson, W.W., Schumacher, T.E., 1992. Quantifying tillage erosion rates due to moldboard plowing. Soil Tillage Research 24, 243-255.

Lobb, D.A., 1991. Soil erosion processes on shoulder slope landscape positions. M.Sc. Thesis. University of Guelph. Guelph. 390 p.

Lobb, D.A., Kachanoski, R.G., Miller, M.H., 1995. Tillage translocation and tillage erosion on shoulder slope landscape positions measured using ^{137}Cs as a tracer. Can. J. Soil Science 75, 211-218.

Lobb, D.A., 1997. Impact of tillage translocation and tillage erosion on the estimation of soil loss using ^{137}Cs (abstract). J. Soil Water Conservation 52, 306.

Lobb, D.A., Kachanoski, R.G., 1999*a*. Modelling tillage erosion in topographically complex landscapes of southwestern Ontario, Canada. Soil Tillage Research 51, 261–278.

Lobb, D.A., Kachanoski, R.G., 1999*b*. Modelling tillage translocation using step, linear-plateau and exponential functions. Soil Tillage Research 51, 317-330.

Lobb, D.A., Kachanoski. R.G., Miller, M.H., 1999. Tillage translocation and tillage erosion in the complex upland landscapes of southwestern Ontario. Soil Tillage Research 51, 189-209.

Lobb, D.A., Lindstrom, M.J., Schumacher, T.E., 2003. Soil erosion processes and their interactions: implications for environmental indicators. In: R. Francaviglia (Ed.).

Agricultural impacts on soil erosion and soil biodiversity: developing indicators for policy analysis. Proceedings from an OECD expert meeting – Rome, Italy, March 2003, pp. 325-336.

Pennock, D.J., 2003. Terrain attributes, landform segmentation, and soil redistribution. Soil Tillage Research 69, 15-26.

Van Muysen, W., Govers, G., Bergkamp, G., Roxo, M., Poesen, J., 1999. Measurement and modelling of the effects of initial soil conditions and slope gradient on soil translocation by tillage. Soil Tillage Research 51, 303-316.

Van Muysen, W., Govers, G., Van Oost, K., 2002. Identification of important factors in the process of tillage erosion: the case of mouldboard tillage. Soil Tillage Research 65, 77-93.

Van Oost, K., Govers, G., Van Muysen W., Quine, T.A., 2000. Modeling translocation and dispersion of soil constituents by tillage on sloping land. Soil Science Society Am. J. 64, 1733-1739.

Van Oost, K., Govers, G., Van Muysen W., 2003*a*. A process-based conversion model for caesium-137 derived erosion rates on agricultural land: an integrated spatial approach. Earth Surface Processes and Landforms 28, 187-207.

Van Oost, K., Van Muysen W., Govers, G., Heckrath, G., Quine, T.A., Poesen, J., 2003*b*. Simulation of the redistribution of soil by tillage on complex topographies. Eur. J. Soil Science 54, 63-76.

Walling, D.E., He, Q., 2001. Models for converting ^{137}Cs measurements to estimates of soil redistribution rates on cultivated and uncultivated soils, and estimating bomb-derived ^{137}Cs reference inventories (including software for model implementation). A

Contribution to the IAEA Coordinated Research Programmes on Soil Erosion (D1.50.05) and Sedimentation (F3.10.01).

Wischmeier, W.H., Smith, D.D., 1965. Predicting rainfall-erosion losses from cropland east of the Rocky Mountains. U.S. Department of Agriculture, Agricultural Research Service, Agriculture Handbook 282.

2. TILLAGE TRANSLOCATION AND TILLAGE EROSION IN CEREAL-BASED PRODUCTION IN MANITOBA, CANADA*

2.1 Abstract

Tillage erosion is a potential contributor to the total soil erosion occurring within cultivated fields. No study has been carried out on tillage erosion associated with cereal-based production systems, which are the predominant form of crop production in the Canadian Prairies. In this study, 77 plots were established within a field site in southern Manitoba, Canada to examine tillage translocation caused by four tillage implements: air-seeder, spring-tooth-harrow, light-cultivator and deep-tiller. Together, these four implements create a typical conventional tillage sequence for cereal-based production in Canadian Prairies. It is determined that secondary tillage implements could be as erosive as primary tillage implements. In addition, the erosivity of the air-seeder was comparable to that of the deep-tiller, the primary tillage implement, when seeding was conducted shortly after the light-cultivator. In the majority of cases, tillage translocation could be explained by slope gradient alone, confirming that slope gradient is the main factor

* Li, S., Lobb, D.A. (University of Manitoba), Lindstrom, M.J. (USDA-ARS, retired). This manuscript was submitted to Soil and Tillage Research in Dec, 2005 and was accepted under the condition of medium revision. Revised version was submitted in Jul, 2006.

driving tillage translocation. However, slope curvature also significantly affected tillage translocation and should be used for future modeling.

2.2 Introduction

Tillage erosion is the redistribution of soil within a landscape caused directly by tillage. For a range of landscapes, it has been shown that tillage erosion is a potential contributor to the total soil erosion on cultivated fields (Govers et al., 1999). Lobb et al. (1995) reported that tillage erosion accounted for at least 70 % of the total soil loss on hilltops in their studies in Ontario, Canada. Tillage erosion is a direct result of tillage translocation, which is defined as the movement of soil by tillage. Progressive net downslope movement of soil by tillage results in soil loss from convex positions within a landscape and soil accumulation within concave positions.

The magnitude of tillage erosion depends on tillage erosivity, the erosivity of the tillage operation, and landscape erodibility, the erodibility of the landscape (Lobb and Kachanoski, 1999*a*). Tillage erosivity is determined by the design of the tillage implement (i.e. the type of equipment, the arrangement and geometry of the cutting tools), and how the tillage is operated (i.e. tillage frequency, tillage speed and depth, the match between the tractor and the implement and the behavior of the operator). Any field operation that disturbs soil has the potential to cause tillage erosion.

Tillage translocation and tillage erosivity must be measured in a much broader range of cropping and tillage systems than what has been examined to date. No one has reported on the erosivity of tillage associated with cereal-based production systems, which are the predominant form of crop production in the Canadian Prairies, the northern-most portion of the North American Great Plains and the largest area of crop production in Canada. Tillage associated with this system a relatively low intensity primary and secondary tillage and relatively high disturbance seeding operations. As well, the size of implements is normally quite large (10 - 25 m in width), which can result in intensive "scalping" of hilltops.

To date, tillage translocation and tillage erosion studies have been focused on the primary tillage implements, such as mouldboard plough and chisel plough (e.g. Lindstrom et al., 1990, 1992; Lobb et al., 1999). Few studies have been carried out to investigate tillage translocation and tillage erosion caused by secondary tillage and seeding implements (e.g. Van Muysen and Govers, 2002); translocation by the former implements has been assumed to be of minor importance, and translocation by the latter has been assumed to be negligible. These assumptions need to be validated.

Studies of tillage systems have investigated each implement separately (e.g. Lobb et al., 1999) or only investigated combinations (e.g. Lindstrom et al., 1990). But in a sequence of tillage operations, when one operation is conducted shortly after the previous operation, the previous one likely will affect the tillage translocation of the following operations. Lobb et al. (1995) and Lobb and Kachanoski (1999b) investigated tillage translocation caused by the same tillage sequence, combined and separately, respectively, but these two studies were conducted on different soil types. To account for the effect of

the previous tillage, Lobb et al. (1999) pre-tilled the field before establishing the plots for the secondary tillage implements, a tandem disc and a field cultivator. Van Muysen et al. (1999) and Van Muysen et al. (2000) compared the translocation caused by mouldboard plough and chisel plough on a pre-tilled field to that on a grass fallow field and on a stubble field, respectively. These authors found that pre-tilling considerably increased the intensity of translocation. Marques da Silva et al. (2004), however, found that pre-tilling decreased the translocation caused by an offset disc harrow. It is probable that soil conditions (including crop residue cover) at the time of tillage will affect the translocation of soil, and these conditions will be affected by the preceding soil and crop management tillage and cropping practices. The effect of one operation on subsequent ones must be examined in greater details.

Landscape erodibility is determined by the topographic properties of the landscape (i.e. slope gradient and slope curvature) and properties of the soil (e.g. bulk density, moisture content, texture, structure, etc.). Studies from different parts of the world have shown that slope gradient is the dominant property in influencing tillage translocation and tillage erosion (e.g. Lindstrom et al., 1990; Govers et al., 1994). However, the variability in tillage translocation which causes tillage erosion cannot be explained by slope gradient alone. The effects of other factors such as tillage depth and speed, tillage direction, soil properties have been stressed by several researchers (e.g. Lobb et al., 1999; Van Muysen et al., 2002). Lobb et al. (1999) suggested the inclusion of slope curvature as a second topographic property and used a multiple linear function to simulate tillage translocation:

$$T_M = \alpha + \beta\,\theta + \gamma\,\varphi \quad (1)$$

where

T_M is translocation in mass over a unit width of tillage (kg m^{-1});

α is the intercept of the linear regression equation, representing tillage translocation unaffected by slope gradient or slope curvature (kg m^{-1} $pass^{-1}$);

β is the coefficient for slope gradient, representing the extra tillage translocation due to slope gradient (kg m^{-1} $\%^{-1}$ $pass^{-1}$);

θ is slope gradient, positive when downslope and negative when upslope (%);

γ is the coefficient for slope curvature, representing the extra tillage translocation due to slope curvature (kg m^{-1} ($\%^{-1}$ m) $pass^{-1}$); and

φ is slope curvature, positive for convex and negative for concave (% m^{-1}).

In this model, α, β and γ characterize the tillage erosivity of a given tillage implement or combination of implements, while slope gradient (θ) and slope curvature (φ) characterize the landscape erodibility. These authors found that for some implements, slope curvature has significant effect on tillage translocation, however the effect of slope curvature was not consistent. Slope curvature may be of greater importance in the Canadian Prairies where landscapes can be highly topographically complex due to the youth of the landscapes and the short history of cultivation. The effect of slope curvature therefore needs to be examined in depth.

The objectives of this study were: 1) to assess the erosivity of tillage implements and practices associated with cereal-based production systems in Manitoba; 2) to examine tillage translocation by and erosivity of individual tillage implements used in

these crop production systems, and, in particular, that of secondary tillage and seeding implements; 3) to examine the effect of one tillage operation on subsequent operations; and 4) to investigate the effect of slope curvature on tillage translocation and its contribution to the erosivity in these production systems.

2.3 Materials and Methods

2.3.1 Study Site

This study was carried out near Deerwood, about 150 km southwest of Winnipeg in Manitoba, Canada, between - 98.3° and - 98.4° East and 49.3° and 49.4° North. This area is referred to as Pembina Hills Upland (Michalyna et al., 1988), a transition area between the lower Manitoba Plain and the higher Saskatchewan Plain and is characterized by undulating to hummocky moraine landscapes. Climate is a subhumid continental with short, cool summers and long cold winters. In Deerwood, the mean annual temperature is 2.9 °C and the mean annual precipitation is 567 mm. Underlying bedrock of this area is shale but the parent material is dominantly glacial till derived from shale, limestone and granite rock and moderately to very strongly calcareous. The dominant soils in this area are Dark Grey Chernozems (Canadian System of Soil Classification, 1998) (Mollisols in the USDA soil classification system). Soil series vary according to landform positions. On the upper and mid slope positions, soils are well

drained and belong to the Dezwood Loam series (Orthic Dark Grey Chernozem); on the lower slope positions, soils are imperfectly drained and belong to the Zaplin Loam series (Gleyed Dark Grey Chernozem); and in the depression positions, soils are poorly drained and belong to the Pouchal Clay Loam series (Humic Luvic Gleysol). For the surface layer, the soil bulk density, based on 72 soil samples collected along a transect in the long slope area after harvest and prior to tillage, is 1170 ± 192 kg m^{-3} (data not shown). The natural vegetation in this area is boreal forest, but most of the area has been cleared for agriculture and is cultivated. Spring wheat is the most popular crop in this area. Other major crops include canola, barley, dry field beans, oats, alfalfa and flaxseed. In the 2001 census year (Statistics Canada, 2002), these major crops covered about 85 % of the seeded area (Figure 2. 1). The intensity of tillage practices has decreased since 1970s: firstly, conservation tillage and/or zero-till systems have been adopted by more and more farmers; secondly, in conventional tillage systems, lighter implements have been used and used less frequently.

The field site used in this study was broken and has been continuously cropped since 1928. Main crops are spring wheat, oat and canola. Tillage implements used in this field have changed over time. Mouldboard plough for primary tillage, tandem disc and heavy cultivator for secondary tillage, diamond harrow for harrowing and disc drill for seeding were used before 1980s. Currently, the sequence of operations in the field includes one primary tillage operation (deep-tiller), one to two secondary tillage operations (usually a light-cultivator, sometimes a tandem disc, fertilizer usually applied with a secondary tillage), one to two harrowing (spring-tooth-harrow) operations, and seeding (air-seeder) (Figure 2. 2). The description of the tillage implements currently

used is summarized in Table 2.1. The farmer considers this tillage system to be conventional by today's standard, although the implements being used are considerably less intensive than the traditional definition of conventional tillage.

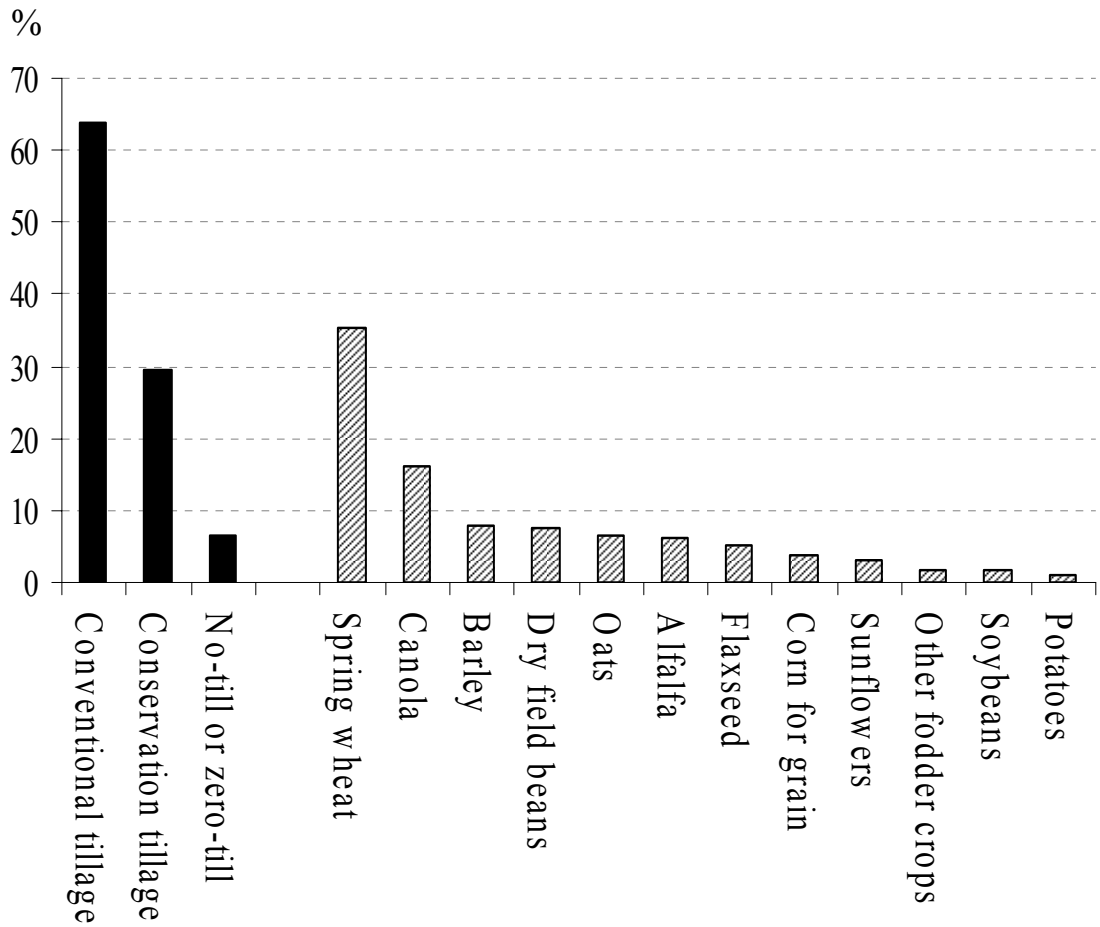

Figure 2.1 Tillage systems and main crops in the study area. The height of the bar represents the respective percent of seeded area in 2001 census year in agricultural region 8, southwest Manitoba, Canada. Conventional tillage refers to tillage incorporating most of the crop residue into the soil and conservation tillage refers to tillage retaining most of the crop residue on the surface (Source: Statistics Canada, 2002) .

Figure 2.2 Photos of the four tillage implements: a) deep-tiller; b) spring-tooth-harrow; c) light-cultivator and d) air-seeder.

Table 2.1 Description of tillage implements.

Implement†	Type	Tools	Spacing m (inch)	Arrangement	W_I m (foot)	D_T m	S_T m s^{-1}
Deep-tiller	primary	sweeps 0.25 m (10") wide	0.31 (12")	4 rows	11.0 (36')	0.10 - 0.13	1.8 - 2.0
Light-cultivator	secondary	sweeps 0.23 m (9") wide	0.18 (7")	4 rows	13.7 (45')	0.04 - 0.08	2.2 -2.5
Spring-tooth-harrow	harrowing	spring-tooth 0.53 m (21") long, 0.01 m (0.5") in diameter	0.05 (2")	5 rows	21.3 (70')	0.01 - 0.02	2.0 -2.5
Air-seeder	seeding	knives 0.03 m (1") wide	0.18 (7")	4 rows	11.0 (36')	0.02 - 0.04	2.2

† The same tractor, John Deer 8970 (400 horsepower), was used for all the implements.

2.3.2 Experiment Design

In 2003 and 2004, 53 plots were established to measure tillage translocation by single passes of deep-tiller (DT), spring-tooth-harrow (SH), light-cultivator (LC) and air-seeder (AS). Another set of 24 field plots was established to examine the combined effect of light-cultivator and air-seeder (LC/AS) due to the fact that seeding operation is usually conducted very shortly after secondary tillage. In total, there were 77 field plots.

Two areas of the field were selected according to their topographic features (Figure 2. 3), the Long Slope Area and the Bowl Area, which represent the two dominant landform types within the field: undulating and hummocky landforms, respectively. The Long Slope Area is part of a large ridge and extends from the top of the ridge to its base, along the northern boundary of the field. Slope gradient in this area ranges from 0 % to about 20 % while slope curvature ranges from –2.5 % m^{-1} to 2.5 % m^{-1}. Although the absolute values of slope gradient are high, the variability along the slope is relatively small because the slope is long (about 500 m). This area is a complex of small knolls located in the middle of the field. The central part of this area is a depression, which gives it a bowl shape. The ranges of both slope gradient (form 0 to 6 %) and slope curvature (from –1.5 % m^{-1} to 1.5 % m^{-1}) in the Bowl Area are narrower than that of the Long Slope Area, especially the range of slope gradient. The change in slope curvature is comparatively high given that all the changes happen within a fairly short distance (about 40 m from the edge of the bowl to its base). It was presumed that the relatively small change in slope gradients and large change in slope curvatures in the Bowl Area would provide for greater isolation of slope curvature's contribution to tillage translocation.

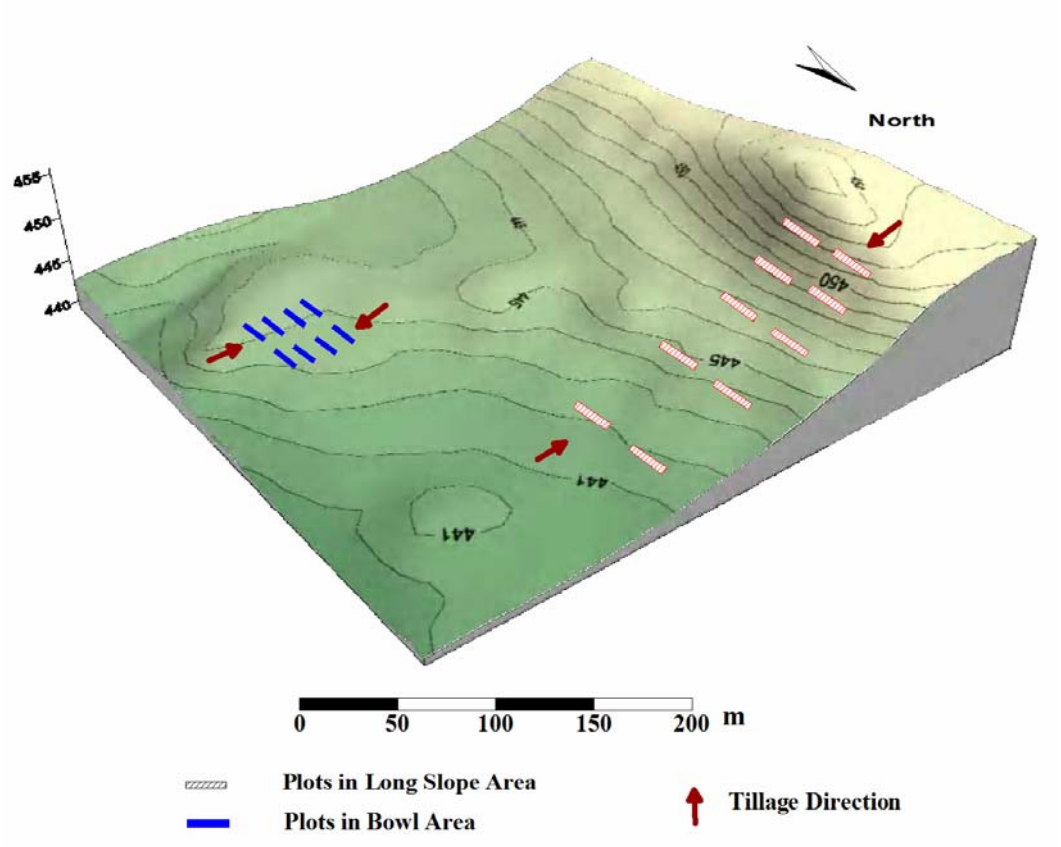

Figure 2.3 Plot positions for deep-tiller to illustrate plot layout. Towards the northern boundary is the Long Slope Area, towards the eastern-southern corner is the Bowl Area. Paired plots were positioned in two parallel lines and tillage operations were undertaken in opposite directions (Note: scale used for the plots were different from the map scale. Plot width = 1.22 m).

In both the Long Slope Area and the Bowl Area, plots were oriented into two parallel rows over a range of topographic conditions (i.e. slope gradient and slope curvature), one row undergoing upslope tillage while the other row undergoing downslope tillage. Plot positions for deep-tiller are illustrated in Figure 2. 3. Plot positions for spring-tooth-harrow and the combination of light-cultivator and air-seeder were similar to those for the deep-tiller. Due to time limitations, for the single pass of light-cultivator and air-seeder, plots were only established in the Long Slope Area.

2.3.3 Topographic Survey

Plot positions and the topography of the plots areas (area of approximately 10 × 10 m) were surveyed by using Total Station (Sokkia set 4110). The survey was georeferenced using a Trimble TSC1 system, a differential GPS system. For the topographic survey, the survey was conducted along two to four lines parallel to the tillage direction at a density of approximately 2 - 3 m. Slope gradient and slope curvature at the plot position were calculated directly by using these topographic survey points. Slope gradient (%) is calculated as the change of elevation over the distance and slope curvature was calculated as the change of slope gradient over the distance (% m^{-1}).

2.3.4 Tillage Translocation Measurement

Dyed limestone chips were used as tracers to measure soil movement by tillage (MacLeod et al., 2000; Zhang et al., 2004). Tracer size was 0.6 - 1.2 cm for all tillage operations, excluding deep-tiller. Larger size tracers (1.2 - 2.5 cm) were used for the deep-tiller to save field labor because the plot size for deep-tiller was considerably larger than that for the other tillage operations (see below for the determination of the plot size) and Rahman et al. (2002) found no significant difference due to tracer size or density.

The tracers were incorporated into the soil in plots. Plots were oriented perpendicular to the tillage direction (Figure 2. 4). The length of the plots (the dimension along the tillage direction) was 20 cm. The width of the plots (the dimension perpendicular to tillage direction) depended on the arrangement of cutting tools (e.g. sweeps and knives) in the tillage implement. Plot width was equal to a multiple of the tool spacing (Figure 2. 4a). A compromise was made for the combination of light-cultivator and air-seeder due to the different tool spacings of these two implements. The

depth of the plots was 5 - 10 cm deeper than the expecting tillage depth (Figure 2. 4b, c). To set up the plot in the field, a base plate and a box (4 walls) were prepared in advance. The inside dimensions of the box were made to be the exact size of the plot. Soil in the plot location was dug out first and the plate was placed and leveled on the bottom of the hole. The box was established on the plate and the soil that was excavated was placed back into the hole, both inside and outside the box, and packed to the original bulk density. Soil inside the box was then taken out and mixed with the tracer (a mass equal to about 5 % of the soil mass). The labeled soil was placed back into the box once again and the plot was packed to the original bulk density. Finally, the box was pulled out and the base plate was left in the field as a reference for exact relocation of the plot.

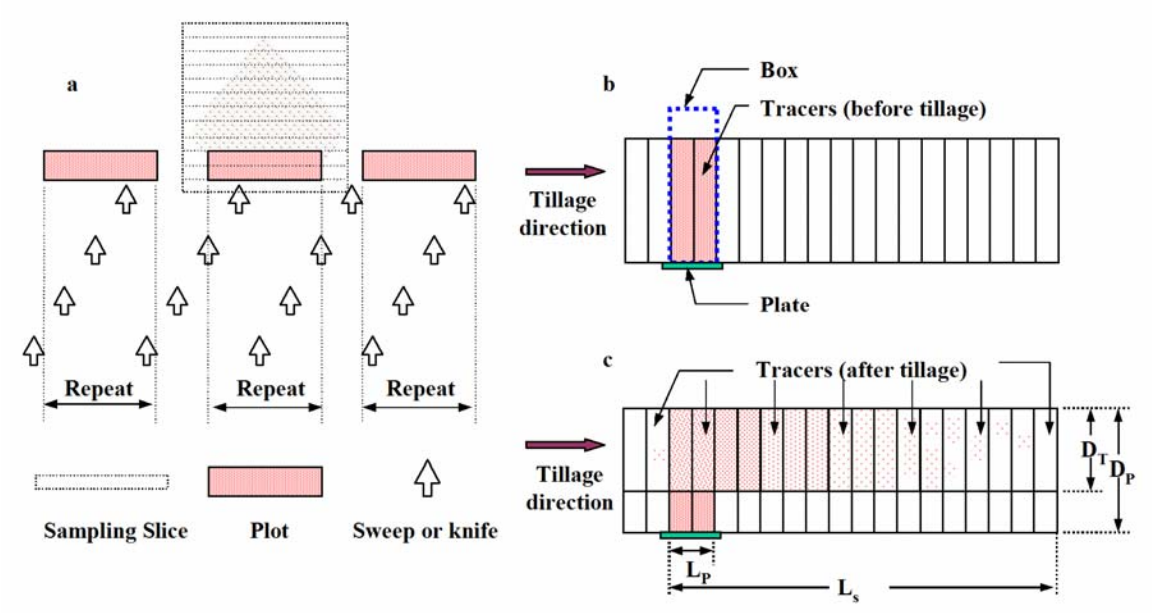

Figure 2.4 Illustration of plot set-up and sampling design. a) Top view. Plot width was determined by the repeating width of the tools according to the tool arrangement of the implement; b) Cross-section view of a plot before tillage. The box is pulled out and the plate is left in the field as a reference for the sampling; c) Corss-section view of a plot after tillage. The plot depth is deeper than the tillage depth, and after tillage only the tracers within the tillage layer are redistributed (D_T: tillage depth, D_P: plot depth, L_P: plot length and L_S: a distance exceeding the maximum translocation distance.)

After tillage operations, the edge of the plate was located and used as a reference for sampling. The tracers were recovered along the tillage direction in slices, each 10 cm in length, until no tracers could be found (Figure 2. 5). The distribution of these plot-tracers was then used to generate a summation curve (Figure 2. 4) as described by Lobb et al. (2001). Using the summation curve method, what is assessed is the volume/mass moving past the zero line of the tracer-labeled plot. The average translocation distance, and the experimental error, can be calculated through a procedure involving convolution:

$$T_P = \int_0^{\infty} (1 - c_s)\, dx - \int_{-\infty}^{0} (c_s)\, dx, \tag{2}$$

$$\varepsilon = \left(\int_{Ls}^{Ls+Lp} |1 - c_s|\, dx \Big/ (T_P + L_p) \right) 100, \tag{3}$$

where:

T_P is the translocation distance averaged over the depth of labeled soil, over a unit width of tillage (m);

x is the distance at which the quantity of tracer is measured (m);

c_s is the proportion of tracer quantity calculated from the summation curve at distance x (kg kg^{-1});

ε is a measure of error, either from the inherent variability of translocation or experimental error, or from both (%);

L_s is a distance exceeding the maximum translocation distance (m); and

L_p is plot length (m).

T_P can be converted to translocation in distance, T_L, by:

$$T_L = T_P \frac{D_P}{D_T} \tag{4}$$

where

T_L is translocation distance averaged over the depth of the tillage layer, over a unit width of tillage (m);

D_T is tillage depth (m); and

D_P is plot depth (m).

T_P can also be converted directly to translocation in mass, T_M , by:

$$T_M = \rho T_L D_T = \rho T_P D_P \tag{5}$$

where

ρ is dry soil bulk density (kg m^{-3}).

T_L provides an indicator of the potential erosivity since T_L relates to how far soil is moved over the land surface. However, it is preferable to use T_M (translocation in mass) rather than T_L because: 1) traditionally, erosion is measured as a mass; 2) the calculation of T_L requires accurate measurements of tillage depth (Equation (4)), and it is difficult to determine tillage depth in the field, particularly for tillage implements with sweeps or knives because the cutting surface can be very uneven. The calculation of T_M uses D_P (Equation (5)), which is accurately measured during the plot set up. Therefore, T_M is considered to be more accurate than T_L; 3) since T_L depends on tillage depth, it is not comparable between tillage implements with different tillage depth; 4) tillage depth varies over the landscape. The summation curve method provides an estimate of the

tillage depth (Figure 2. 5). It also provides an approach to estimate the distance to a cumulative percentile of translocated soil mass along tillage direction, e.g. λ_{75} (m) is the distance to which 75 % of soil mass (75th percentile) is translocated (Figure 2. 5). These percentiles characterize the behavior of the translocated soil and how soil is distributed along the path of tillage.

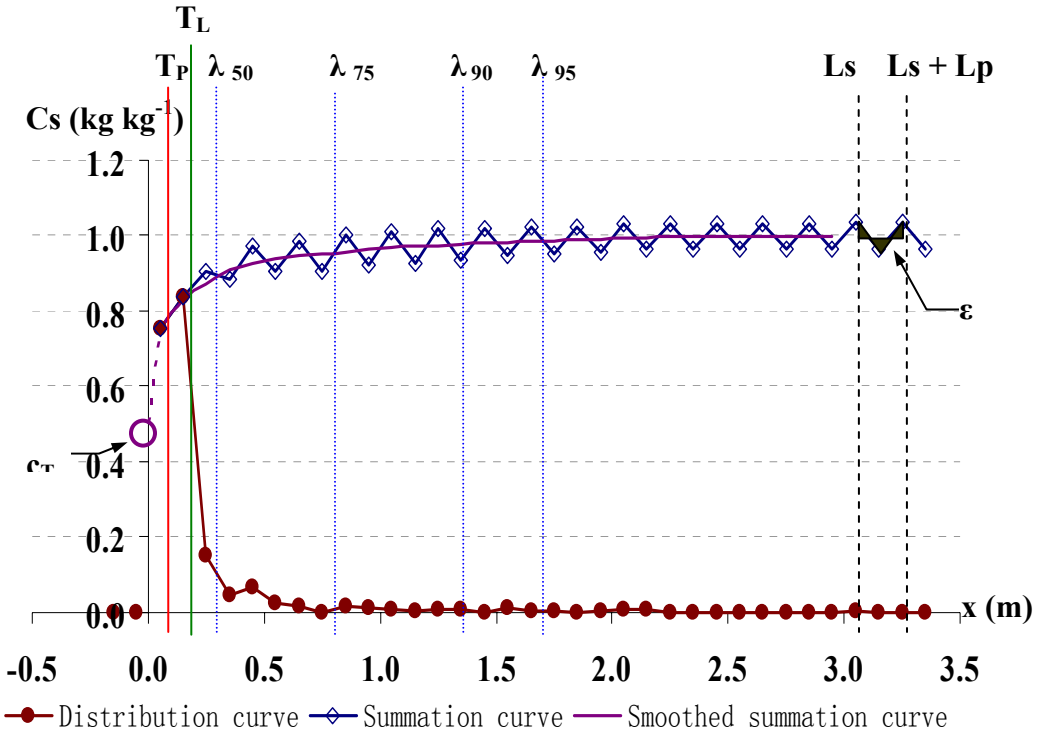

Figure 2.5 Tracer distribution and summation curve of deep-tiller, plot 4. Plot depth (D_P) = 0.25 m. c_T represents the proportion of the untouched tracer on the bottom of the plot. Tillage depth (D_T) was estimated by $D_T = D_P\ (1- c_T)$ = 0.13 m. $T_L = T_P D_P / D_T$ = 0.23 m. λ_{50}, λ_{75}, λ_{90} and λ_{95} represent the distances to which 50 %, 75 %, 90 % and 95 % of soil mass is translocated, respectively. Experiment errors (ε) associated with T_P was represented by shaded area (T_P = 0.115 m, L_P (plot length) = 0.20 m, L_s (a distance exceeding the maximum translocation distance) = 3.05 m, ε = 7.6 %).

2.3.5 Statistical Analysis

Tillage translocation data were examined with SAS 9.0® for statistical analyses. Means were used to indicate the averages, and standard deviation (SD) and coefficient of variance (CV) were used to indicate the variability of the data. A Tukey-Kramer test was used for multiple comparisons and to determine whether there was a significant difference between those means. Due to the inherent variability of the data, 10 % significance level was used as the threshold for the Tukey-Kramer tests of multiple comparisons. The Tukey-Kramer test was designed for pairwise comparisons of means with unequal-sized samples. It controls the maximum-experimentwise-error-rate (SAS institute, Inc, 2002).

In the regression analyses, a F-test was used to determine the significance of the regression model and a student t-test was used to determine the significance of the individual coefficients (i.e. α, β and γ). The significance of the tests were indicated by the $P > F$ or $P > |t|$ values, which were grouped into three categories, i.e. ≤ 0.10, ≤ 0.05, ≤ 0.01, and are stated as 10 %, 5 % and 1 % levels, respectively. Coefficient of determination, R^2, was used as another indicator for evaluating to what extent the regression models could explain the observed variation of the dependent variable(s).

2.3.6 Tillage Translocation Modeling

Tillage translocation models were established based on the regression analysis of translocation in distance (T_L) or translocation in mass (T_M) against slope gradient (θ) and slope curvature (φ), as shown in Equation (1). By using Equation (1), (4) and (5), the translocation in mass can be calculated by:

$$T_M = T_P \rho D_P = T_L \rho D_T = (A + B \theta + C \varphi) \rho D_T \quad (6)$$

$$= \alpha + \beta \theta + \gamma \varphi$$

where

A is the intercept of the linear multiple regression model (m pass^{-1});

B is the slope of the linear multiple regression model associated with slope gradient (m %$^{-1}$ pass^{-1}); and

C is the slope of the linear multiple regression model associated with slope curvature (m %$^{-1}$ m pass^{-1}).

β and γ indicate tillage erosivity. The model is more sensitive to β than to γ because the range of slope gradient observed in the field typically exceeds those of slope curvature by about one to two orders of magnitude (Lobb et al., 1999). β is commonly referred to as tillage transport coefficient and has been widely used as the indicator of tillage erosivity. α indicates the dispersivity of translocated soil. In general, the greater is the α value, the wider is the range of the soil being translocated, i.e. the greater the dispersivity is. α also serves as a means for comparison of research data between tillage implements and practices.

In order to examine the contributions of slope gradient (θ) and slope curvature (φ) on tillage translocation, in this study, we used two regression models:

$$T_M = \alpha + \beta \theta \quad (M1)$$

$$T_M = \alpha + \beta \theta + \gamma \varphi \quad (M2)$$

M1 is a simple regression model used to examine the effect of slope gradient (θ) as shown in Figure 2.6. M2 used both θ and φ as independent variables and was the

model of primary interest in this study. M2 was compared to M1 to determine whether M2 could better explain the observed tillage translocation. Data from the Long Slope Area and the Bowl Area were analyzed separately and then the combined data sets were analyzed as well.

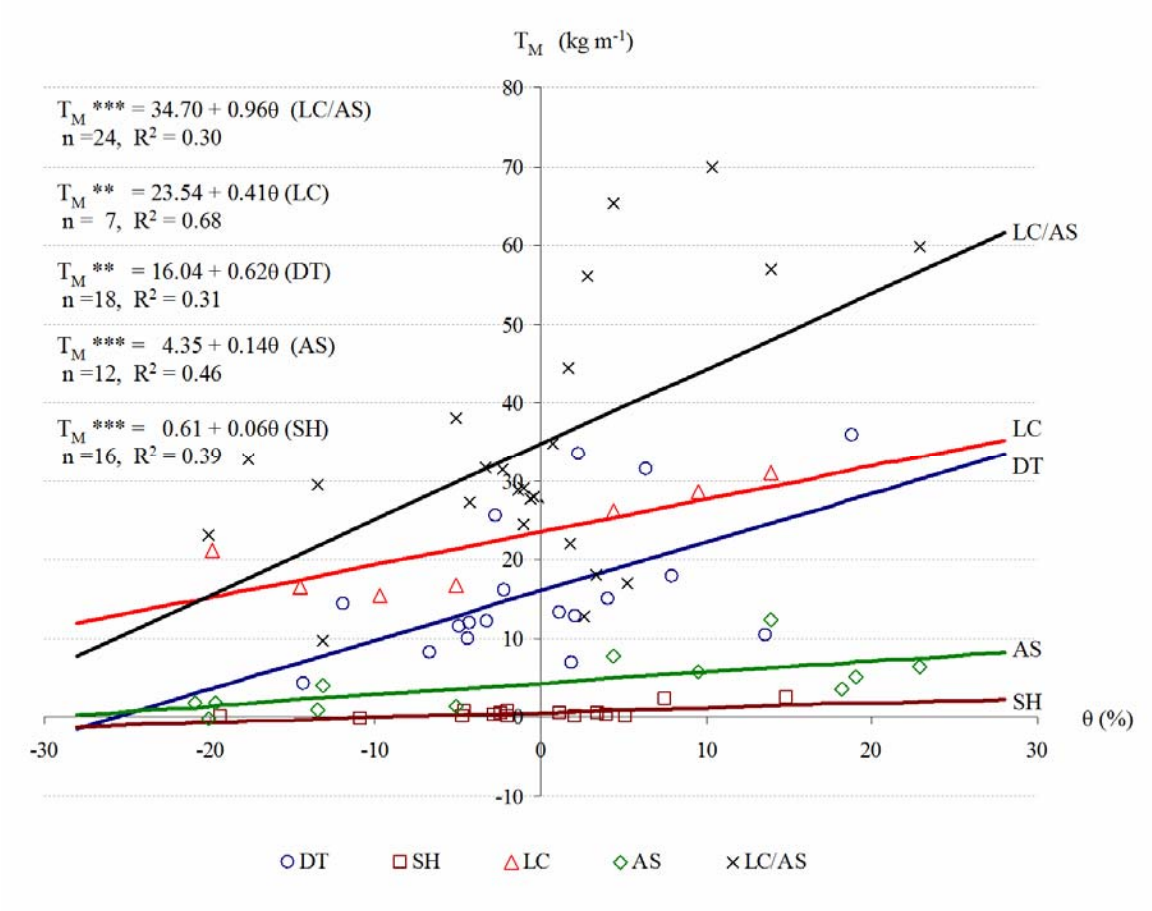

Figure 2.6 Regression analyses of translocation in mass (T_M) against slope gradient foreach tillage treatment.

Four translocation percentiles, i.e. λ_{50}, λ_{75}, λ_{90} and λ_{95}, were also regressed against slope gradient and/or slope curvature as:

$$\lambda_p = \alpha_p + \beta_p \theta \qquad \text{(M3)}$$

$$\lambda_p = \alpha_p + \gamma_p \varphi \qquad \text{(M4)}$$

$$\lambda_p = \alpha_p + \beta_p \theta + \gamma_p \varphi \quad \text{(M5)}$$

where

p denotes the p^{th} percentile of translocated soil mass;

λ_p is the distance to which p % of soil mass is translocated (m);

α_p is the intercept of the regression model for the p^{th} percentile (m);

β_p is the coefficient of slope gradient for the p^{th} percentile (m $\%^{-1}$); and

γ_p is the coefficient of slope curvature for the p^{th} percentile (m $\%^{-1}$ m).

These regression models were used to evaluate how slope gradient and slope curvature could affect tillage translocation. More pronounced relationships between soil movement and slope gradient and possibly slope curvature (i.e. greater β_p and γ_p values, respectively) are expected at the higher percentiles (Lobb et al., 2001). However, due to the increased variability that occurs in the tail region of the distribution curves, the significance levels may not be the highest at λ_{95}.

After the translocation models for each tillage operation and their combinations were determined, the overall translocation after a full sequence, which includes several operations, was calculated by:

$$T_{Mt} = \sum_{i=1}^{n} T_{Mi} = \sum_{i=1}^{n} \alpha_i + \left(\sum_{i=1}^{n} \beta_i \right) \theta + \left(\sum_{i=1}^{n} \gamma_i \right) \varphi \quad (7)$$

where

T_{Mt} is the total translocation in mass after a full sequence (kg m^{-1});

i is the denotation for the i'th tillage operation; and

n is the number of tillage operations in one full sequence.

2.4 Results and Discussion

2.4.1 Tillage Translocation

The tillage translocation data are shown in Table 2.2. Plot positions evenly covered the range of slope gradient (θ) for all the implements and in Both Areas. Because only one factor could be controlled, slope curvature (φ) is not as evenly distributed as slope gradient, i.e. some plots have very similar φ values. However, the range of slope curvature (φ), i.e. typical and extreme φ values have also been covered. The estimated average tillage depth for DT, SH, LC and AS was 0.11 m, 0.01 m, 0.08 m and 0.03 m (Table 2.2), respectively. These estimates corresponded well with our field measurements (3 – 10 measurements for each implement, Appendix A.1). T_L calculated based on the estimated tillage depth was highly variable within the same implements (Table 2.2). T_M was also highly variable within implements. Firstly, the CVs of T_M were high, 57 %, 133 %, 29 %, 82 % and 48 % for DT, SH, LC, AS and LC/AS, respectively. Secondly, plots with similar topographic features (i.e. similar θ and φ values) have considerably different T_M values (e.g. DT Long Slope Area plot 8 vs plot 10). However, the differences between the implements were obvious.

Table 2.2 Summary of tillage translocation data.

		Deep Tiller (DT)									Spring Tooth Harrow (SH)									Light Cultivator followed by Air Seeder (LC/AS						
		θ	φ	ρ	D_T †	RR	T_P	T_L	T_M	ε	θ	φ	ρ	D_T †	RR	T_P	T_L	T_M	ε	θ	φ	ρ	RR	T_P	T_M	ε
	Plot	%	% m^{-1}	kg m^{-3}	m	%	m	m	kg m^{-1}	%	%	% m^{-1}	kg m^{-3}	m	%	m	m	kg m^{-1}	%	%	% m^{-1}	kg m^{-3}	%	m	kg m^{-1}	%
Long Slope Area	1	-11.9	2.52	1122	0.09	98.3	0.051	0.146	14.3	18.5	14.8	-0.46	1250	0.02	98.4	0.021	0.139	2.6	9.3	-13.2	1.38	1198	90.8	0.055	9.8	1.9
	2	13.6	-0.43	1122	0.10	98.9	0.037	0.094	10.5	0.3	-19.3	-1.03	1250	0.01	98.6	0.002	0.016	0.2	24.4	-20.1	0.08	1214	92.5	0.127	23.0	2.8
	3	-14.4	-0.18	1246	0.10	98.7	0.013	0.034	4.2	7.6	7.5	-0.51	1250	0.03	98.2	0.018	0.071	2.2	11.4	-17.7	0.06	1283	92.6	0.170	32.7	3.7
	4	18.8	1.09	1246	0.13	97.9	0.115	0.230	35.8	7.6	-10.9	-0.64	1250	0.01	98.4	-0.001	-0.016	-0.1	8.5	-13.4	-0.57	1298	85.1	0.151	29.4	1.3
	5	-6.7	-2.19	1246	0.10	98.9	0.026	0.065	8.1	0.1	4.0	0.15	1289	0.01	98.3	0.003	0.059	0.4	8.0	-5.1	0.07	1292	92.1	0.196	38.1	3.0
	6	7.9	0.47	1246	0.13	97.9	0.058	0.115	17.9	0.4	-4.7	0.13	1289	0.01	98.0	0.000	0.002	0.0	8.0	-4.3	0.44	1292	90.2	0.141	27.4	7.7
	7	-4.4	0.22	1265	0.10	98.4	0.031	0.078	9.9	6.6	2.1	0.41	1201	0.01	98.4	0.001	0.013	0.1	11.7	-2.3	-0.20	1247	87.7	0.169	31.5	0.1
	8	2.1	0.05	1265	0.10	98.8	0.041	0.102	12.9	7.6	-2.8	-0.05	1201	0.01	97.9	0.003	0.027	0.3	16.8	-0.4	-0.04	1197	85.0	0.156	28.1	3.8
	9	-2.2	-0.15	1166	0.09	97.8	0.055	0.158	16.2	5.6										13.9	1.58	1198	88.8	0.318	57.1	6.2
	10	1.9	0.45	1166	0.10	98.4	0.024	0.060	7.0	6.1										22.9	-0.22	1214	92.9	0.328	59.7	5.8
	11																			10.4	0.63	1298	88.5	0.359	69.8	2.6
	12																			4.4	0.24	1292	87.3	0.337	65.4	6.7
	13																			5.2	-0.37	1292	87.8	0.088	17.0	9.9
	14																			2.8	1.04	1247	82.1	0.299	56.0	6.1
	15																			2.6	-0.48	1197	89.0	0.071	12.8	19.1
Bowl Area	1	4.1	0.18	1260	0.13	97.6	0.047	0.095	14.9	11.1	3.5	0.47	1260	0.01	97.7	0.004	0.044	0.6	9.2	-3.3	0.63	1260	88.8	0.168	31.7	2.9
	2	-4.9	0.11	1208	0.13	97.9	0.038	0.076	11.5	34.8	-2.4	1.11	1208	0.01	98.7	0.004	0.044	0.5	9.5	-1.4	-0.46	1262	91.4	0.153	28.9	4.0
	3	6.3	-0.52	1301	0.13	97.1	0.097	0.194	31.6	2.0	5.1	-0.27	1301	0.01	98.8	0.001	0.022	0.1	21.4	0.7	0.00	1216	89.7	0.191	34.8	1.2
	4	-4.3	-0.28	1259	0.09	99.0	0.038	0.108	11.9	13.3	-4.6	0.15	1259	0.02	97.5	0.005	0.036	0.7	12.8	-0.7	-0.11	1166	90.9	0.159	27.8	7.7
	5	2.3	-1.55	1259	0.13	96.9	0.106	0.212	33.4	5.4	1.1	-0.17	1259	0.01	97.7	0.004	0.036	0.4	8.9	1.7	0.12	1237	93.8	0.119	22.1	6.1
	6	-3.2	-1.13	1289	0.09	98.1	0.038	0.107	12.1	2.6	-2.0	-0.27	1289	0.01	99.4	0.001	0.020	0.1	17.2	3.4	0.29	1276	90.3	0.095	18.1	10.8
	7	-2.7	1.46	1194	0.14	97.4	0.086	0.156	25.5	8.0	-1.9	0.11	1194	0.02	99.6	0.007	0.048	0.9	16.0	1.7	-0.10	1324	89.7	0.224	44.4	4.5
	8	1.1	0.14	1301	0.09	99.1	0.041	0.116	13.2	10.9	2.1	0.10	1301	0.01	98.8	0.001	0.020	0.1	15.6	-1.0	-0.21	1305	92.9	0.149	29.1	9.1
	9																			-1.0	0.45	1237	91.5	0.131	24.4	13.5
Average ‡				1231	0.11	98.2[c]			16.2	8.2[ab]			1253	0.01	98.4[c]			0.6	13.0[bc]			1252	89.6[b]		34.1	5.8[a]
SD				56	0.02	0.7			9.3	8.2			36	0.01	0.6			0.8	5.0			44	2.8		16.4	4.3

Table 2.2 (Continued)

		Light Cultivator (LC)									Air Seeder (AS)								
	Plot	θ %	φ % m^{-1}	ρ kg m^{-3}	D_T† m	RR %	T_P m	T_L m	T_M kg m^{-1}	ε %	θ %	φ % m^{-1}	ρ kg m^{-3}	D_T† m	RR %	T_P m	T_L m	T_M kg m^{-1}	ε %
Long Slope Area	1	-9.7	1.26	1198	0.07	86.8	0.087	0.193	15.6	0.9	-13.2	1.38	1198	0.03	95.1	0.034	0.115	4.1	6.9
	2	-19.9	0.06	1283	0.09	85.1	0.110	0.183	21.2	8.2	-20.1	0.33	1214	0.02	97.6	-0.001	-0.007	-0.1	37.4
	3	-14.5	-0.44	1298	0.06	81.7	0.085	0.212	16.5	12.0	-20.9	-0.46	1283	0.04	97.6	0.015	0.044	2.0	9.7
	4	-5.1	-0.33	1292	0.08	88.4	0.086	0.172	16.7	7.2	-13.4	-0.57	1298	0.02	96.8	0.008	0.054	1.1	3.4
	5	13.9	1.58	1198	0.09	69.1	0.172	0.287	31.0	7.3	13.9	1.58	1292	0.04	93.4	0.096	0.240	12.4	14.9
	6	9.5	-0.52	1298	0.08	79.5	0.148	0.268	28.7	3.6	22.9	-0.22	1198	0.04	97.4	0.054	0.135	6.4	5.5
	7	4.4	-0.06	1292	0.09	88.0	0.136	0.226	26.3	6.9	19.1	-0.26	1214	0.06	97.0	0.042	0.077	5.1	19.6
	8										-5.1	-0.3	1283	0.02	94.9	0.011	0.075	1.4	17.0
	9										9.5	-0.5	1298	0.04	94.7	0.046	0.130	5.9	2.0
	10										4.4	-0.1	1292	0.04	99.7	0.060	0.171	7.7	8.4
	11										18.2	-2.5	1283	0.04	99.0	0.029	0.080	3.7	21.4
	12										-19.7	0.6	1283	0.04	98.3	0.014	0.041	1.8	27.6
Average ‡				1266	0.08	82.7[a]			22.3	6.6[ab]			1261	0.03	96.8[c]			4.3	14.5[c]
SD				46	0.01	6.8			6.4	3.5			42	0.01	1.9			3.5	10.7

† Estimated using the summation curve method. Plot depth for DT, SH, LC, LC/AS were 0.25 m, 0.10 m, 0.15 m and 0.15 m, respectively. For AS, plot depth of plot 11 and 12 were 0.18 m and 0.175 m, respectively, and of all the other plots were 0.10 m.

‡ Different letters denote different groups according to Tukey-Kramer test of multiple comparisons at 10 % significance level.

The order of the averages of T_M for implements was SH < AS < DT < LC < LC/AS. The T_M for LC/AS, LC and DT were in the same order of magnitude and exceeded the T_M for AS by about one order of magnitude, which in turn exceeded the T_M for SH by about another one order of magnitude. So, in respect to tillage translocation, LC/AS, LC and DT were much more intensive than AS, and AS was much more intensive than SH. It is important to note that AS and SH do move soil and need to be taken into account for tillage erosion studies.

2.4.2 Deep-tiller

The results of the regression analyses are summarized in Table 2.3. For deep-tiller, in the Long Slope Area, M1 was significant at 5 % level, which indicates that tillage translocation is significantly affected by slope gradient. The R^2 of M2 (0.59) was greater than that of M1 (0.45), indicating there is a improvement from M1 to M2. This improvement of M2 was attributed to the contribution of slope curvature because the only change from M1 to M2 is that slope curvature has been added into the model. Therefore, for DT, slope curvature has an effect on tillage translocation.

Data from the Bowl Area are much more difficult to explain. Neither model was significant. A stronger relationship between tillage translocation and slope curvature was not found, contrary to what was expected. This could be explained by the narrower range of both slope gradient and slope curvature in this area. Generally, the narrower the independent data range is, the more difficult it is to establish a significant regression line. For the Both Areas, M1 was significant at the 5 % level. γ in M2 was not significant, but

M2 was significant at the 10 % level and R^2 of M2 (0.32) was almost the same as that of M1.

Table 2.3 Summary of regression analyses of T_M against slope gradient and slope curvature.

		Regression	Model			Intercept	Slope Gradien		Slope Curvature	
		Model	n	Pr>F	R^2	$\alpha^{\dagger}$	β	Pr>| t |	γ	Pr>| t |
Deep-tiller (DT)	Long Slope Area	$T_M=\alpha+\beta\theta$	10	0.03	0.45	13.41	0.56	0.03	-------	-------
		$T_M=\alpha+\beta\theta+\gamma\varphi$	10	0.04	0.59	12.90	0.54	0.03	2.82	0.16
	Bowl Area	$T_M=\alpha+\beta\theta$	8	0.13	0.35	19.47	1.31	0.13	-------	-------
		$T_M=\alpha+\beta\theta+\gamma\varphi$	8	0.34	0.35	19.33	1.28	0.18	-0.69	0.86
	Both Areas	$T_M=\alpha+\beta\theta$	18	0.02	0.31	16.04	0.62	0.02	-------	-------
		$T_M=\alpha+\beta\theta+\gamma\varphi$ [a!]	18	0.06	0.32	16.02	0.62	0.02	0.90	0.63
Spring-tooth-harrow (SH)	Long Slope Area	$T_M=\alpha+\beta\theta$	8	0.03	0.56	0.80	0.07	0.03	-------	-------
		$T_M=\alpha+\beta\theta+\gamma\varphi$	8	<<0.01	0.95	0.46	0.10	<<0.01	-1.50	<<0.01
	Bowl Area	$T_M=\alpha+\beta\theta$	8	0.21	0.25	0.44	-0.04	0.21	-------	-------
		$T_M=\alpha+\beta\theta+\gamma\varphi$	8	0.36	0.34	0.41	-0.03	0.32	0.18	0.45
	Both Areas	$T_M=\alpha+\beta\theta$	16	0.01	0.39	0.61	0.06	0.01	-------	-------
		$T_M=\alpha+\beta\theta+\gamma\varphi$ [a!]	16	0.01	0.51	0.59	0.07	<<0.01	-0.54	0.10
Light-cultivator (LC)	Long Slope Area	$T_M=\alpha+\beta\theta$	7	0.02	0.68	23.54	0.41	0.02	-------	-------
		$T_M=\alpha+\beta\theta+\gamma\varphi$ [a]	7	0.10	0.68	23.59	0.42	0.05	0.19	0.72
Air-seeder (AS)	Long Slope Area	$T_M=\alpha+\beta\theta$	12	0.01	0.46	4.35	0.14	0.01	-------	-------
		$T_M=\alpha+\beta\theta+\gamma\varphi$ [a]	12	<<0.01	0.77	4.52	0.18	<<0.01	1.95	0.01
Light-cultivator followed by Air-seeder (LC/AS)	Long Slope Area	$T_M=\alpha+\beta\theta$	15	0.01	0.38	38.16	1.01	0.01	-------	-------
		$T_M=\alpha+\beta\theta+\gamma\varphi$	15	0.03	0.44	36.42	0.97	0.02	7.03	0.30
	Bowl Area	$T_M=\alpha+\beta\theta$	9	0.64	0.03	29.05	-0.68	0.64	-------	-------
		$T_M=\alpha+\beta\theta+\gamma\varphi$	9	0.67	0.12	29.51	-0.81	0.60	-6.79	0.46
	Both Areas	$T_M=\alpha+\beta\theta$	24	0.01	0.30	34.70	0.96	0.01	-------	-------
		$T_M=\alpha+\beta\theta+\gamma\varphi$ [a!]	24	0.01	0.35	33.53	0.93	0.01	6.53	0.20

[!] All significant at 1 % level.
[a] The model used for the respective implement.
[b] Coefficients being used to generate the translocation model for a full sequence

For the regression of the translocation percentiles (Table 2.4), the general pattern is that the values of α_p, β_p and γ_p all increase as the percentile increases. In addition, the amount of per percentile increase of the α_p values increases with the respective increase of percentiles. Taking the Both Areas data as an example (Figure 2. 7), $(\alpha_{95} - \alpha_{90}) / (95 - 90) > (\alpha_{90} - \alpha_{75}) / (90 - 75) > (\alpha_{75} - \alpha_{50}) / (75 - 50) > \alpha_{50} / 50$, indicating that most soil was translocated within a short distance and in the tail region, the soil was distributed in a much wider range, e.g. 75 % within about 0.51 m but 20 % for the next about 0.58 m (from about 0.51 m to 1.09 m). This pattern is also illustrated on the summation curve (Figure 2. 5). The respective increases of β_p and γ_p values with the increase of percentiles indicate the stronger effect of slope gradient and slope curvature in the tail region. For M3, β_{50} was extremely low (0.002 m $\%^{-1}$), indicating that slope gradient has almost no effect within the corresponding distance (about 0.29 m). β_{95} was much greater (0.019 m $\%^{-1}$) and M3 was significant at the 10 % level, indicating that within the range of the two percentiles (from about 0.24 m to 1.09 m), the amount of soil being translocated is strongly affected by slope gradient. Similarly, for M4, γ_p value increases considerably with the increase of the percentiles indicating the more profound effect of slope curvature in the tail region. For M5, β_p and γ_p values were very close to those of M3 and M4 of the respective percentiles, respectively, but the R^2 values were much greater than either those of M3 or M4 of the respective percentiles, indicating the possible interaction between slope gradient and slope curvature and that including both slope gradient and slope curvature might explain the translocation better.

Table 2.4 Summary of regression analysis of translocation percentiles (λ_p) over slope gradient and/or slope curvature.

				$\lambda_p = \alpha_p + \beta_p \theta$ (M3)				$\lambda_p = \alpha_p + \gamma_p \varphi$ (M4)				$\lambda_p = \alpha_p + \beta_p \theta + \gamma_p \varphi$ (M5)				
		T_{Mp}	n	α_p †	β_p ‡	R^2	P_M	α_p †	γ_p ‡	R^2	P_M	α_p †	β_p	γ_p	R^2	P_M
Deep-tiller (DT)	Long Slope Area	λ_{50}	10	0.28	0.001	0.03		0.27	0.041	0.37	*	0.27	0.001	0.041 *	0.40	
		λ_{75}	10	0.54	0.006	0.12		0.53	0.098	0.40	*	0.53	0.006	0.096 *	0.50	*
		λ_{90}	10	0.94	0.012	0.13		0.90	0.201	0.42	**	0.90	0.011	0.197 **	0.52	*
		λ_{95}	10	1.17	0.020	0.21		1.14	0.211	0.29		1.14	0.019	0.204	0.47	
	Bowl Area	λ_{50}	8	0.30	0.011	0.36		0.30	-0.005	0.00		0.30	0.011	0.006	0.36	
		λ_{75}	8	0.58	0.015	0.16		0.58	0.034	0.04		0.59	0.017	0.051	0.25	
		λ_{90}	8	0.90	0.016	0.09		0.91	0.063	0.06		0.92	0.020	0.083	0.20	
		λ_{95}	8	1.10	0.012	0.03		1.12	0.084	0.07		1.13	0.017	0.101	0.12	
	Both Area	λ_{50}	18	0.29	0.002	0.06		0.29	0.024	0.11		0.29	0.002	0.024	0.17	
		λ_{75}	18	0.56	0.007	0.11		0.56	0.073	0.21	*	0.56	0.007	0.073 **	0.32	*
		λ_{90}	18	0.92	0.013	0.12		0.92	0.156	0.29	**	0.92	0.013	0.156 **	0.41	**
		λ_{95}	18	1.14	0.019	0.16	*	1.14	0.172	0.22	**	1.14	0.019 *	0.172 **	0.38	**
Spring-tooth-harrow (SH)	Long Slope Area	λ_{50}	7	0.19	0.000	0.00		0.16	-0.125	0.63	**	0.16	0.002	-0.140 **	0.71	*
		λ_{75}	7	0.32	0.004	0.13		0.29	-0.142	0.34		0.28	0.007	-0.191 *	0.68	
		λ_{90}	7	0.48	0.007	0.17		0.44	-0.218	0.34		0.42	0.012 *	-0.301 **	0.75	*
		λ_{95}	7	0.57	0.011	0.27		0.52	-0.243	0.27		0.50	0.017 **	-0.362 **	0.80	**
	Bowl Area	λ_{50}	8	0.20	-0.003	0.08		0.20	0.011	0.03		0.20	-0.002	0.007	0.09	
		λ_{75}	8	0.35	-0.005	0.10		0.35	0.021	0.03		0.35	-0.005	0.011	0.10	
		λ_{90}	8	0.53	-0.011	0.13		0.53	0.016	0.01		0.53	-0.011	-0.005	0.13	
		λ_{95}	8	0.64	-0.017	0.22		0.63	0.029	0.01		0.64	-0.018	-0.004	0.22	
	Both Area	λ_{50}	15	0.20	0.000	0.00		0.19	-0.011	0.15		0.19	0.000	-0.044	0.15	
		λ_{75}	15	0.34	0.003	0.06		0.34	-0.040	0.05		0.34	0.004	-0.048	0.13	
		λ_{90}	15	0.51	0.005	0.08		0.51	-0.068	0.06		0.50	0.006	-0.081	0.16	
		λ_{95}	15	0.60	0.008	0.12		0.60	-0.068	0.03		0.60	0.009	-0.088	0.18	
Light-cultivator (AS)	Long Slope Area	λ_{50}	7	0.30	0.003	0.47	*	0.29	0.006	0.01		0.31	0.003	-0.005	0.47	
		λ_{75}	7	0.59	0.005	0.31		0.58	-0.008	0.00		0.60	0.005	-0.028	0.35	
		λ_{90}	7	0.94	0.006	0.22		0.93	-0.032	0.03		0.96	0.006	-0.056	0.31	
		λ_{95}	7	1.16	0.006	0.18		1.16	-0.053	0.08		1.18	0.007	-0.079	0.34	
Air-seeder (AS)	Long Slope Area	λ_{50}	11	0.23	0.001	0.09		0.24	0.016	0.05		0.24	0.002	0.023	0.18	
		λ_{75}	11	0.44	0.004	0.15		0.44	0.026	0.03		0.44	0.004	0.045	0.24	
		λ_{90}	11	0.69	0.006	0.19		0.70	0.043	0.04		0.69	0.007	0.072	0.30	
		λ_{95}	11	0.86	0.008	0.29	*	0.87	0.047	0.04		0.86	0.010 *	0.087	0.42	
Light cultivator followed by air-seeder (LC/AS)	Long Slope Area	λ_{50}	15	0.37	0.006	0.60	***	0.35	0.032	0.06		0.36	0.006 ***	0.020	0.62	***
		λ_{75}	15	0.68	0.010	0.62	***	0.66	0.045	0.04		0.68	0.010 ***	0.025	0.63	***
		λ_{90}	15	1.05	0.013	0.64	***	1.03	0.051	0.03		1.05	0.013 ***	0.024	0.64	***
		λ_{95}	15	1.29	0.014	0.62	***	1.27	0.050	0.02		1.29	0.014 ***	0.020	0.63	***
	Bowl Area	λ_{50}	9	0.44	0.032	0.24		0.43	0.209	0.27		0.43	0.037 *	0.233 *	0.57	*
		λ_{75}	9	0.74	0.041	0.68	***	0.73	0.107	0.13		0.73	0.043 ***	0.136 **	0.89	***
		λ_{90}	9	1.07	0.017	0.11		1.07	0.021	0.00		1.07	0.018	0.033	0.12	
		λ_{95}	9	1.28	-0.004	0.00		1.29	-0.073	0.02		1.29	-0.005	-0.076	0.02	
	Both Area	λ_{50}	24	0.40	0.007	0.29	***	0.39	0.043	0.04		0.39	0.006 ***	0.033	0.31	**
		λ_{75}	24	0.70	0.011	0.54	***	0.69	0.044	0.03		0.70	0.010 ***	0.027	0.55	***
		λ_{90}	24	1.06	0.013	0.56	***	1.04	0.042	0.02		1.06	0.013 ***	0.022	0.56	***
		λ_{95}	24	1.29	0.014	0.43	***	1.27	0.032	0.01		1.29	0.014 ***	0.010	0.43	***

† All significant at 1 % level.

‡ Significance level the same as that of the model.

*, **, *** Model or coefficient significant at 10 %, 5 % and 1 % level, respectively.

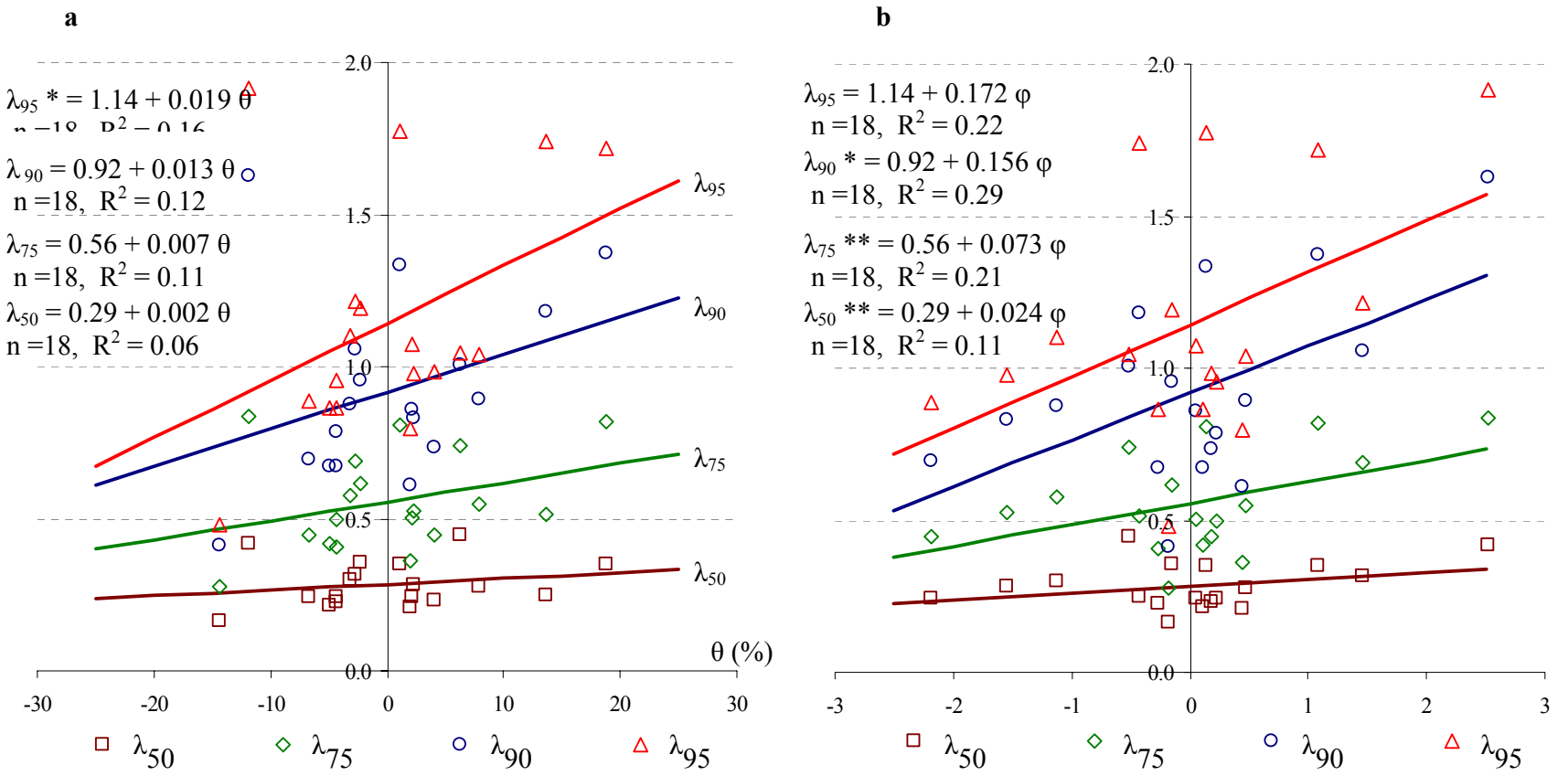

Figure 2.7 Regression analysis for deep-tiller (DT), Both Areas data of translocation percentiles (λ_{50}, λ_{75}, λ_{90} and λ_{95}) against: a) slope gradient; and b) slope curvature.

2.4.3 Spring-tooth-harrow

For Spring-tooth-harrow, in Long Slope Area, M1 was significant at the 5% level (Table 2.3). Compared to M1, M2 had a slightly higher significance (<<0.01 vs 0.03) and both β and γ in M2 were significant at 1 % level. Furthermore, the R^2 of M2 (0.95) was much greater than that of M1 (0.56). The comparison of M2 to M1 strongly supports that, in the case of SH, slope curvature has significant effect on tillage translocation and M2 was significantly superior to M1.

The results of the Bowl Area data for SH were similar to that of DT. Neither model was significant. For the Both Areas, M2 was significant at the 1 % level, γ in M2 is significant at 10 % level, and the R^2 of M2 (0.51) was greater than that of M1 (0.39), which confirms the conclusion drawn from the Long Slope Area: M2 was superior to M1 and including slope curvature as a secondary factor has improved the model with respect to explaining the observed tillage translocation. The patterns of α_p, β_p and γ_p in M3, M4 and M5 for SH, especially in the Long Slope Area, were similar to those for DT (Table 2.4).

2.4.4 Light-cultivator and Air-seeder

Plots for light-cultivator and air-seeder were only established in the Long Slope Area. For light-cultivator, M2 was significant but compared to M1, M2 had a lower significance (0.10 vs 0.02); the R^2 of M2 (0.68) was the same as the R^2 of M1 (0.68, which is the highest R^2 value for M1 found among all the examined implements) and γ in M2 was not significant (Table 2.3). All of these indicate that, for LC, slope gradient has largely explained the observed translocation.

For air-seeder, the significances of M2 and M1 were similar (<<0.01vs 0.01), but the R^2 of M2 (0.77) was much greater than that of M1 (0.46) and γ in M2 was significant at 1 % level. All of these indicate that M2 is superior to M1 in explaining the observed translocation data. Therefore, slope curvature was considered to have a significant effect on tillage translocation for the AS. The patterns of α_p, β_p and γ_p in M3, M4 and M5 for AS were similar to those for DT, which also indicate the possible strong effect of slope gradient and slope curvature, especially in the tail region (Table 2.4).

2.4.5 Light-cultivator Followed by Air-seeder

For LC/AS, in the Long Slope Area, the significance of M2 (0.03) and the R^2 of M2 (0.44) were similar to those of M1 (0.01 and 0.38, respectively) (Table 2.3). γ in M2 was not significant. For the Both Areas, compared to M1, M2 also had similar R^2 value (0.35 vs 0.30) and significance level (0.01 vs 0.01). The significance of γ in M2 (0.20) exceeded the 10 % level but as a secondary factor, it is considered to be close and therefore the effect of slope curvature to exist. The translocation percentiles analyses also show the strong effect of slope gradient (much higher R^2 values and significance levels of M3 when compared to those for other implements, of the respective percentile) (Table 2.4). The effect of slope curvature might be masked by the effect of slope gradient, given that slope curvature was considered as a secondary factor in the models.

2.4.6 Comparison of the Implements

Based on the statistic analyses, M2 established on the Both Areas data (for DT, SH and LC/AS) and on the Long Slope Area data (for LC and AS) was chosen as the tillage translocation model for the respective implements (Table 2.3 and Table 2.5).

Table 2.5 Summary of results from this study and those of other researchers.

Data source	Implement	ρ kg m^{-3}	S_T m s^{-1}	D_T m	α kg m^{-1}	β kg m^{-1}%$^{-1}$	γ kg %$^{-1}$	P_M	R^2	n
This study	Deep tiller	1230	1.90	0.11	16.02	0.62	0.90	*	0.32	18
Manitoba, Canada	Spring tooth harrow	1250	2.35	0.01	0.59	0.07	-0.54	***	0.51	16
	Light cultivator	1250	2.23	0.08	23.59	0.42	0.19	*	0.68	7
	Air seeder	1270	2.23	0.03	4.52	0.18	1.95	***	0.77	12
	Light cultivator and air seeder	1260			33.53	0.93	6.53	***	0.35	24
	One full sequence				50.73	1.69	6.35			
	Extra [a]				5.42	0.33	4.39			
	ASX [a]				9.94	0.51	6.34			
Van Muysen and Govers, 2002 Huldenberg, Belgium	Rotary harrow and seeder	1130	2.20	0.07	29.94	1.23		**	0.51	10
Van Muysen et al., 2000	Chisel plough [b]	1560	1.57	0.15	53.82	1.69 [c]		***	0.51	56
Huldenberg, Belgium	Chisel plough [d]	1250	2.02	0.20	102.50	3.38 [c]		***	0.67	24
Lobb et al., 1999 [e]	Chisel plough	1580	2.66	0.17	54.8	1.03	3.34	**	0.27	19
Ontario, Canada	Field cultivator	1210	1.92	0.15	56.7	0.07	-3.63	*	0.11	23
Lobb et al., 1998 [e] Ontario, Canada	One conventional tillage sequence [f]	1520	0.8 - 1.1	0.10 - 0.19	81.6	5.41	38.89	***	0.66	16
Poesen et al., 1997	Duckfoot chisel	1580	0.65	0.16	n.a.	2.82		n.a.	0.78	5
Murcia, Spain	Duckfoot chisel [j]	1580	0.65	0.14	n.a.	1.39		n.a.	0.65	5
Govers et al., 1994 [e] Huldenberg, Belgium	Chisel plough	1350	1.25	0.15	73	1.11		*	0.39	12

[a] Refer to the text for the explanation of the term.
[b] Stubble soil surface.
[c] Assuming upslope translocation to be constant.
[d] Pre-tilled soil surface.
[e] After Lobb et al. 1999.
[f] One pass of mould plough, two passes of tandem disc, one pass of field cultivator.
[j] Lateral translocation.

n.a. Data not available.
*, **, *** Model or coefficient significant at 10 %, 5 % and 1 % level, respectively.

Of the four implements, LC has the highest α value while DT has the highest β and γ values. The α value for LC (23.59 kg m^{-1}) was about one and a half of that for DT (16.02 kg m^{-1}), demonstrating that LC moves considerably more soil than DT, i.e. dispersivity of LC is higher. This is probably due to the fact that tillage speed of LC is higher than DT and the overlaps between cutting tools for LC (Table 2.1). The β and γ values for LC (0.42 kg $\%^{-1}$ m^{-1} and 0.19 kg $\%^{-1}$ m m^{-1}, respectively) were considerably lower than those of DT (0.62 kg $\%^{-1}$ m^{-1} and 0.90 kg $\%^{-1}$ m m^{-1}, respectively). Taking both β and γ into account, it is reasonable to conclude that, with respect to erosivity, LC was considerably lower than DT. For AS, the α value (4.52 kg m^{-1}) was only about one third of that for DT and about one fifth of that for LC, and the β value (0.18 kg $\%^{-1}$ m^{-1}) was about one third of that for DT and one half of that for LC, indicating that both the dispersivity and erosivity of AS was much lower than those of LC and DT. For SH, the α value (0.59 kg m^{-1}) was about one order of magnitude lower than that for AS and both the β and γ values (0.07 kg $\%^{-1}$ m^{-1} and –0.54 kg $\%^{-1}$ m m^{-1}, respectively) were much lower than those for AS, indicating that the dispersivity and erosivity of SH were considerably lower than AS. Compared to those for DT and LC, both the dispersivity and erosivity of AS and SH were considerably lower, which was not a surprise. What is important is that the effects of AS and SH were not negligible. Based on a simple calculation on the β value ($4\ \beta_{AS} > 9\ \beta_{SH} > \beta_{DT}$), tillage erosion after four passes of AS or nine passes of SH will exceed one pass of DT.

For the combination of light-cultivator and air-seeder (LC/AS), both α and β values exceed the summation of those for the two single passes (LC + AS) by about 30 %. Since for LC, the conditions for the single pass and the combination were the same,

the extra translocation was presumed to be caused by the effect of LC on AS. The magnitude of this effect (referred to as Extra) was estimated by subtracting the translocation of both LC and AS from the translocation of the combination: Extra = LC/AS – LC – AS, which gave us the model for the Extra (Table 2.5). Compared to AS, the Extra exceeded AS itself on both dispersivity and erosivity given that the values of α, β and γ of Extra were all greater than those of AS, respectively. To think of it another way, the translocation due to AS as affected by LC (referred to as ASX) can be estimated by subtracting the translocation of LC from the translocation of the combination: ASX = LC/AS – LC, which gave us the model for ASX (Table 2.5). Compared to the models of the other implements, dispersivity and erosivity of ASX were found close to those of DT. The effect of air-seeder, based on this point of view, was far from negligible and should be taken into account. The extra effects also suggested that pre-tilling must be taken into account when measuring translocation due to a tillage operation, which is conducted shortly after previous tillage operation(s) and taking the measurement separately without considering the previous tillage operation(s) might considerably under estimate the overall translocation. Our explanations for these extra effects were: 1) More power acts on moving the soil because less power is required for cutting and lifting the soil; 2) With less cohesion and adhesion, soil particles are more likely to move (e.g. rolling) under the effect of gravity; 3) the furrow pattern generated by LC may match up with the AS cutting tools to increase the translocation by AS.

2.4.7 The Effect of Slope Curvature

Except for the Bowl Area datasets, M1 was found significant for all the implements, indicating the strong effect of slope gradient on tillage translocation. In

contrast, similar simple regression of T_M against slope curvature (Appendix A.2) was found not to be significant for all the implements. However, with the inclusion of slope curvature, M2 explains the observed tillage translocation better than M1 in most cases (except for LC), indicating the necessity of taking slope curvature as a secondary factor into tillage translocation modeling. The insignificance of the effect of slope curvature probably is due to the fact that very few data points (n = 7) were available and, therefore, requires further investigation to adequate statistical evidence.

The negative γ value found for SH means tillage translocation on the concave positions exceeds that on the convex positions, which contradicts the theoretical relationship (Lobb and Kachanoski, 1999a). However this might be a special feature (e.g. due to the size of the implement and the location of the tractor related to the implement) of SH under the examined scale given that the R^2 of M2 was so high (0.95) when compared to that of M1 (0.56) (Table 2.3). A possible reason for that is the lead effect, defined by Lobb et al. (1999) as the translocation affected by the position of the tractor. These authors suggested that the magnitude of lead effect to be determined by "the distance between the center of the tillage implement and the center of the combined mass of the tractor, implement and the soil being carried by the tillage tools". This is due to the fact that the topography at the position of the tractor wheels determines tillage speed and tillage depth and, therefore, affects the intensity of tillage translocation. The size of the SH is large, which means that the center of the tillage implement was further behind the wheels when compared to other implements. On the other hand, SH caries very little soil during the operation so that the combined mass approaches the tractor. Both of these enhance the lead effect.

The analysis of the translocation percentiles suggests that the effect of slope gradient and/or slope curvature is more profound in the tail region of the distribution curve but due to the inherent variability of tillage translocation, noise increases in the tail region as well, which might mask the effect of slope gradient and/or slope curvature. This masking effect is comparatively stronger for slope curvature because the effect of slope curvature is considerably less significant than slope gradient. Therefore, more data are required for testing the effect of slope curvature and obtaining an accurate γ value than those for testing the effect of slope gradient and obtaining an accurate β value.

Another approach to test the effect of slope curvature is to isolate the effect slope curvature from the effect of slope gradient, as we tried on the Bowl Area. However, the Bowl Area data show no physical evidence of the stronger effect of slope curvature when compared to the Long Slope Area data. Part of the problem with the Bowl area is the possible stronger lead effect in this area. In this study, the scale of tillage and the scale of the topographic features in the Bowl Area are such that the effects of slope gradient and curvature on soil movement are confounded by the fact that the implements are quite large relative to the size of the land surface feature. Consequently, what is observed as soil movement at one point can be greatly affected by what is occurring all across the frame of the implement and at some distance in front of the implement, as topography affects the operation of the tractor – the lead effect. Lobb et al. (1999) suggested using the topographic data of the points in front of the plots positions (closer to the tractor) for the regression analysis. Further study on the effect of slope curvature might need a different experiment design to isolate slope curvature from slope gradient.

2.4.8 Comparison of This Study to Those of Other Researchers

Some of the published tillage translocation data is summarized in Table 2.5. For the same type of implements, large differences exist between different studies. This is understandable since implements may have very different designs, and the operations in different part of the world can be very different. Furthermore, the materials and methods used to measure tillage translocation vary among researchers and, therefore, systematic differences between results may exist. However, these differences are expected to be less than the experimental errors. A weakness in all of the studies is the small dataset.

The large differences between different researchers make comparisons difficult. For the single implements, both α and β values of deep-tiller found in this study were considerably lower than those found by other researchers of chisel plough, indicating that the dispersivity and erosivity of the primary implement used in this study was considerably lower. Other than the different design of the implements, lower soil bulk density and shallower tillage depth observed in this study might be the major reasons for the less intensive dispersivity and erosivity. α and β values for the combination of light-cultivator and air-seeder were found similar to those of rotary harrow and seeder in Van Muysen and Govers' study (2002), which is a typical secondary tillage operation in central Belgium.

For the field site used in this study, one full tillage sequence (one year) would normally consist of one pass of deep-tiller, two passes of spring-tooth-harrow and one pass of light-cultivator followed by one pass of air-seeder (LC/AS, not LC+AS). Translocation models for the implements were summed to establish a model for one full sequence by using Equation (7) (Table 2.5). For one full sequence, α, β and γ values

found in this study were about one half, one third and one fifth, respectively, of those found by Lobb and Kachanoski (1999*b*) in Ontario, Canada, indicating that tillage translocation in a cereal-based production system, which represents the predominant cropping system of the Canadian Prairies region, was considerably less intensive than in a conventional tilled corn-based production system in Canadian Great Lakes region.

2.4.9 Experiment Errors

The unexplained variability in the regression data is a result of the inherent variation of tillage translocation and experiment errors. The major errors of this study might come from the sampling. The loss of tracer during sampling was one ineviTable 2.source of experiment errors. The further the tracer is translocated, the more difficult it is to find. The loss of tracer normally causes an under-estimation of tillage translocation. In this study, except for LC, the tracer recovery rate (RR) was quite high, an average of 98 %, 98 %, 97 % and 90 % for DT, SH, AS and LC/AS, respectively (Table 2.2). Errors due to the loss of tracer were considered to be very low. The lowest RR was found for LC (83 %). A possible reason for this is the limited sampling time. Between the LC and AS, we had only one week to recover the tracers of the LC plots and to put another set of plots in place for the AS, so field activities were rushed. While after the seeding, we had plenty of time to recover the tracer of LC/AS, hence higher RR values. During sampling, even though a frame was set up as a reference, it was difficult sampling lengths of exactly 10 cm. When the soil is dry and loose, soil and tracer from the adjacent sampling slice might fall into the slice being sampled. Also, when sampling to greater depths it was difficult to cut each slice normal to the soil surface. Sampling length, which was supposed to be 10 cm, could vary at depth by up to 1 cm. However, such errors are

compensatory, i.e. 1 cm longer on one slice results in 1 cm shorter in the adjacent slice, so that these errors will not affect the translocation estimates (T_P, T_L and T_M) but might cause under estimation of the translocation percentiles (λ_p).

Another source of experiment error is the topographic survey. In theory the accuracy of Total Station was adequate (less than 1 cm); however, in practice the accuracy may have been less than adequate. It has been found that slope gradient and slope curvature typically vary about ± 5 % and ± 30 %, respectively, when different survey points were used. Errors due to the surveyors and the surface roughness may contribute the most to these variations.

The tillage translocation calculation was based on the assumption that all plots were oriented perpendicular to tillage direction; however, it is very difficult to ensure that. Even with plots oriented to perpendicular to the intended path of tillage, the operation of the tillage implement does not follow exactly the intended path, a straight line. The plots deviated up to ± 5° from perpendicular to the actual tillage direction. Assuming forward translocation exceeds lateral translocation, tillage translocation would be under estimated due to this error.

The summation curve method used in this study provides a parameter, ε, to evaluate the experiment error and the inherent variation of tillage translocation (Figure 2. 5). The ε value is not a direct measure of the errors but it indicates the level of the errors associated with the summation curve for different plots and different implements. In this study, for all the plots, the value of ε ranges from 0.1 % to 37.4 % and overall averages at 9.3 % (Table 2.2). In general, the experiment errors were considered to be low. A Tukey-Kramer test showed that ε for AS is significantly greater than those for DT, LC and

LC/AS with that for SH in between (Table 2.2). No significant difference was found between the Long Slope Area and the Bowl Area (data not shown). A test was conducted by averaging the first two samples' data (this will not change the estimated T_P and T_M values) and recalculating ε (Appendix A.1). The overall average of the ε values dropped down to 1.8 %. This indicates that the major contributor to ε is the variability of the data in the first two samples (within the original tracer-labeled region). This high variability is mainly due to the much deeper plot depth than the tillage depth and does not affect the accuracy of the estimated T_P and T_M values.

2.5 Conclusions

Tillage translocation was found to be highly variable for all the tillage implements. Regression analysis showed that there were significant relationships between tillage translocation and slope gradient. This confirmed slope gradient to be the predominant factor driving tillage translocation. Except for the light-cultivator, slope curvature was also found to have an effect on tillage translocation and, therefore, we recommend including slope curvature in the tillage translocation model as a secondary factor. For light-cultivator, though it is a secondary tillage implement, its dispersivity was greater than that of the deep-tiller, the primary tillage implement, but its erosivity was lower than that of the deep-tiller. The erosivity of air-seeder and spring-tooth-harrow were much lower than that of light-cultivator and deep-tiller, but their effects were not

negligible, especially when they were conducted shortly after another tillage operation. The erosivity of air-seeder after one pass of light-cultivator was found comparable to the deep-tiller. For a full sequence, the erosivity of the tillage system in our study site was considerably lower than a traditional defined conventional tillage system (i.e. with a moldboard plough) indicating the considerably less intensive tillage system associated with the cereal-based production system in the Canadian Prairies. The different relationships between tillage translocation and slope gradient/slope curvature in the Long Slope Area and the Bowl Area suggested that landform type might also affect tillage translocation and different experiment design may be needed for different landform types.

2.6 Acknowledgements

Financial support for this study was provided by Natural Sciences and Engineering Research Council of Canada (NSERC) as part of the "Tillage erosion and its impacts on soil characteristics and pesticide fate processes at the large-scale" project. The authors would like to thank Dr. A. Farenhorst for her support and B. Turner, C. Sawka, A. Jeninga and K. Archibald for their help with the field experiments. We would also like to thank K. Tiessen for reviewing the manuscript.

2.7 References

De Alba, S., 2001. Modeling the effects of complex topography and patterns of tillage on soil translocation by tillage with mouldboard plough. J. Soil Water Conservation 56, 335-345.

Govers, G., Vandaele, K., Desmet, P.J.J., Poesen, J., Bunte, K., 1994. The role of tillage in soil redistribution on hillslopes. Eur. J. Soil Science 45, 469-478.

Govers, G., Lobb, D.A., Quine, T.A., 1999. Tillage erosion and translocation emergence of a new paradigm in soil erosion research. Soil Tillage Research 51, 167-174.

Lindstrom, M.J., Nelson, W.W., Schumacher, T.E., Lemme, G.D., 1990. Soil movement by tillage as affected by slope. Soil Tillage Research 17, 255-264.

Lindstrom, M.J., Nelson, W.W., Schumacher, T.E., 1992. Quantifying tillage erosion rates due to moldboard plowing. Soil Tillage Research 24, 243-255.

Lobb, D.A., Kachanoski, R.G., Miller, M.H., 1995. Tillage translocation and tillage erosion on shoulder slope landscape positions measured using ^{137}Cs as a tracer. Can. J. Soil Science 75, 211-218.

Lobb, D.A., Kachanoski, R.G., 1999*a*. Modelling tillage erosion in topographically complex landscapes of southwestern Ontario, Canada. Soil Tillage Research 51, 261-278.

Lobb, D.A., Kachanoski, R.G., 1999*b*. Modelling tillage translocation using step, linear-plateau and exponential functions. Soil Tillage Research 51, 317-330.

Lobb, D.A., Kachanoski, R.G., Miller, M.H., 1999. Tillage translocation and tillage erosion in the complex upland landscapes of southwestern Ontario. Soil Tillage Research 51, 189-209.

Lobb, D.A., Quine, T.A., Govers, G., Heckrath, G.J., 2001. Comparison of methods used to calculate tillage translocation using plot-tracers. J. Soil Water Conservation 56, 321-328.

Marques da Silva, J.R., Soares, J.M.C.N., Karlen, D.L., 2004. Implement and soil condition effects on tillage-induced erosion. Soil Tillage Research 78, 207-216.

MacLeod, C.J., Lobb, D.A., Chen, Y., 2000. The relationships between tillage translocation, tillage depth and draught force for sweeps. Proceeding of 43rd Annual Meeting, Manitoba Soil Science Society, Winnipeg, Canada, January 2000.

Michalyna, W., Podolsky, G., St. Jacques, E., 1988. Soils of the rural municipalities of Grey, Dufferin, Roland, Thompson and part of Stanley. Canada-Manitoba Soil Survey, Soils Report No. D60.

Poesen, J., Van Wesemael, B., Govers, G., Martinez-Fernandez, J., Desmet, P.J.J., Vandaele, K., Quine, T.A., Degraer, G., 1997. Patterns of rock fragment cover generated by tillage erosion. Geomorphology 18, 183-197.

Quine, T.A., Zhang, Y., 2004. Re-defining tillage erosion: quantifying intensity-direction relationships for complex terrain. 1. Derivation of a directional soil transport coefficient. Soil Use and Management 20, 114-123.

Rahman, S., Lobb, D.A., Chen, Y., 2002. Size and density of point-tracers for use in soil translocation studies. Proceeding of 45th Annual Meeting, Manitoba Soil Science Society, Winnipeg, Canada, January 2002.

SAS institute, Inc., 2002. SAS® 9 help and documents. SAS Institute, Inc., Cary, NC 27513, USA.

Soil Classification Working Group, 1998. The Canadian System of Soil Classification. 3rd ed. Agriculture and Agri-Food Canada Publication 1646.

Statistics Canada, 2002. Farm data for the 2001 Census of Agriculture (Initial release). Available at http://www.statcan.ca/english/agcensus2001/index.htm.

Van Muysen, W., Govers, G., Bergkamp, G., Roxo, M., Poesen, J., 1999. Measurement and modelling of the effects of initial soil conditions and slope gradient on soil translocation by tillage. Soil Tillage Research 51, 303-316.

Van Muysen, W., Govers, G., Van Oost, K., Van Rompaey, A., 2000. The effect of tillage depth, tillage speed, and soil condition on chisel tillage erosivity. J. Soil Water Conservation 55, 355-365.

Van Muysen, W., Govers, G., 2002. Soil displacement and tillage erosion during secondary tillage operations: the case of rotary harrow and seeding equipment. Soil Tillage Research 65, 185-191.

Van Muysen, W., Govers, G., Van Oost, K., 2002. Identification of important factors in the process of tillage erosion: the case of mouldboard tillage. Soil Tillage Research 65, 77-93.

Zhang, J.H., Lobb, D.A., Li, Y., Liu, G.C., 2004. Assessment of tillage translocation and tillage erosion by hoeing on the steep land in hilly areas of Sichuan, China. Soil Tillage Research 75, 99-107.

2.8 Nomenclature

A	the intercept of the linear regression equation (m $pass^{-1}$)
AS	air-seeder
ASX	tillage translocation due to air-seeder as affected by the previous tillage operation, one pass of light-cultivator
B	the slope of the linear multiple regression model associated with slope gradient (m $\%^{-1}$ $pass^{-1}$)
C	the slope of the linear multiple regression model associated with slope curvature (m $\%^{-1}$ m $pass^{-1}$)
c_s	the proportion of tracer quantity calculated from the summation curve at distance x (kg kg^{-1})
c_T	the proportion of untouched tracer on the bottom of the plots, which can be used to estimate tillage depth (kg kg^{-1})
D_P	plot depth (m)
D_T	tillage depth (m)
DT	deep-tiller
Extra	the extra effect of combining light-cultivator and air-seeder when compared to the sum of the single passes of these two implements
LC	light-cultivator
LC/AS	light-cultivator followed by air-seeder

LC+AS	the sum of one single pass of light-cultivator and one single pass of air-seeder
L_P	plot length (m)
L_s	a distance exceeding the maximum translocation distance (m)
P_M	model significance level
RR	tracer recovery rate (%)
S_T	tillage speed (m s^{-1})
SH	spring-tooth-harrow
T_L	the average translocation distance over tillage depth over a unit width of tillage (m)
T_M	translocation in mass over a unit width of tillage (kg m^{-1})
T_P	the averaged translocation distance over the depth of labeled soil over a unit width of tillage (m)
T_{Mt}	the total translocation in mass after a full sequence (kg m^{-1})
W_I	implement width (m)
i	the denotation for the i'th tillage operation
n	the number of tillage operations in one full sequence
x	the distance at which the quantity of tracer is measured (m)
α	the intercept of the linear regression equation, representing tillage translocation unaffected by slope gradient or slope curvature and indicating the dispersivity of the given tillage operation (kg m^{-1} $pass^{-1}$)
α_p	the intercept of the regression model for the p^{th} percentile (m)

β the coefficient for slope gradient, representing the extra tillage translocation due to slope gradient and indicating the erosivity of the given tillage operation (kg m^{-1} $\%^{-1}$ $pass^{-1}$)

β_p the coefficient of slope gradient for the p^{th} percentile (m $\%^{-1}$)

γ the coefficient for slope curvature, representing the extra tillage translocation due to slope curvature and indicating the erosivity of the given tillage operation (kg m^{-1} ($\%^{-1}$ m) $pass^{-1}$)

γ_p the coefficient of slope curvature for the p^{th} percentile (m $\%^{-1}$ m)

θ slope gradient, positive when downslope and negative when upslope (%)

φ slope curvature, positive for convex and negative for concave (% m^{-1})

λ_p the distance to which p % of soil mass is translocated (m)

ε a measure of error, either from the inherent variability of translocation or experimental error, or from both (%)

ρ soil dry bulk density (kg m^{-3})

3. TILLAGE AND WATER EROSION IN CULTIVATED FIELDS OF THE NORTHERN NORTH AMERICAN GREAT PLAINS EVALUATED USING ^{137}CS MEASUREMENTS AND SOIL EROSION MODELS*

3.1 Abstract

Total soil erosion is the integrated result of all forms of soil erosion – wind, water and tillage. It has been recognized that in topographically complex landscapes, individual soil erosion processes and their interactions all contribute towards total soil erosion. In this study, two field sites located in the northern region of the North American Great Plains were examined. These two field sites are characterized by undulating slopes and hummocky knolls, respectively. Water and tillage erosion were estimated using the established water and tillage erosion models; total soil erosion was estimated using the ^{137}Cs technique; and the landscapes were segmented using the LandMapR program.

The results showed that using any of the water or tillage erosion models alone provides acceptable estimation of total soil erosion when either one of the two erosion

* Li, S., Lobb, D.A. (University of Manitoba), Lindstrom, M.J. (USDA-ARS, retired) and Annemieke Farenhorst (University of Manitoba). This manuscript was submitted to Catena in Jun, 2006.

processes is dominant. However, combining water and tillage erosion models generally provided better estimations of total soil erosion than the component models on their own. On undulating slopes, tillage and water erosion both contribute considerably to total soil erosion: tillage erosion contributes about 50 to 70 % on upper-slopes and water erosion dominates on mid-slopes. On hummocky knolls, tillage erosion dominates the pattern of total soil erosion: tillage erosion contributes about 65 to 80 % soil loss on upper-slopes and about 40 to 50 % soil loss on mid-slopes. At both sites, the highest water-induced soil loss occurred on mid-slopes, while the highest tillage-induced soil loss occurred on upper-slopes. We found that the major patterns and variations of water, tillage and total soil erosion within given landform elements is predictable., and therefore, the landscape segmentation procedure can be used as a tool to assess soil erosion in topographically complex landscapes.

3.2 Introduction

Soil erosion affects both soil properties and soil processes, and is widely recognized as a major cause of soil degradation in arable land. Historically, water and wind erosion were assumed to be the major forms of soil erosion. Since the "rediscovery" of tillage erosion in the 1990s, field evidence from different parts of the world has shown that tillage erosion is another major form of soil erosion (e.g. Lindstrom et al., 1990, 1992; Govers et al., 1994; Lobb et al., 1995). Due to the complexity of the individual

erosion processes, researchers usually deal with each soil erosion process independently and assume for a given region, one process dominates over the other processes (e.g. Lobb and Kachanoski, 1999; Schumacher et al., 1999). However, each soil erosion process has its characteristic pattern across the landscape and each will contribute to some degree to the total soil erosion evident within a field. The general patterns of water and tillage erosion along a hypothetical slope are illustrated in Figure 3.1a. The rate of water erosion at a given point is not only determined by the local relief at this point but also by its upslope catchment area. From the crest, water-induced soil loss gradually increases until it reaches the highest level at the lower backslope and then gradually decreases. Towards the lower end of the footslope and in the toeslope, water-induced soil accumulation occurs.

Conversely, the rate of localized tillage erosion (tillage erosion rate at a given point) is determined largely by the local relief (relief at a given point), in particular slope curvature. Tillage-induced soil loss occurs on convex portions and soil accumulation occurs in concave portions of the landscape. Tillage erosivity influences the amplitude, but not the pattern of tillage erosion, whereas water erosivity (rainfall and runoff) influences both the amplitude of water erosion and the pattern of water erosion in the toeslope (i.e. the rate of water-induced soil accumulation is higher but the spatial extent of soil accumulation is over less of the slope under high water erosivity when compared to those under low water erosivity).

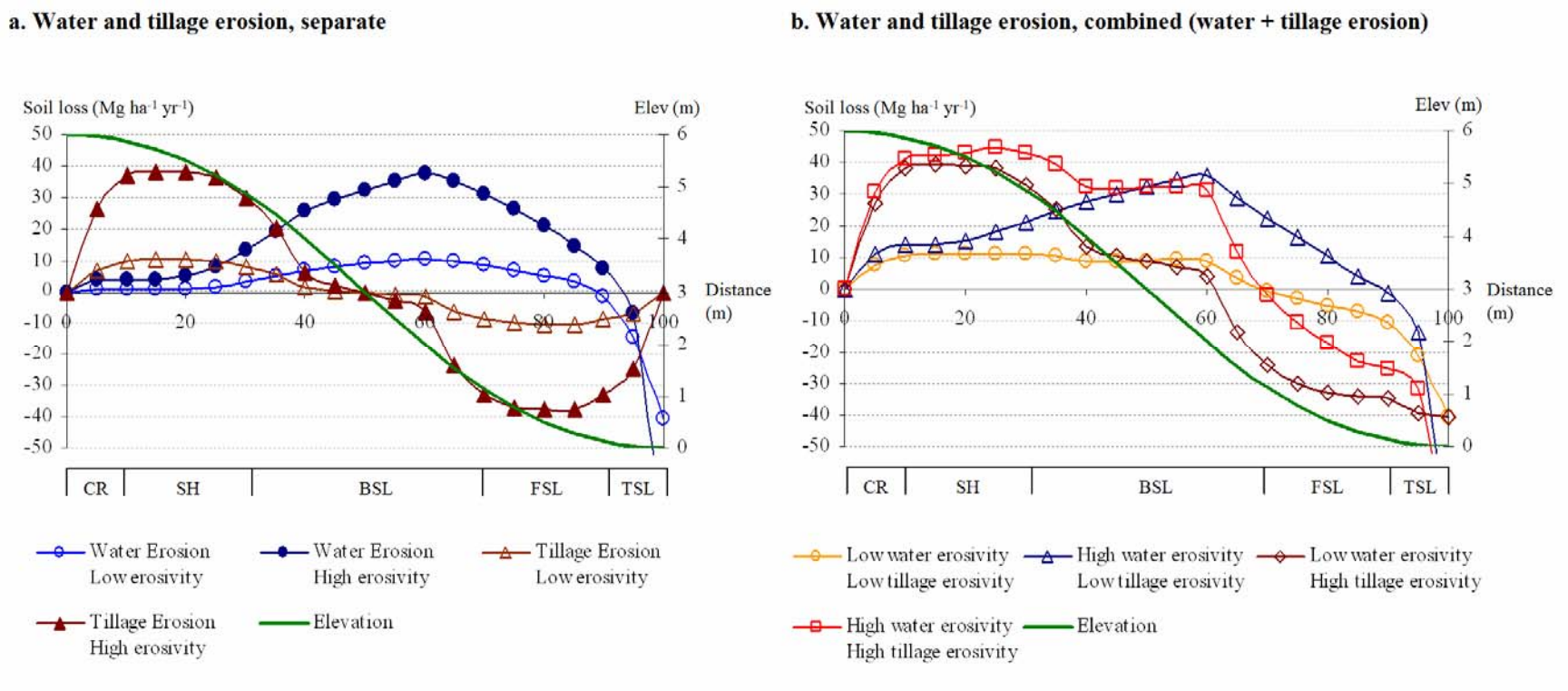

Figure 3.1 The patterns of: a. Water and tillage erosion, separate; and b. Water and tillage erosion, combined, on a hypothetical slope (CR: crest, SH: should slope, BSL: back slope, FSL: foot slope and TSL: toeslope)

The pattern of total soil erosion is complicated due to the linkages and interactions between the erosion processes. Linkages refer to the simple additive effects between different erosion processes. Interactions occur when one erosion process changes the erodibility of the landscape for another erosion process or when one process works as a delivery mechanism for another erosion process (Lobb, 1991; Lobb et al., 2003). Figure 3.1b illustrates the potential linkages between water and tillage erosion on a hypothetical slope: 1) in the crest and the shoulder sections, both water and tillage erosion cause soil loss and tillage erosion dominates the combined water + tillage erosion pattern; 2) in the backslope section, water erosion causes soil loss and dominates the combined water + tillage erosion pattern (here tillage erosion might cause soil loss or soil accumulation); 3) in the footslope section, water erosion causes soil loss while tillage erosion causes soil accumulation and the pattern of the combined water + tillage erosion is determined by the relative intensity of water vs. tillage erosion; and 4) in the toeslope section, tillage erosion causes soil accumulation, water erosion might cause soil loss or soil accumulation and neither one of the two erosion processes dominates the other erosion process. A possible interaction between water and tillage erosion occurs in the footslope section where tillage accumulated soil is more susceptible to water-induced soil loss and the overall soil loss might be greater than that estimated by the combined water + tillage erosion.

For a given set of conditions, especially in topographically complex landscapes, the observed soil redistribution pattern in agricultural land is an integrated result of all forms of soil erosion, including the contributions of individual erosion processes and the interactions between different erosion processes. Due to the geological youth of the

landscape and the relatively short cultivation history, soil-landscapes in the northern region of the North American Great Plains (northern NAGP) are generally more complex than those in Europe and Asia. More than 75 percent of the agricultural land in this region is classified as hilly (rolling, undulating and hummocky) landscapes. Both water and tillage erosion have been reported to contribute to the total soil erosion in the northern NAGP (Pennock, 2003; De Alba, 2004; Papiernik et al., 2005; Schumacher et al., 2005). However, no previous field study to date has been conducted to examine the interactions between tillage and water erosion in topographically complex landscapes. It is important to examine both erosion processes, their linkages and interactions because the redistribution of soil mass causes the variability of soil properties across the landscape and, therefore, influences other landscape-driven soil processes such as water contamination, pesticide fate and greenhouse gas emission. For example, Gaultier et al. (2006) found that the spatial variability of 2,4-D sorption was similar to that of soil organic carbon.

Established water erosion models, such as the Revised Universal Soil Loss Equation (RUSLE) and the Water Erosion Prediction Project (WEPP), are widely used to estimate water erosion (Flanagan et al., 1995; Renard et al., 2001). Tillage erosion models have been developed and used to estimate tillage erosion (e.g. Lobb and Kachanoski, 1999). However, one major limitation to these models is that they require field scale topographic data, which is not always available nation-wide. Therefore, these models are not always practicable for soil conservation. For this reason, there is renewed interest in using landscape segmentation as a simple tool to estimate soil erosion and to help decision makers with soil conservation practices. In Canada, landscape segmentation

was used in the National Soil Database (NSDB) to better represent the spatial specificity of landscape processes. The NSDB was further used to develop several Agri-environmental Indicators (AEIs), including indicators of wind, water and tillage erosion, for various agricultural regions in Canada within the Agriculture and Agri-Food Canada National Agri-Health Analysis and Reporting Program (NAHARP) (Lefebvre et al., 2005). In Saskatchewan, Canada, Pennock et al. (2001) used a landscape segmentation procedure and demonstrated that both soil organic carbon (SOC) storage and N_2O emissions are controlled by the predominant water or soil redistribution processes occurring in different landform elements. It is important to examine the relative contributions of, and the linkages and interactions between different erosion processes in different landform elements to evaluate the pattern of total soil erosion.

The objectives of this study are: 1) to estimate water, tillage and total soil erosion on topographically complex landscapes; 2) to compare the relative contributions of water and tillage erosion to the total soil erosion on different landscapes; 3) to investigate the patterns of water and tillage erosion, their linkages and interactions in different landform elements; and 4) to demonstrate and evaluate the use of landscape segmentation in estimating water, tillage and total soil erosion in topographically complex landscapes.

3.3 Materials and Methods

3.3.1 Study Sites and Laboratory Analysis

Two field sites were examined in this study. The first site is a 2.7 ha portion of a 16 ha field near the town of Cyrus, in west central Minnesota, USA (Figure 3.2a). The sampling area features a trough in the western part, a knoll in the middle and a slightly concave slope towards the eastern side of the field. The second site is a 0.8 ha portion of a 42 ha field near the town of Deerwood, in south-western Manitoba, Canada (Figure 3.2b). The sampling area is a complex of small knolls. The central part of this area is a depression, which gives it a bowl shape. The two sites are typical of the landscapes in the northern NAGP: undulating (the Cyrus site) and hummocky (the Deerwood site) landscapes. A general overview of the field sites and the associated tillage and cropping systems employed at each site are summarized in Table 3.1.

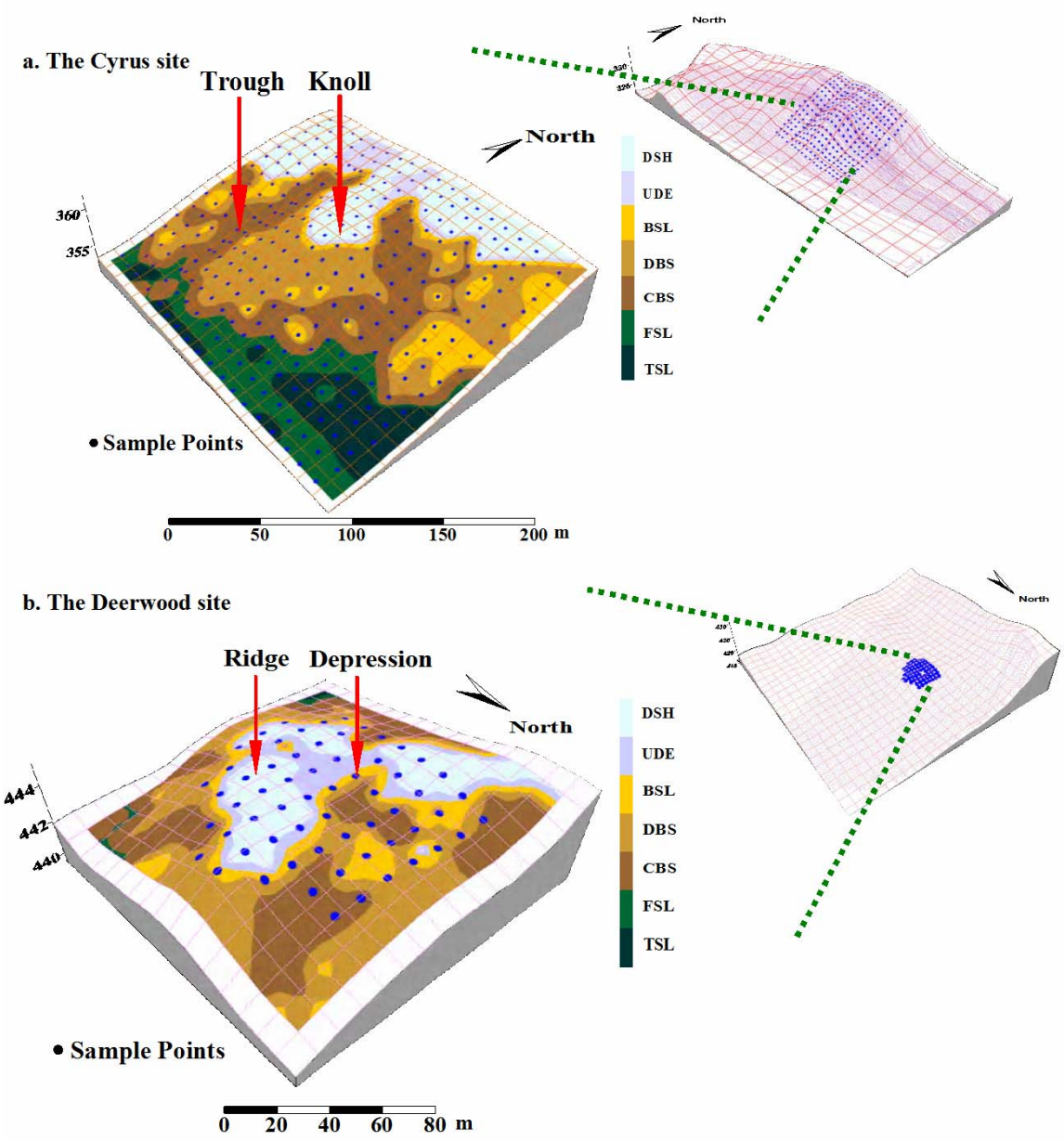

Figure 3.2 Landscape segmentation of a. The Cyrus site and b. The Deerwood site.

Table 3.1 Characteristics of the field sites.

Item	Cyrus site	Deerwood site
Location	Minnesota, USA	Manitoba, Canada
Coordinates	45.67° N, - 95.75° E	49.35° N, - 98.35° E
Soil texture of the Ap horizon *	Loam	Sandy loam
Annual precipication	595 mm	567 mm
Crops	Corn, winter wheat, soybean	Winter wheat, oat, canola
Major tillage implements	Mouldboard plough, tandem disc	Heavy cultivator, light cultivator

* of the sampling area not of the whole field.

The background field information, and the collection and processing of soil samples (except for ^{137}Cs radioactivity) at the Cyrus site was described in Papiernik et al. (2005) and De Alba (2004). To summarize, depth-incremental soil samples were collected at 288 points on a 10 × 10 m grid. Each sampling location was surveyed using a Trimble AgGPS-132 system. Soil samples were air-dried, sieved through a 2-mm screen, and both soil and stone fractions were weighed. ^{137}Cs radioactivity was detected at 662 keV using Broad Energy Germanium Gamma spectrometers (Canberra BE3830, Landscape Dynamics Laboratory, University of Manitoba, Canada) with counting time ranging from 4 to 12 hrs, providing a detection error < 10 %. A reference site for ^{137}Cs analysis was established on a native grassland adjacent to the Cyrus field site. At the reference site, seven soil cores were taken in 2-cm depth increments to one meter. The profile ^{137}Cs radioactivity was examined and the inventory was used as the reference ^{137}Cs radioactivity for the Cyrus site (2093 Bq m^{-2}).

For the Deerwood site, detailed field information can be found in Li et al. (Section 2.3.1). Depth-incremental soil samples were collected at 63 points on a 10 × 10 m grid. Each sampling location was surveyed using a Total Station (Sokkia set 4110) and georeferenced using a Trimble TSC1 GPS system. The procedures for soil sample analyses were the same as those used at the Cyrus site. The reference ^{137}Cs level (2060 Bq m^{-2}) was determined based on the average ^{137}Cs radioactivity of the samples taken from three sites located within 10 km of the study area (two pasture sites and one old farm yard site). Soil samples in both the Cyrus and the Deerwood sites were collected in the spring of 2002 and January 1, 2002 was used as the reference date of ^{137}Cs radioactivity.

The topographic data of the two sites were used to generate Digital Elevation Models (DEM, 10 m and 8 m spacing for the Cyrus and the Deerwood site, respectively) by using GS+ 5.1.1® point kriging interpolation. The DEMs were used as the topographic input data for the water and tillage erosion modeling and the landscape segmentation.

3.3.2 Water Erosion ----WEPP and WaTEM

Due to the uncertainty associated with water erosion modeling, two established models, WEPP (2002 Hillslope version) and the water erosion component of the Water and Tillage Erosion Model (WaTEM, Van Oost et al., 2000), were used to estimate water erosion.

WEPP is a two-dimensional model and calculates point-water-erosion rates along a two-dimensional slope (Flanagan et al., 1995). To simulate water erosion in three-dimensions, WEPP was run on both North-South and East-West oriented transects in the

DEMs. As required by WEPP, transects were divided into sub-slopes at the summit and/or nadir points to ensure there was no negative slope gradient point. In total, 67 and 55 slopes were generated for the Cyrus and the Deerwood sites, respectively. For a given point, this procedure tracked water flows from two perpendicular directions, and therefore, to some degree, it took into account the effect of convergent and divergent water flows. In addition, this procedure accounted for the directionality of water erosion caused by cropping and tillage (i.e. water flows along the furrows created by tillage operations and crop rows rather than the direction of the steepest slope).

The climate data necessary for WEPP were generated using the CLIGEN v. 5.2 program incorporated in WEPP. For the Cyrus site, the Morris MN climate station data was used and the simulated 48 yr mean annual precipitation was 594 mm. For the Deerwood site, linear interpolation of the data from the two closest climate stations in the USA (Edmore ND and Grafton ND, located about 100 – 125 km away from the site) was used and the simulated 48 yr mean annual precipitation was 422 mm. Management data were generated based on the cropping history and the current tillage practices employed at the two sites (Table 3.1, detailed data not shown). For the Cyrus site, the dominant soil SVEA (Loam) (Lindstrom et al., 2000) was used. For the Deerwood site, soil data were generated based on the measurements of the soil samples (soil texture is sandy loam). Single soil types were used on both sites for the simplification of the modeling.

The WEPP program was run for 48 iterations (representing 48 yrs) to match the duration of ^{137}Cs fallout (from 1954 to 2002). The output point-water-erosion rates (100 points per slope) were regrouped into the DEM transects and were averaged so that the water erosion rates on the grid nodes of the DEMs represented the average water erosion

rates of the respective sections (length = DEM spacing). Each individual grid node had two values, calculated from the North-South transect and the East-West transect, and the sum of these two values was the water erosion rate assigned to this grid node.

To compare the two sites and to isolate the effect of topography, WEPP was run for a second time on the Deerwood site using the Cyrus site's climate, management and soil data. This reanalysis was also performed, because: 1) heavier implements, similar to those used on the Cyrus site, had previously been used on the Deerwood site during the early-1950s to the late-1980s; and 2) the local annual precipitation on the Deerwood site (567 mm, Table 3.1) is considerably greater (about 30 - 65 mm) than that of the other climate stations in southwestern Manitoba, Canada (Environment Canada, 2006) and greater than the simulated annual precipitation (422 mm). This indicates that using the coarse scale climate data in the WEPP database might have considerably underestimated the local precipitation at the Deerwood site.

The water erosion component of WaTEM is a three-dimensional model based on RUSLE but incorporates routing algorithms to simulate both convergent and divergent water flows. At each site, The Govers (1991)-routing-algorithm was used, and the Transport Capacity Coefficient (k_{Tc}) was assumed to be 170 m. Additional parameter settings for the Cyrus site were based on Papiernik et al. (2005) and included: 1) a rainfall-runoff erosivity factor (R-factor) of 1532 MJ mm ha^{-1} h^{-1} yr^{-1}; 2) a soil erodibility factor (K-factor) of 0.037 Mg ha h ha^{-1} MJ^{-1} mm^{-1}; 3) a cover / management factor (C-factor) of 0.21; and 4) a support practice factor (P-factor) of 1.0. The parameter settings for the Deerwood site were: 1) a R-factor of 865 MJ mm ha^{-1} h^{-1} yr^{-1}; 2) a K-factor of

0.017 Mg ha h ha^{-1} MJ^{-1} mm^{-1}; 3) a C-factor of 0.27; and 4) a P-factor of 1.0 (Wall et al., 2002).

3.3.3 Tillage Erosion ---- TillEM

Tillage erosion was estimated for the two sites using the tillage translocation model described in detail by Lobb and Kachanoski (1999). In brief, tillage translocation is simulated using a multiple linear function:

$$T_M = \alpha + \beta\,\theta + \gamma\,\varphi \qquad (1)$$

where: T_M is the translocation in mass per unit width of tillage (kg m^{-1} $pass^{-1}$); α is the intercept of the linear regression equation, representing tillage translocation unaffected by slope gradient or slope curvature (kg m^{-1} $pass^{-1}$); β is the coefficient for slope gradient, representing the additional tillage translocation due to slope gradient (kg m^{-1} $\%^{-1}$ $pass^{-1}$); θ is slope gradient, positive when downslope and negative when upslope (%); γ is the coefficient for slope curvature, representing the additional tillage translocation due to slope curvature (kg m^{-1} ($\%^{-1}$ m) $pass^{-1}$); and φ is slope curvature, positive for convex and negative for concave (% m^{-1}).

Tillage erosion is calculated as:

$$E_{Ti} = -\frac{\partial M}{\partial t} = -\frac{\partial T_M}{\partial s} = -\left(\beta\frac{\partial \theta}{\partial s} + \gamma\frac{\partial \varphi}{\partial s}\right) \qquad (2)$$

where: E_{Ti} is the estimated tillage erosion, positive for soil loss and negative for soil accumulation (kg m^{-2} $pass^{-1}$); M is the mass of soil per unit area above some specified base elevation (kg m^{-2}); t is time (yr); and s is the length in any specified horizontal direction (m).

Based on Eq. 2, the TillEM, written in Visual Basic 6.0® code, was developed to calculate point-tillage-erosion rates using topographic data. Technically, the TillEM runs on lines both parallel and perpendicular to the direction of tillage, representing forward and lateral tillage translocation, respectively. For the forward tillage translocation, β and γ were determined by previous translocation experiments. At the Deerwood site, Li et al. (Section 2.4.6) reported that for a full sequence of tillage operations (one pass of deep-tiller, one pass of light-cultivator followed by air-seeder and two passes of spring-tooth-harrow) , β = 1.7 kg m^{-1} $\%^{-1}$ yr^{-1} and γ = 6.4 kg m^{-1} ($\%^{-1}$ m) yr^{-1}. Using the tillage translocation data of Lobb et al. (1999), a sequence of one pass of mouldboard plow, two passes of tandem disc and one pass of field cultivator was estimated to have a β = 6 kg m^{-1} $\%^{-1}$ yr^{-1} and a γ = 12 kg m^{-1} ($\%^{-1}$ m) yr^{-1} at the Cyrus site. For the lateral tillage translocation, the values of β and γ were assumed to be one-half of those for the forward tillage translocation (Lobb et al., 1999). The β and γ values of the Cyrus site were also used on the Deerwood site to isolate the effect of topography on tillage erosion in the comparison of the two sites.

3.3.4 Total Soil Erosion --- ^{137}Cs Measurements

The ^{137}Cs technique has previously been shown to be an effective tool to estimate point-total-soil-erosion rates and has been widely used to validate both water and tillage erosion models (e.g. de Jong et al., 1983; Quine et al., 1997; Walling et al., 1998; Lobb et al., 1999; Pennock, 2003). The Mass Balance Model 2 (MBM2) in the Cs-137 Erosion Calibration Models software (Walling et al., 2001) was used to convert point-^{137}Cs inventories into point-total-soil-erosion rates. The MBM2 takes into account the time-variant fallout ^{137}Cs input rate and the fate of the freshly deposited fallout before it is incorporated into the till-layer by tillage. The MBM2 is generally considered superior to the proportional model and the simplified mass balance model (Walling et al., 2001; Hassouni et al., 2006).

For both sites, the estimated northern hemisphere annual ^{137}Cs deposition flux data supplied with the software were used as the ^{137}Cs fallout data (starting from 1954). The "start year of cultivation" was set at 1954, even though the actual cultivation history to 2002 is approximately 100 and 75 yrs for the Cyrus and Deerwood sites, respectively. The "mass plough depth" was calculated from the measured average tillage depth and soil bulk density (ρ) and was 294 kg m^{-2} and 205 kg m^{-2} for the Cyrus and Deerwood site, respectively. The "relaxation mass depth" (H_{MBM2}) and the "particle size correction factor" (P_{MBM2}) were assumed to be 4.0 kg m^{-2} and 1.0, respectively (He et al., 1997; Walling et al., 2001).

The proportion of annual ^{137}Cs input susceptible to removal by erosion (γ_{MBM2}) was estimated using the WEPP-simulated average monthly runoff pattern and the associated tillage operations. At the Cyrus site, intensive rainfall runoff events typically

occur from April to September and the spring and fall tillage operations generally occur in May and October. The minimum γ_{MBM2} was calculated as the ratio of precipitation between May and October to the total annual precipitation (0.65). The γ_{MBM2} value for the Cyrus site was adjusted to 0.70 to account for spring and late-fall snowmelt runoff events. Using similar methods, the γ_{MBM2} value for the Deerwood site was estimated to be 0.75.

3.3.5 Landscape Segmentation

The LandMapR® toolkit of programs (including FlowMapR, FormMapR, FacetMapR and WeppMapR) developed by MacMillan (2003) was used for the landscape segmentation of the two sites. LandMapR uses a DEM to automatically extract a variety of topographic features of the landscape to classify the landscape into landform elements through user-defined fuzzy rules (based on tacit knowledge of landform segmentation and soil mapping). Following a specified order, FlowMapR computes flow topology for simulated surface water flow in both the down-slope and up-slope directions, FormMapR computes a series of terrain derivatives for the input DEM, and FacetMapR automatically applies the user-defined fuzzy rules to segment the landscape into different landform elements.

The DEMs of the two sites were imported into the programs and the parameter settings included: 1) FlowMapR, a "maximum area of pit to remove" of 10 cells (1000 m^2 and 640 m^2 for the Cyrus site and the Deerwood site, respectively) and a "maximum depth of pit to remove" of 0.15 m were used; 2) FormMapR, the threshold values for the "upslope area" and the "depression area" were both set at 420 cells (larger than the entire area of each DEM); and 3) FacetMapR, program-supplied fuzzy-facet-attribute-rule and

facet-classification-rule files (which have been widely applied in Canada) were used. Fifteen landform elements (15-class LE) were classified and were further grouped into four landform elements (4-class LE) (Table 3.2). The 4-class landform classification primarily characterizes the relative position to the hilltops and/or depressions (i.e. pits) and the profile topographic feature; whereas the 15-class landform classification characterizes plan topographic feature as well.

Table 3.2 General characteristics of the landform elements.

4-class LE		15-class LE		Slope Curvature		Slope Gradient
Name	Code	Name	Code	Profile	Plan	
Upper-slope	UP	Divergent-shoulder	DSH	Convex	Convex	Low
		Upper-depression	UDE	Concave	Concave	Low
Mid-slope	MID	Backslope	BSL	Linear	Linear	High
		Divergent-backslope	DBS	Linear	Convex	High
		Convergent-backslope	CBS	Linear	Concave	High
Lower-slope	LOW	Footslope	FSL	Concave	Concave	Low
		Toeslope	TSL	Linear	Linear	Low

* adapted from MacMillan, 2003. Only three 4-class and seven 15-class landform elements were observed at the scale of analyses in this study.

3.3.6 Statistical Analysis

Model-estimated water and tillage erosion rates and landform element data were determined for each DEM grid node and these points did not necessarily coincide with the sampling points. GS+ 5.1.1® point kriging was used to interpolate the erosion rate data onto the sampling points. To avoid smoothing, the searching radius of the interpolation was set to equal the DEM spacing, so that for a given point, data from a maximum of the five closest points were used in the interpolation. The landform element

assigned to each sampling point was that of its closest grid node(s) in the DEM (Figure 3.2a and b).

The interpolated data and the ^{137}Cs estimated total soil erosion of the sampling points were examined with SAS 9.0®. Pearson correlation coefficients (r) were used to indicate the correlations between different variables (SAS 2002). The significance of r was grouped into three categories, i.e. $P \leq 0.10$, ≤ 0.01, ≤ 0.001, and were denoted using †, ** and ***, respectively. For each variable, the Ryan-Einot-Gabriel-Welsch multiple-range test (REGWQ test) was used to test the significance of differences ($P \leq 0.05$) between the means in different landform elements. REGWQ test was chosen because the test controls both type I errors and type II errors (SAS 2002).

3.4 Results and Discussion

3.4.1 The Cyrus Site

3.4.1.1 Patterns of Estimated Water, Tillage and Total Erosion. At the Cyrus site, WEPP-estimated water erosion rates ranged from 0.2 to 57.5 Mg ha $^{-1}$ yr^{-1} (Figure 3.3a), averaged 18.8 Mg ha $^{-1}$ yr^{-1} (Table 3.3) and the entire mapped field area showed soil loss. The basic pattern was that lower soil loss occurred in the upper-slope areas and higher soil losses occurred in the mid-slope and lower-slope areas, with the highest rates of soil loss located on the lower part of the knoll (Figure 3.3a). WaTEM-estimated water erosion rates ranged from –127.8 to 98.2 Mg ha $^{-1}$ yr^{-1} (Figure 3.3b) and averaged 24.9 Mg ha $^{-1}$

yr^{-1} (Table 3.3). The major patterns of WaTEM- and WEPP- estimated water erosion were similar. However, WaTEM estimated considerably greater soil loss on the upper part of the trough and the slightly concave slope towards the east, and considerably greater soil accumulation near the lower end of the trough (Figure 3.3b). This suggests that WaTEM captured the major convergent water flows better than the WEPP procedure used in this study. These noticeable differences between the WEPP and WaTEM estimations reinforce that there is a great deal of uncertainty associated with water erosion modeling.

TillEM-estimated tillage erosion rates ranged from –25.6 to 44.9 Mg ha^{-1} yr^{-1} and averaged 1.1 Mg ha^{-1} yr^{-1} (Figure 3.3c and Table 3.3, respectively). The pattern, as expected, varied with the local relief, in particular with slope curvature. Overall, the total area of soil loss was approximately the same as that of soil accumulation. The highest rates of soil loss were found on the top of the knoll, which has a convex shape, and the highest soil accumulation was found in the trough and on the eastern side-slope of the knoll, which are both concave in shape (Figure 3.3c).

The ^{137}Cs-estimated total soil erosion rates ranged from -97.2 to 25.5 Mg ha^{-1} yr^{-1} and averaged 20.3 Mg ha^{-1} yr^{-1} (Figure 3.3f and Table 3.3). More than 90 % of the mapped field area showed soil loss. The highest soil losses were located on the lower part of the knoll and the trough, while soil accumulation was mainly found in the footslope and toeslope areas (Figure 3.3f).

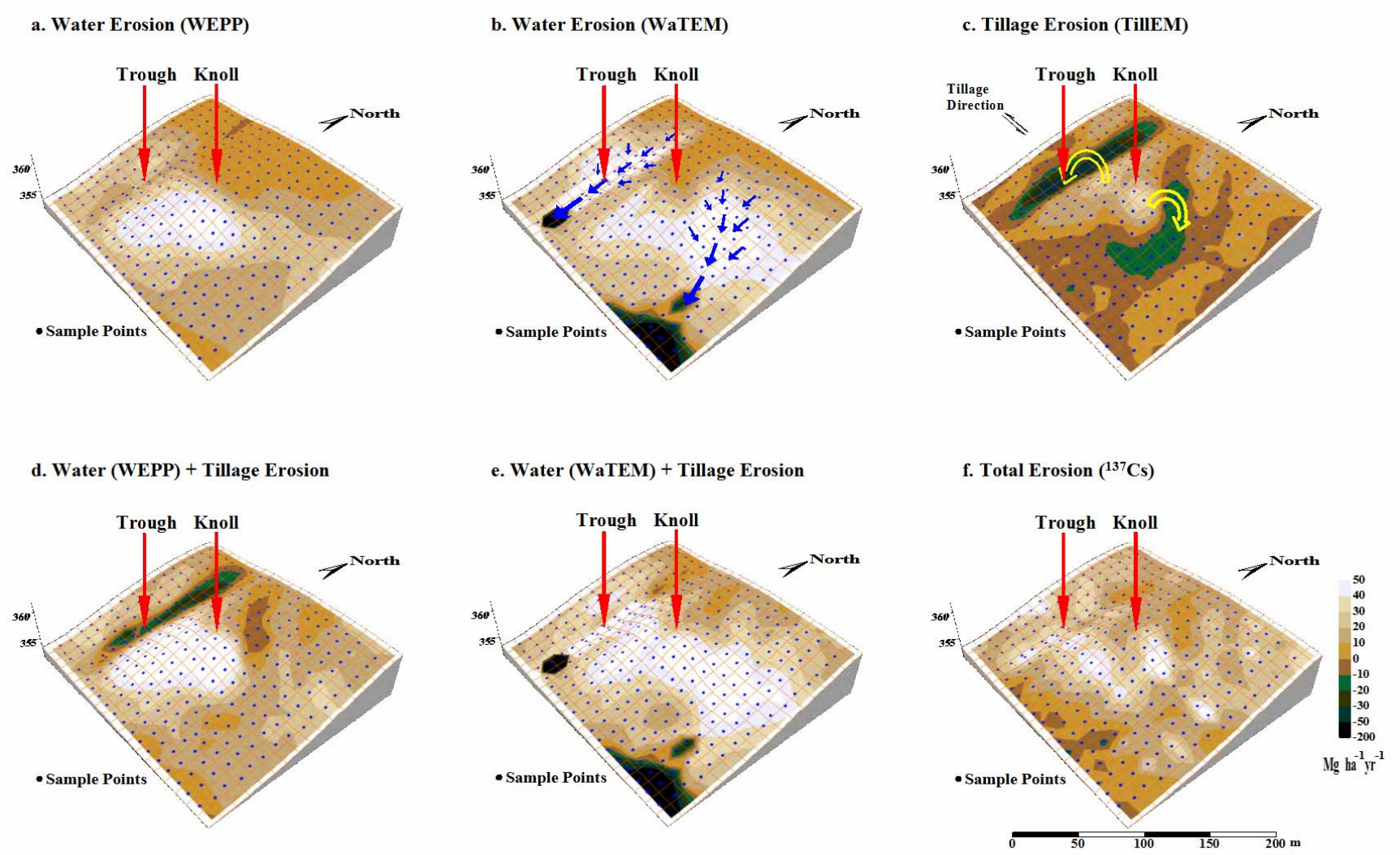

Figure 3.3 Estimated a. Water (WEPP), b. Water (WaTEM), c. Tillage (TillEM), d. Water (WEPP) + Tillage, e. Water (WaTEM) + Tillage, and f. Total (^{137}Cs) soil erosion at the Cyrus site.

Table 3.3 Erosion estimates in different landscape elements at the Cyrus site.

		4-class LE			15-class LE							
		UP	MID	LOW	DSH	UDE	BSL	DBS	CBS	FSL	TSL	All
	n *	69	150	69	58	11	38	57	55	43	26	288
E_{Cs}	Mean	19.5 ^{B}	26.1 ^{A}	8.6 ^{C}	20.3 ^{bc}	14.8 ^{cde}	26.4 ^{ab}	33.2 ^{a}	18.2 ^{bcd}	9.1 ^{de}	7.9 ^{e}	20.3
(Mg ha^{-1})	SD	8.9	16.0	12.1	9.0	7.3	15.1	15.8	13.3	11.8	12.8	15.4
E_{Wepp}	Mean	4.1 ^{C}	24.9 ^{A}	20.3 ^{B}	4.5 ^{d}	1.7 ^{d}	27.0 ^{ab}	30.0 ^{a}	18.2 ^{c}	22.2 ^{bc}	17.3 ^{c}	18.8
(Mg ha^{-1})	SD	3.7	13.5	9.0	3.9	1.2	13.0	13.1	11.4	10.0	6.0	13.8
E_{Usle}	Mean	9.6 ^{B}	39.9 ^{A}	7.7 ^{C}	9.3 ^{b}	11.2 ^{b}	41.3 ^{a}	31.7 ^{a}	47.5 ^{a}	5.7 ^{b}	10.9 ^{b}	24.9
(Mg ha^{-1})	SD	5.8	23.4	36.4	5.6	6.5	10.8	10.1	34.5	42.5	23.5	29.2
E_{Ti}	Mean	8.6 ^{A}	-0.8 ^{B}	-2.2 ^{B}	11.0 ^{a}	-4.0 ^{b}	-0.5 ^{b}	11.7 ^{a}	-13.9 ^{c}	-4.0 ^{b}	0.7 ^{b}	1.1
(Mg ha^{-1})	SD	8.4	14.2	4.5	5.9	8.6	3.6	9.6	10.4	4.6	2.4	12.0
$E_{Wepp+Ti}$	Mean	12.7 ^{C}	24.1 ^{A}	18.1 ^{B}	15.5 ^{c}	-2.3 ^{d}	26.5 ^{b}	41.7 ^{a}	4.3 ^{d}	18.2 ^{bc}	18.0 ^{bc}	20.0
(Mg ha^{-1})	SD	10.4	22.3	9.5	8.1	8.5	12.4	17.6	14.7	11.3	5.6	18.1
$E_{Usle+Ti}$	Mean	18.2 ^{B}	39.1 ^{A}	5.5 ^{C}	20.3 ^{bc}	7.2 ^{cd}	40.8 ^{a}	43.4 ^{a}	33.6 ^{ab}	1.8 ^{d}	11.6 ^{cd}	26.1
(Mg ha^{-1})	SD	9.0	20.7	36.1	8.2	3.9	10.2	9.9	30.9	41.8	23.5	27.5

* some data points were missing for some variables.

A - C denote the group of the 4-class clasiffiation means, REGWQ test, $P \leq 0.05$.

a - e denote the group of the 15-class clasiffiation means, REGWQ test, $P \leq 0.05$.

The pattern of ^{137}Cs-estimated total erosion did not agree well with the patterns of either the model-estimated tillage or water erosion, indicating that neither water or tillage erosion alone was able to explain the total soil erosion evident at this site. In addition, the patterns of water (WEPP) + tillage erosion (Figure 3.3d) and water (WaTEM) + tillage erosion (Figure 3.3e) did not agree well with the pattern of the ^{137}Cs estimated total erosion. The absence of wind erosion data and the errors associated with the models and ^{137}Cs estimations might partly explain these discrepancies. However, wind erosion is comparatively uniform within a small area and should not greatly affect the results (Pennock et al., 1999). Also the errors associated with the models and ^{137}Cs estimations primarily affect the magnitude of the estimated value, not the pattern (see the discussion

of errors below). Therefore, a further explanation for these discrepancies could be that tillage and water erosion might not always be additive and more complicated interactions between these two processes may exist.

3.4.1.2 Correlation Analyses. The correlation analyses for erosion estimates at the Cyrus site (Table 3.4) show that both WEPP- and WaTEM-estimated water erosion (E_{Wepp} and E_{Usle}, respectively) and TillEM-estimated tillage erosion (E_{Ti}) were significantly correlated with ^{137}Cs-estimated total soil erosion (E_{Cs}). Therefore, both water and tillage erosion contributed to the total soil erosion at this site. However, overall, the correlations were weak since each of the three models explained only a small part of the variance of the total soil erosion. The estimates of the two water erosion models were significantly correlated with each other, but the correlation ($r = 0.40^{***}$) was also considered to be weak given that in theory, the two models should have produced identical results. Again, this confirms that there is a high degree of uncertainty associated with water erosion modeling. In addition, no significant differences were found between E_{Wepp} ($r = 0.31^{***}$) and E_{Usle} ($r = 0.22^{***}$) when correlated with E_{Cs}. The r-value of E_{Ti} ($r = 0.19^{**}$) was significantly lower than, but still close to, the r-values of E_{Wepp} and E_{Usle} when correlated with E_{Cs}. This suggests that the influence of water erosion is stronger than tillage erosion at this site, but still not strong enough to dominate the total erosion pattern across the field.

The r-values of the sum of water and tillage erosion ($E_{Wepp+Ti}$, $r = 0.35^{***}$ and $E_{Usle+Ti}$, $r = 0.31^{***}$), when correlated with E_{Cs}, were both larger than those of the component model estimates (i.e. E_{Wepp}/E_{Usle} and E_{Ti}), indicating the superiority of

combining water and tillage erosion models. The correlation between $E_{Wepp+Ti}$ and E_{Wepp} ($r = 0.75^{***}$) was larger than the correlation between $E_{Wepp+Ti}$ and E_{Ti} ($r = 0.65^{***}$), the correlation between $E_{Usle+Ti}$ and E_{Usle} ($r = 0.91^{***}$) was much larger than the correlation between $E_{Usle+Ti}$ and E_{Ti} ($r = 0.08^{NS}$). Again, this suggests that based on the models, water erosion contributed more than tillage erosion at the Cyrus site. To avoid the effects of systematic errors associated with the model and ^{137}Cs estimations, multiple-correlation analyses of E_{Cs} against both E_{Wepp} and E_{Ti}, and of E_{Cs} against both E_{Usle} and E_{Ti} were conducted ($r = 0.39^{***}$ and 0.34^{***}, respectively). The multiple-correlation coefficients were very close to those of $E_{Wepp+Ti}$ and $E_{Usle+Ti}$, respectively. This suggests that the systematic errors were not the reason for the observed weak correlations and further suggests that a possible interaction exists between the two erosion processes.

Further correlation analyses of the models estimates with the ^{137}Cs estimates were conducted on each transect parallel and perpendicular to tillage direction (Appendix B.1). The r-values of $E_{Wepp+Ti}$ and $E_{Usle+Ti}$, in general, were much greater than those of E_{Wepp} / E_{Usle} and E_{Ti}, which again confirms that combining water and tillage erosion model provides better estimation of total soil erosion. The r-values of E_{Wepp}, in general, were considerably greater than those of E_{Usle} for transects parallel to the tillage direction. This could be explained by the fact that the WEPP procedure used in this study accounted for the influences of tillage on the directionality of water flows and, therefore, water erosion.

Table 3.4 Correlation coefficients for erosion estimates at the Cyrus site*.

	E_{Cs}	E_{Wepp}	E_{Usle}	E_{Ti}	$E_{Wepp+Ti}$
E_{Wepp}	0.31 ***				
E_{Usle}	0.22 ***	0.40 ***			
E_{Ti}	0.19 **				
$E_{Wepp+Ti}$	0.35 ***	0.75 ***		0.65 ***	
$E_{Usle+Ti}$	0.31 ***		0.91 ***	0.08	0.37 ***

* n = 279 -288.

, * significant at the 0.10, 0.01 and 0.001 probability levels, respectively.

3.4.1.3 Landscape Segmentation. At the Cyrus site, only three of the 4-class landform elements and seven of the 15-class landform elements defined in LandMapR were expressed (Table 3.3). For the three 4-class LEs, ^{137}Cs-estimated soil loss (E_{Cs}) was ranked mid-slope (MID) >> upper-slope (UP) >> lower-slope (LOW) (REGWQ test, significant at $P \leq 0.05$). For water erosion, both WEPP and WaTEM estimated the highest soil loss in MID and significantly lower soil loss in UP and LOW. Overall, the E_{Usle} was much greater than E_{Wepp} in MID and UP but much less than E_{Wepp} in LOW. In addition, high variability was found for the E_{Usle} in LOW (SD = 36.4 Mg ha^{-1} yr^{-1}). TillEM-estimated tillage erosion showed soil loss in UP, negligible soil accumulation in MID and considerable soil accumulation in LOW. Comparing E_{Wepp}, E_{Usle} and E_{Ti} to $E_{Wepp+Ti}$ and $E_{Usle+Ti}$, tillage erosion contributed about 50 - 70 % soil loss in the upper-slope landscape positions. These results are comparable to those reported by Lobb et al. (1995) and Lobb and Kachanoski (1999). In addition, water erosion dominated in MID and tillage-induced soil accumulation compensated for about 10 - 30 % water-induced soil loss in LOW.

Noticeable differences were found between the 15-class LEs corresponding to the same 4-class LEs (Table 3.3). The most significant differences were found for E_{Ti}, of which: in UP, divergent-shoulder (DSH) >> upper-depression (UDE); in MID, divergent-backslope (DBS) >> backslope (BSL) >> convergent-backslope (CBS); and in LOW, toeslope (TSL) > footslope (FSL). Landform elements with similar local topographic features appeared to have close E_{Ti} means. For example: UDE, CBS and FSL were concave and showed tillage-induced soil accumulation (-4.0, -13.9 and –4.0 Mg ha^{-1} yr^{-1}, respectively); both DSH and DBS were convex and showed high tillage-induced soil loss (11.0 and 11.7 Mg ha^{-1} yr^{-1}, respectively); and both BSL and TSL were linear and showed near zero tillage erosion (-0.5 and 0.7 Mg ha^{-1} yr^{-1}, respectively). For the other erosion estimates, a common pattern emerged in that the differences between the 4-class LEs were considerably greater than the differences between the subdivided 15-class LEs. For example, for E_{Wepp}, no significant differences were found between DSH and UDE (UP), between BSL and DBS (MID) and between FSL and TSL (LOW), whereas BSL and DBS >> FSL and TSL >> DSH and UDE. The two water erosion estimates, E_{Wepp} and E_{Usle}, showed quite different patterns. Within the same 4-class LEs, E_{Wepp} and E_{Usle} of the 15-class LEs were ranked in opposite orders (e.g. in UP, for E_{Wepp}, DSH > UDE, but for E_{Usle}, DSH < UDE). The means of E_{Usle} were much greater than E_{Wepp} in UP and MID (except for DBS), but were much lower than E_{Wepp} in LOW. A possible reason for this discrepancy was that WaTEM captured the major divergent and convergent water flows better than the WEPP procedure used in this study and, therefore, estimated more soil loss in convergent landforms (UDE and CBS), less soil loss in divergent landforms (DSH and DBS) and probably more soil accumulation in FSL and TSL as well. However, much

greater uncertainty was found for E_{Usle} (e.g. in CBS, FSL and TSL, SD = 34.5, 42.5 and 23.5 Mg ha^{-1} yr^{-1}, respectively). This is likely due to the fact that in these landform elements, WaTEM estimated stronger runoff, which can cause either more intensive soil loss when the transportation capacity was not exceeded or intensive soil accumulation when the transportation capacity was exceeded.

For the 15-class LEs, the patterns of $E_{Wepp+Ti}$ and $E_{Usle+Ti}$ were similar to the pattern of E_{Cs} in the five UP and MID elements but not in the two LOW elements (Table 3.3). According to the model estimates: in BSL and TSL, total soil erosion was largely determined by water erosion; in DSH and DBS, tillage erosion contributed about 55 – 70 % and 25 - 30 % to the total soil loss, respectively; and in UDE, CBS and FSL, tillage-induced soil accumulation compensated for about 35 – 100 %, 30 - 75 % and 15 - 70 % of the water-induced soil loss, respectively. The large discrepancies found between $E_{Wepp+Ti}$, $E_{Usle+Ti}$ and E_{Cs} in UDE, CBS, FSL and TSL suggests that there is a high uncertainty associated with the modeling, especially the water erosion modeling, and/or there is high variability of soil erosion that actually occurred in these landform elements. It is possible that the interactions between water and tillage erosion was another major cause of this high variability. However, since we were limited by the high uncertainty associated with the modeling, it was difficult to examine the pattern of the interactions and to isolate the contributions of the interactions from those of water and tillage erosion alone and those of their linkages.

The landscape segmentation analyses at the Cyrus site suggests that the use of landscape segmentation procedure provides valuable information on the variations of soil erosion across the landscape. The data also suggests that the 4-class landform

classification captured the major pattern of these variations. However, the 15-class landform classification differentiated tillage erosion pattern more precisely and provided more information on the pattern of water erosion as affected by the convergent and divergent water flows.

3.4.2 The Deerwood Site

3.4.2.1 Patterns of Estimated Water, Tillage and Total Erosion. At the Deerwood site, the WEPP-estimated water erosion rates ranged from –1.6 to 8.4 Mg ha $^{-1}$ yr^{-1} (Figure 3.4a) and averaged 1.9 Mg ha $^{-1}$ yr^{-1} (Table 3.5). About 70 % of the mapped field area showed soil loss between 0 and 3 Mg ha $^{-1}$ yr^{-1}, while the bottom of the bowl (depression) showed soil accumulation. The pattern of the WaTEM estimates (Figure 3.4b) was similar to that of the WEPP estimates, except that WaTEM estimated soil loss over the entire mapped field area, including the depression area. Compared to the Cyrus site, estimated water-induced soil loss at the Deerwood site was considerably lower. The primary reason for this is due to the shorter slope lengths at the Deerwood site. The TillEM-estimated tillage erosion rates ranged from –6.5 to 14.5 Mg ha $^{-1}$ yr^{-1} (Figure 3.4c) and averaged 2.2 Mg ha $^{-1}$ yr^{-1} (Table 3.5) with the highest soil losses at the top of the ridge and soil accumulation in the bowl area. In comparison to the three models, the ^{137}Cs-estimated total soil erosion rates ranged from –27.5 to 42.0 Mg ha $^{-1}$ yr^{-1} (Figure 3.4f) and averaged 12.1 Mg ha $^{-1}$ yr^{-1} (Table 3.5).

The patterns of the ^{137}Cs-estimated total soil erosion, water (WEPP) + tillage erosion (Figure 3.4d) and water (WaTEM) + tillage erosion (Figure 3.4e) were both more similar to that of tillage erosion than water erosion. This suggests that tillage erosion is

the dominant erosion process at the Deerwood site. The large discrepancy between the model and ^{137}Cs estimates suggests that there might be systematic errors in the models. These errors were likely caused by the absence of data relating to the historically used heavier tillage implements and the low accuracy of the climate data.

With the use of the Cyrus climate, management and soil data, the WEPP-estimated water erosion (E_{WeppC}) and the TillEM-estimated tillage erosion (E_{TiC}) showed patterns almost identical to that of E_{Wepp} and E_{Ti}, respectively (maps not shown). The data range of the combined model ($E_{WeppC+TiC}$) (-17.5 to 66.2 Mg ha $^{-1}$ yr^{-1} with an average at 12.4 Mg ha $^{-1}$ yr^{-1}), were close to the range of E_{Cs}, suggesting that the climate and management data from the Cyrus site might be more realistic than the generated climate and management data used at the Deerwood site.

3.4.2.2 Correlation Analyses. Correlation analyses provided further evidence that tillage erosion is the dominant erosion process at the Deerwood site (Table 3.6). For example: 1) E_{Ti} was significantly correlated with E_{Cs} ($r = 0.56^{***}$); 2) The r-values of E_{Wepp} ($r = 0.30^{\dagger}$) and E_{Usle} ($r = -0.20^{NS}$) were significantly lower than that of E_{Ti}, when correlated with E_{Cs}; 3) The combined models, $E_{Wepp+Ti}$ and $E_{Usle+Ti}$, had r-values ($r = 0.59^{***}$ and 0.49^{***}, respectively) which are similar to that of E_{Ti}, when correlated with E_{Cs}; 4) The correlation coefficients determined for $E_{Wepp+Ti}$ and E_{Ti} ($r = 0.94^{***}$) and for $E_{Usle+Ti}$ and E_{Ti} ($r = 0.92^{***}$) were very strong and were considerably larger than the correlations between $E_{Wepp+Ti}$ and E_{Wepp} ($r = 0.55^{***}$) and between $E_{Usle+Ti}$ and E_{Usle} ($r = 0.17^{NS}$), respectively; and 4) D and C_{St} were significantly correlated with E_{Ti} ($r = -0.24^{\dagger}$ and 0.39^{**}, respectively).

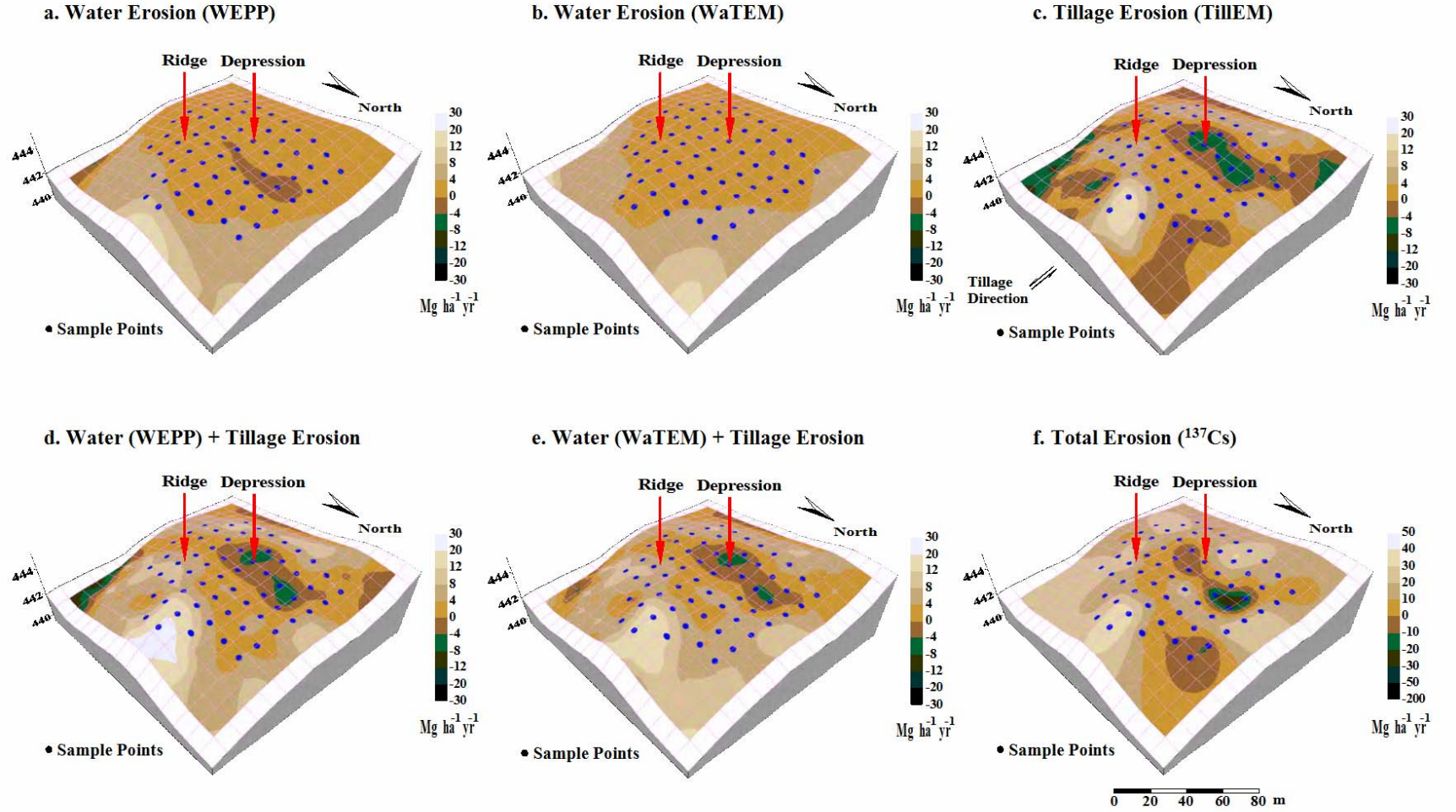

Figure 3. 4 Estimated a. Water (WEPP), b. Water (WaTEM), c. Tillage (TillEM), d. Water (WEPP) + Tillage, e. Water (WaTEM) + Tillage, and f. Total (^{137}Cs) soil erosion at the Deerwood site.

Table 3.5 Erosion estimates in different landscape elements at the Deerwood site.

		4-class LE		15-class LE					
		UP	MID	DSH	UDE	BSL	DBS	CBS	All
	n	34	29	26	8	12	10	7	63
E_{Cs}	Mean	13.5 ^{A}	10.5 ^{A}	16.2 ^{ab}	4.7 ^{bc}	13.3 ^{ab}	20.1 ^{a}	-7.9 ^{c}	12.1
(Mg ha^{-1})	SD	11.7	18.1	10.2	12.6	15.8	12.9	15.9	14.9
E_{Wepp}	Mean	1.4 ^{B}	2.5 ^{A}	1.6 ^{ab}	0.9 ^{b}	1.8 ^{ab}	3.2 ^{a}	2.8 ^{a}	1.9
(Mg ha^{-1})	SD	0.8	2.2	0.8	0.5	1.3	2.8	2.3	1.7
E_{Usle}	Mean	0.9 ^{B}	2.9 ^{A}	0.9 ^{c}	1.0 ^{c}	2.5 ^{b}	2.4 ^{b}	4.4 ^{a}	1.8
(Mg ha^{-1})	SD	0.6	1.8	0.7	0.6	1.4	1.0	2.4	1.6
E_{WeppC}	Mean	2.9 ^{B}	6.7 ^{A}	3.2 ^{c}	2.0 ^{c}	4.5 ^{bc}	7.9 ^{ab}	8.9 ^{a}	4.7
(Mg ha^{-1})	SD	2.0	5.4	2.1	0.9	2.4	6.9	6.1	4.4
E_{Ti}	Mean	2.6 ^{A}	1.8 ^{A}	4.1 ^{a}	-2.6 ^{c}	0.9 ^{b}	5.9 ^{a}	-2.7 ^{c}	2.2
(Mg ha^{-1})	SD	4.1	4.3	3.2	1.8	2.2	3.4	2.2	4.2
E_{TiC}	Mean	9.2 ^{A}	6.1 ^{A}	14.2 ^{a}	-7.1 ^{c}	3.5 ^{b}	19.1 ^{a}	-8.1 ^{c}	7.8
(Mg ha^{-1})	SD	12.9	13.6	9.9	5.8	6.6	11.6	7.1	13.2
$E_{Wepp+Ti}$	Mean	4.0 ^{A}	4.3 ^{A}	5.7 ^{ab}	-1.7 ^{d}	2.6 ^{bc}	9.1 ^{a}	0.2 ^{cd}	4.1
(Mg ha^{-1})	SD	4.5	5.3	3.6	1.7	2.4	5.2	3.6	4.8
$E_{Usle+Ti}$	Mean	3.4 ^{A}	4.7 ^{A}	5.0 ^{b}	-1.6 ^{c}	3.4 ^{b}	8.4 ^{a}	1.7 ^{b}	4.0
(Mg ha^{-1})	SD	3.9	4.3	3.0	1.5	2.7	3.4	4.2	4.1
$E_{WeppC+TiC}$	Mean	12.1 ^{A}	12.8 ^{A}	17.4 ^{ab}	-5.1 ^{d}	8.0 ^{bc}	26.9 ^{a}	0.8 ^{cd}	12.4
(Mg ha^{-1})	SD	14.1	15.8	11.3	5.8	6.6	16.1	12.3	14.8

$^{A-B}$ denote the group of the 4-class clasiffiation means, REGWQ test, $P \leq 0.05$.
$^{a-d}$ denote the group of the 15-class clasiffiation means, REGWQ test, $P \leq 0.05$.

Table 3.6 Correlation coefficients for erosion estimates at the Deerwood site*.

	E_{Cs}	E_{Wepp}	E_{Usle}	E_{WeppC}	E_{Ti}	E_{TiC}	$E_{Wepp+Ti}$
E_{Wepp}	0.30 †						
E_{Usle}	-0.20	0.51 ***					
E_{WeppC}	0.13	0.94 ***	0.66 ***				
E_{Ti}	0.56 ***						
E_{TiC}	0.65 ***				0.97 ***		
$E_{Wepp+Ti}$	0.59 ***	0.55 ***		0.44 ***	0.94 ***	0.95 ***	
$E_{Usle+Ti}$	0.49 ***		0.17		0.92 ***		0.95 ***
$E_{WeppC+TiC}$	0.62 ***	0.58 ***		0.49 ***		0.96 ***	0.98 ***

* n = 63.
†,**,*** significant at the 0.10, 0.01 and 0.001 probability levels, respectively.

Similar to the Cyrus site, E_{Wepp} and E_{Usle} were significantly correlated ($r = 0.51^{***}$) but the correlation was not that strong and the uncertainty associated with water erosion modeling was considered to be high (Table 3.6). The strong correlations found between E_{Wepp} and E_{WeppC} ($r = 0.94^{***}$), between E_{Ti} and E_{TiC} ($r = 0.97^{***}$) and between $E_{Wepp+Ti}$ and $E_{WeppC+TiC}$ ($r = 0.98^{***}$) suggest that at the Deerwood site, the patterns of the model estimates were not sensitive to the input climate, management and soil data and, therefore, were considered largely determined by the topographic data

For the transect data, correlation analyses of model estimates against ^{137}Cs estimates also demonstrated the dominant effect of tillage erosion (Appendix B.2). The r-values of E_{Ti} were generally much greater than the respective r-values of E_{Wepp} and E_{Usle} and were close to the respective r-values of $E_{Wepp+Ti}$ and $E_{Usle+Ti}$. For transects parallel to the tillage direction, the r-values of E_{Wepp} again were found to be considerably greater than those of E_{Usle}, suggesting the existence of the directionality of water erosion induced by tillage operations.

3.4.2.3 Landscape Segmentation. At the Deerwood site, only two of the 4-class landform elements and five of the 15-class landform elements defined in LandMapR were expressed (Table 3.5). For the two expressed 4-class LEs, the three water erosion estimates showed a consistent pattern with MID >> UP (REGWQ test, $P \leq 0.05$). These results are similar to those found at the Cyrus site. No significant differences were found between MID and UP for all the other erosion estimates. Based on the model estimates, tillage erosion contributed about 65 - 80 % soil loss in UP and about 40 – 50 % soil loss in MID at the Deerwood site.

Except for the three water erosion estimates, all the other model estimates showed significant differences between DSH and UDE, and between BSL, DBS and CBS (Table 3.5). The differences were largely dependent on the values of E_{Ti} and varied in a similar pattern to that of E_{Ti}, with the highest soil losses observed in the DBS and DSH and the greatest soil accumulation and/or the lowest soil loss occurring in the UDE and CBS. The differences between the individual 15-class LEs appeared to be greater than the differences between the two 4-class LEs. For the 15-class LEs, the respective patterns of E_{Ti}, E_{Wepp} and E_{Usle} were the same as those at the Cyrus site. However, variations of model-estimated water erosion over the different 15-class LEs were comparatively smaller than those at the Cyrus site. Based on the model estimates, tillage erosion contributed about 70 - 85 %, 65 – 70 % and 25 – 45 % soil loss in the DSH, DBS and BSL, respectively. Tillage erosion also compensated for most of the water-induced soil loss in CBS and caused soil accumulation in UDE.

3.4.3 Errors

3.4.3.1 Errors Associated With Erosion Model Estimates. Inaccuracy of the climate, soil, management (i.e. tillage, crop rotation) and topographic data may have all contributed errors to the water erosion model estimates. For both WEPP and WaTEM, the patterns of the estimated water erosion were largely determined by the topography. The effect of the climate, soil and management data on the estimated water erosion rates was expected to be the largest in the lower-slope, as shown in Figure 3.1. This might be a major reason for the large discrepancies between E_{Cs} and $E_{Wepp+Ti}$ / $E_{Usle+Ti}$ in the FSL and

TSL observed at the Cyrus site. However, the use of Cyrus site's climate, soil and management data on the Deerwood site and a sensitivity test of WaTEM demonstrated that the general patterns of the estimated water erosion were not sensitive to different climate and management data. Also, WEPP output was not sensitive to the alteration of the three major soil types at the Cyrus site. In addition, the alteration of K-factor values in WaTEM did not make noticeable changes on the pattern of the estimated water erosion. Overall, the major patterns of both WEPP- and WaTEM-estimated water erosion in this study were similar. However, the fact that large discrepancies existed between E_{Wepp} and E_{Usle}, indicates that there is still high uncertainty associated with water erosion modeling. Neither model was considered to be superior to the other, but it appears that WaTEM captures the major water flows better, while the WEPP procedure was better able to account for the tillage-induced directionality of water erosion.

Compared to water erosion, tillage erosion is relatively simple to model. The magnitude of the estimated tillage erosion varies across the landscape as a result of only two coefficients, β and γ. Based on previous research, tillage erosion was expected to be more sensitive to β (Lobb et al., 1999). However, as evident by using the Cyrus site's coefficients at the Deerwood site, the pattern of estimated tillage erosion was not sensitive to β and γ. WaTEM also provides a tillage erosion model, but this model does not account for the effect of the variation of slope curvature (i.e. $\gamma = 0$) and, therefore, was not used in this study. Nonetheless, a test with the Cyrus data showed that the WaTEM estimates were very similar to the TillEM estimates ($r = 0.89$).

3.4.3.2 Errors Associated With ^{137}Cs Estimates. The MBM2 used in this study is one of the most sophisticated models for converting ^{137}Cs inventories into total erosion rates,

but it requires more data inputs (i.e. γ_{MBM2}, P_{MBM2} and H_{MBM2}) than the widely used proportional or simplified mass balance model. Calculating γ_{MBM2} using the averaged climate data, assuming that P_{MBM2} was equal to 1.0 and taking H_{MBM2} values from the literature were unavoidable simplifications. Further field experiments are needed to obtain more accurate measurements of γ_{MBM2}, P_{MBM2} and H_{MBM2}. A sensitivity analysis showed that the output total erosion rates were sensitive to both γ_{MBM2} and P_{MBM2}, but not H_{MBM2}. However, within reasonable γ_{MBM2} and P_{MBM2} ranges, the output varied by no more than 10 %. Therefore, the accuracy of these parameters was considered to be sufficient in this study.

Another input parameter, and potential source of error was the reference ^{137}Cs level used in this study. It was difficult to obtain an accurate value of the reference ^{137}Cs level due to the fact that ideal reference sites are rare. The measured reference ^{137}Cs level at the Deerwood site had a coefficient of variation of 9.3 %. Nonetheless, the measured ^{137}Cs levels at both reference sites used this study were comparable to those reported by other researchers in the northern NAGP (e.g. de Jong et al., 1983, Pennock et al., 1999). In addition, the errors associated with the reference ^{137}Cs level primarily cause a shift between soil loss and accumulation, however, the relative differences remain constant and, therefore, will not affect the results of the correlation analyses.

It should be noted that the same software used in this study provides a more complicated converting model, the Mass Balance Model 3 (MBM3). MBM3 incorporates a two-dimensional tillage erosion model, which does not take into account lateral translocation and the effect of changing slope curvature (i.e. $\gamma = 0$), and, therefore, might not be suitable for topographically complex landscapes.

3.4.3.3 Errors Associated With Landscape Segmentation. Potential errors in the landscape segmentation are associated with the fuzzy rules used to classify the landform elements. It was recommended that specific rules be created by the user for different landscapes. To maintain consistency within this study, the same fuzzy rules supplied by the software were used for both sites. However, these fuzzy rules have not been fully validated on undulating and/or hummocky landscapes. Had more accurate classification rules been available, the variability of soil erosion estimates within a given landform element could be reduced and the interactions between water and tillage erosion might be easier to identify.

3.5 Conclusions

Patterns of water and tillage erosion are fundamentally different within topographically complex landscapes. We determined that water and tillage erosion models tested alone provide acceptable estimation of total soil erosion only when that process is dominant over the other process(es). We found that combining water and tillage erosion models generally provided a better estimation of total soil erosion than the component models on their own.

The contributions of water and tillage erosion vary in different landscapes and in different landform elements. On undulating slopes, tillage and water erosion both

contribute considerably to total soil erosion. Tillage erosion contributes about 50 to 70 % towards total soil erosion on upper-slopes; water erosion is the dominant erosion process on mid-slopes, and in lower-slopes, tillage-induced soil accumulation compensates for approximately 10 to 30 % of the water-induced soil loss. On hummocky knolls, tillage erosion dominates the pattern of total soil erosion and the effects of water erosion are minor, with tillage erosion contributing for 65 to 80 % of the total soil loss on upper-slopes and about 40 to 50 % soil loss on mid-slopes.

Localized water erosion is primarily influenced by the local slope gradient and the upslope catchment area. In this study, the highest water-induced soil loss occurred on mid-slope landscape positions. Localized tillage erosion is more dependent on the local relief, with tillage-induced soil losses occurring on convex landform elements (such as divergent-shoulder and divergent-backslope) and tillage-induced soil accumulation occurring in convergent landform elements (such as upslope-depression, convergent-backslope and footslope). In linear landform elements (such as backslope and toeslope landscape positions), tillage erosion is minor. The pattern of total soil erosion is further complicated in certain landform elements (such as convergent-backslope, footslope and toeslope) by the interactions between water and tillage erosion. However, it is difficult to isolate the contributions of the interactions from those of water, tillage erosion and their linkages. We suspect that the accuracy of the estimations would be enhanced if the interactions between water and tillage erosion could be clearly identified.

The 4-class landscape segmentation captured the major erosion patterns and the 15-class landscape segmentation provided additional detail with regards to the variability of soil erosion across the landscape. Landform information, which can be used for

landscape segmentation, is available in some nationwide soil databases (e.g. Canada and China). With these data, landscape segmentation could be used as an effective tool for the assessment of water, tillage and total erosion in topographically complex landscapes.

3.6 Acknowledgements

Financial support for this study was provided by Natural Sciences and Engineering Research Council of Canada (NSERC) as part of the "Tillage erosion and its impacts on soil characteristics and pesticide fate processes at the large-scale" project. The authors would like to thank K. Stephens who provided a major part of the soil properties data at the Cyrus site. We would also like to acknowledge Dr. K. Van Oost for the help of WaTEM application; Dr. R. MacMillan for the permission to use the LandMapR software; Dr. A. Moulin for the help of LandMapR application and K. Tiessen for reviewing the manuscript.

3.7 References

De Alba, S., Lindstrom, M.J., Schumacher, T.E., Malo, D.D., 2004. Soil landscape evolution due to soil redistribution by tillage: a new conceptual model of soil catena evolution in agricultural landscapes. Catena 58, 77-100.

de Jong, E., Begg, C.B.M., Kachanoski, R.G., 1983. Estimates of soil erosion and deposition for some Saskatchewan soils. Can. J. Soil Science 63, 607–617.

Environment Canada, 2006. Canadian Climate Normals or Averages 1971-2000 [Online]. Available at: http://www.climate.weatheroffice.ec.gc.ca/climate_normals/index_e.html.

Flanagan, D.C., Nearing, M.A. (Eds.), 1995. USDA-Water Erosion Prediction project: Hillslope profile and watershed model documentation. NSERL Report No. 10. USDA-ARS National Soil Erosion Research Laboratory, West Lafayette, IN 47097-1196.

Gaultier, J., Farenhorst, A., Crow, G., 2006. Spatial variability of soil properties and 2,4-D sorption in a hummocky field as affected by landscape position and soil depth. Can. J. Soil Science 86, 89-95.

Govers, G., Vandaele, K., Desmet, P.J.J., Poesen, J., Bunte, K., 1994. The role of tillage in soil redistribution on hillslopes. Eur. J. Soil Science 45, 469–478.

Hassouni, K., Bouhlassa, S., 2006. Estimation of soil erosion on cultivated soils using ^{137}Cs measurements and calibration models: a case study form Nakhla watershed, Morocco. Can. J. Soil Science 86, 77-87.

He, Q., Walling, D.E., 1997. The distribution of fallout ^{137}Cs and ^{210}Pb in undisturbed and cultivated soils. Applied Radiation and Isotopes 48, 677-690.

Lefebvre, A., Eilers, W., Chunn, et B. (Eds.), 2005. Environmental Sustainability of Canadian Agriculture: Agri-Environmental Indicator Report Series – Report #2. Agriculture and Agri-Food Canada, Ottawa, Ontario.

Lindstrom, M.J., Nelson, W.W., Schumacher, T.E., 1992. Quantifying tillage erosion rates due to moldboard plowing. Soil Tillage Research 24, 243-255.

Lindstrom, M.J., Nelson, W.W., Schumacher, T.E., Lemme, G.D., 1990. Soil movement by tillage as affected by slope. Soil Tillage Research 17, 255-264.

Lindstrom, M.J., Schumacher, T.E., Malo, D.D., 2000. Soil quality alterations across a complex prairie landscape due to tillage erosion. In: 15th Conf. Of the Intl. Soil Tillage Research Organization. July 2000. Fort Worth, TX, USA.

Lobb, D.A., 1991. Soil erosion processes on shoulder slope landscape positions. M.Sc. Thesis. University of Guelph. Guelph. 390 p.

Lobb, D.A., Kachanoski, R.G., Miller, M.H., 1995. Tillage translocation and tillage erosion on shoulder slope landscape positions measured using ^{137}Cs as a tracer. Can. J. Soil Science 75, 211-218.

Lobb, D.A., Kachanoski, R.G., 1999. Modelling tillage erosion in topographically complex landscapes of southwestern Ontario, Canada. Soil Tillage Research 51, 261–278.

Lobb, D.A., Kachanoski, R.G., Miller, M.H., 1999. Tillage translocation and tillage erosion in the complex upland landscapes of southwestern Ontario. Soil Tillage Research 51, 189-209.

Lobb, D.A., Lindstrom, M.J., Schumacher, T.E., 2003. Soil erosion processes and their interactions: implications for environmental indicators. In R. Francaviglia (Ed.). Agricultural impacts on soil erosion and soil biodiversity: developing indicators for policy analysis. Proceedings from an OECD expert meeting – Rome, Italy, March 2003, pp. 325-336.

MacMillan, R.A., 2003. LandMapR© Software Toolkit- C++ Version: Users manual. LandMapper Environmental Solutions Inc., Edmonton, AB. 110 p.

Papiernik, S.K., Linstrom, M.J., Schumacher, J.A., Farenshorst, A., Stephens, K.D., Schumacher, T.E., Lobb, D.A., 2005. Variation in soil properties and crop yield across and eroded prairie landscape. J. Soil Water Conservation 60, 388-395.

Pennock, D.J., 2003. Terrain attributes, landform segmentation, and soil redistribution. Soil Tillage Research 69, 15-26.

Pennock, D.J., Corre, M.D., 2001. Development and application of landform segmentation procedures. Soil Tillage Research 58, 151-162.

Pennock, D.J., McCann, B.L., de Jong, E., Lemmen, D.S., 1999. Effects of soil redistribution on soil properties in a cultivated Solonetzic-Chernozemic landscape of southwestern Saskatchewan. Can. J. Soil Science 79, 593-601.

Quine, T.A, Govers, G., Walling, D.E., Zhang, X., Desmet, P.J.J., Zhang, Y., Vandaele, K., 1997. Erosion processes and landform evolution on agricultural land - new

perspectives from caesium-137 measurements and topographic-based erosion modelling. Earth Surface Processes and Landforms 22, 799-816.

SAS institute, Inc., 2002. SAS® 9 help and documents. SAS Institute, Inc., Cary, NC 27513, USA.

Schumacher, J.A., Kaspar, T.C., Ritchie, J.C., Schumacher, T.E., Karlen, D.L., Venteris, E.R., McCarty, G.W., Colvin, T.S., Jaynes, D.B., Lindstrom, M.J., Fenton, T.E., 2005. Identifying spatial patterns of erosion for use in precision conservation. J. Soil Water Conservation 60, 355-362.

Schumacher, T.E., Lindstrom, M.J., Schumacher, J.A., Lemme, G.D., 1999. Modeling spatial variation in productivity due to tillage and water erosion. Soil Tillage Research 51, 331-339.

Renard, K.G., Foster, G.R., Weesies, G.A., McCool, D.K., Yoder, D.C., 2001. Predicting soil erosion by water - a guide to conservation planning with the revised universal soil loss equation (RUSLE). Agriculture Handbook No. 703, USDA-ARS, Washington, D.C.

Van Oost, K., Govers, G., Desmet, P., 2000. Evaluating the effects of changes in landscape structure on soil erosion by water and tillage. Landscape Ecology 15, 577-589.

Wall, G.J., Coote, D.R., Pringle, E.A., Shelton, I.J. (Eds), 2002. RUSLEFAC --- Revised Universal Soil Loss Equation for Application in Canada: A handbook for estimating soil loss from water erosion in Canada. Research Branch, Agriculture and Agri-Food Canada. Ottawa. Contribution No. 02-92. 117pp.

Walling, D.E., 1998. Use of ^{137}Cs and other fallout radionuclides in soil erosion investigations: Progress, problems and prospects. In: Use of ^{137}Cs in the study of soil erosion and sedimentation, IAEA-TECDOC-1028, pp 117-121.

Walling, D.E., He, Q., 2001. Models for converting ^{137}Cs measurements to estimates of soil redistribution rates on cultivated and uncultivated soils, and estimating bomb-derived ^{137}Cs reference inventories (including software for model implementation). A Contribution to the IAEA Coordinated Research Programmes on Soil Erosion (D1.50.05) and Sedimentation (F3.10.01).

3.8 Nomenclature

BSL	backslope
C-factor	cover / management factor (dimensionless ratio)
CBS	convergent-backslope
CR	crest
DBS	divergent-backslope
DSH	divergent-shoulder
E_{Cs}	^{137}Cs estimated total soil erosion, positive for soil loss, negative for soil accumulation (Mg ha^{-1} yr^{-1})
E_{Ti}	TillEM estimated tillage erosion, positive for soil loss, negative for soil accumulation (Mg ha^{-1} yr^{-1})

E_{TiC}	TillEM estimated tillage erosion on the Deerwood site using the Cyrus site's tillage erosivity data, positive for soil loss, negative for soil accumulation (Mg ha^{-1} yr^{-1})
E_{Usle}	WaTEM estimated water erosion, positive for soil loss, negative for soil accumulation (Mg ha^{-1} yr^{-1})
$E_{Usle+Ti}$	the sum of WaTEM estimated water erosion and TillEM estimated tillage erosion, positive for soil loss, negative for soil accumulation (Mg ha^{-1} yr^{-1})
E_{Wepp}	WEPP estimated water erosion, positive for soil loss, negative for soil accumulation (Mg ha^{-1} yr^{-1})
E_{WeppC}	WEPP estimated water erosion on the Deerwood site using the Cyrus site's climate, management and soil data, positive for soil loss, negative for soil accumulation (Mg ha^{-1} yr^{-1})
$E_{Wepp+Ti}$	the sum of WEPP estimated water erosion and TillEM estimated tillage erosion, positive for soil loss, negative for soil accumulation (Mg ha^{-1} yr^{-1})
$E_{WeppC+TiC}$	the sum of WEPP estimated water erosion and TillEM estimated tillage erosion on the Deerwood site using the Cyrus site's climate, management, soil and tillage erosivity data, positive for soil loss, negative for soil accumulation (Mg ha^{-1} yr^{-1})
FSL	footslope
H_{MBM2}	the relaxation mass depth of the initial distribution of fallout ^{137}Cs in the soil profile used in MBM2 (kg m^{-2})
K-factor	soil erodibility factor (Mg ha h ha^{-1} MJ^{-1} mm^{-1})
k_{Tc}	Transport capacity coefficient used in WaTEM (m)

LE	landform element
LOW	lower-slope
M	the mass of soil per unit area above a specified base elevation (kg m^{-2})
MBM2	Mass Balance Model 2 in the Cs-137 Erosion Calibration Models software
MBM3	Mass Balance Model 3 in the Cs-137 Erosion Calibration Models software
MID	mid-slope
NAGP	North American Great Plains
P-factor	support practice factor (dimensionless ratio)
P_{MBM2}	particle size correction factor used in MBM2 (dimensionless ratio)
R-factor	rainfall-runoff erosivity factor (MJ mm ha^{-1} h^{-1} yr^{-1})
REGWQ test	Ryan-Einot-Gabriel-Welsch multiple-range test
RUSLE	Revised Universal Soil Loss Equation
s	the length in any specified horizontal direction (m)
SH	shoulder-slope
t	time (yr)
TillEM	Tillage Erosion Model
T_M	translocation in mass over a unit width of tillage (kg m^{-1} $pass^{-1}$)
TSL	toeslope
UDE	upper-depression
UP	upper-slope
WaTEM	Water and Tillage Erosion Model
WEPP	Water Erosion Prediction Project

α the intercept of the linear regression equation, representing tillage translocation unaffected by slope gradient or slope curvature and indicating the dispersivity of the given tillage operation (kg m^{-1} $pass^{-1}$)

β the coefficient for slope gradient, representing the extra tillage translocation due to slope gradient and indicating the erosivity of the given tillage operation (kg m^{-1} $\%^{-1}$ $pass^{-1}$)

γ the coefficient for slope curvature, representing the extra tillage translocation due to slope curvature and indicating the erosivity of the given tillage operation (kg m^{-1} ($\%^{-1}$ m) $pass^{-1}$)

γ_{MBM2} the proportion of the annual ^{137}Cs input susceptible to removal by erosion used in the MBM2 model (dimensionless ratio)

θ slope gradient, positive when downslope and negative when upslope (%)

φ slope curvature, positive for convex and negative for concave (% m^{-1})

ρ dry soil bulk density (kg m^{-3})

4. MODELING TILLAGE-INDUCED REDISTRIBUTION OF SOIL MASS AND ITS CONSTITUENTS WITHIN DIFFERENT LANDSCAPES*

4.1 Abstract

Tillage is a driving force of soil movement in cultivated fields. Soil constituents, together with the mass of soil, are redistributed over landscapes by tillage. The pattern of tillage-induced soil constituent redistribution is not determined by the pattern of tillage-induced soil mass redistribution alone because the translocation extent and the transfers between the till-layer and the subsoil layer also strongly affect soil constituent redistribution.

In this study, we used a convoluting procedure and developed a model (TillTM) to simulate the tillage translocation process, by which to demonstrate tillage-induced soil mass and soil organic carbon (as an example of soil constituents) redistribution on four hypothetical landscapes: plane slope, symmetric hill, asymmetric hill and irregular hill, under different tillage patterns and over different temporal scales. The model was

* Li, S., Lobb, D.A. (University of Manitoba), Lindstrom, M.J. (USDA-ARS, retired), Papiernik, S.K. (USDA-ARS) and Annemieke Farenhorst (University of Manitoba).

validated against field data collected at a site near Cyrus, Minnesota, USA. It was determined that tillage erosion is mainly dependent on topography and the effects of tillage pattern and temporal scale on tillage erosion are relatively minor. Soil constituent content in the till-layer is mainly determined by the number and size of soil loss positions in the landscape and the intensity of soil loss occurring on these positions. Net loss of soil organic carbon over the landscape occurs in the till-layer and this loss increases over time. In contrary, increase of soil organic carbon content in the sub-layer occurs at soil accumulation positions. The application of the TillTM on the Cyrus site demonstrated that using the model, the pattern of soil organic carbon and inorganic carbon redistribution can be precisely estimated and it is possible to use a simpler diffusion model to assess the pattern of the soil constituent redistribution through the estimation of tillage erosion.

4.2 Introduction

The redistribution of soil mass and soil constituents has important implications for the understanding of the variation of soil properties within landscapes. It has been recognized that tillage erosion is a major cause of soil mass redistribution in cultivated landscapes (Govers et al., 1999). During tillage, soil constituents are translocated together with the soil mass. The redistribution of soil constituents is strongly affected by the redistribution of soil mass. In addition, it is affected by the mixing of subsoil into the till-

layer. For example, on convex positions, due to tillage-induced soil loss, organic-poor subsoil is exposed and brought up into the till-layer, which results in the decrease of soil organic carbon (OC) content in the till-layer. During the subsequent tillage, the OC-diluted soil is translocated to further distances and eventually will propagate over the landscape and will cause a decrease in OC content in the till-layer over the entire landscape, even in concave positions, where soil mass is accumulated. Similarly, in landscapes with high-carbonate parent materials, tillage can cause an increase in soil inorganic carbon (IC) in the till-layer due to the transfer of carbonate-rich subsoil into the till-layer (De Alba et al., 2004). This vertical mixture of soil from different soil horizons induced by tillage is referred to as the mixing effect herein. In order to investigate the redistribution of soil constituents, the redistribution of soil mass and the mixing effect both must be taken into account.

Studies of tillage translocation and tillage erosion have been focused on the redistribution of soil mass. A diffusion model, proposed by Lindstrom et al. (1990) and Govers et al. (1994), is used and developed by researchers worldwide to describe tillage translocation in different tillage systems (e.g. Quine et al., 1997; Lobb and Kachanoski, 1999*a*; Li et al., Chapter 2). In the diffusion models, the intensity of tillage translocation is generally characterized by the tillage transport coefficient(s) but no information is provided on the transferring of surface soil and subsoil. Kachanoski et al. (1984) analyzed the possible effect of vertical mixture due to tillage translocation. Lobb (1997) demonstrated the impact of the dispersion of translocated soil and the mixing effect on the redistribution of ^{137}Cs. Lobb and Kachanoski (1999*b*) suggested the use of an exponential function to simulate tillage translocation. Van Oost et al. (2000) proposed the

use of a convoluting procedure to simulate the translocation process and established a model to predict soil constituent redistributions. In further studies, Van Oost et al. (2003*a*, *b*) extended this model to two dimensions, which accounts for both forward and lateral translocation. These researchers concluded that the convoluting procedure is superior to the diffusion model in estimating tillage-induced soil constituent redistribution.

We propose to improve upon these preceding studies by furthering the investigation into the redistribution of soil mass and soil constituents under the context of different topographic features, tillage patterns and temporal scales. Unlike flat landscapes, topographically complex landscapes usually include isolated convexities so that there are more areas of tillage-induced soil loss and, therefore, more sources of subsoil transfer into the till-layer. The tillage pattern can also affect the redistribution of soil mass and soil constituents. For example, when there is a predominant tillage direction, continuous soil output from the start-boundary can result in the mixing of subsoil into the till-layer in the start-boundary region. This mixed soil (including the subsoil material) will be continuously spread out over the rest of the landscape. Temporal scales affect the expression of tillage-induced redistribution of soil mass and soil constituents. The mixing effect is limited by the translocation distance and may only propagate further under continuous tillage.

Furthermore, although the convoluting procedure is considered to be more sophisticated, it requires more detailed information about the translocation process, which is not available in most cases. The diffusion model, on the other hand, requires less data but still provides acceptable accuracy in estimating the redistribution of soil mass. It is important for future modeling practices to examine the differences between the

redistribution of soil mass and the redistribution of soil constituents, and to evaluate the possibility of using the diffusion model to predict soil constituent redistribution.

The objectives of this study were: 1) to examine the redistribution of OC (as an example of soil constituents) and soil mass on landscapes with different topographic features, particularly on topographically complex landscapes; 2) to investigate the effects of tillage patterns (directions) and temporal scales on the redistribution of OC and soil mass; 3) to compare the differences and/or correlations between the redistribution of soil mass and soil constituents; and 4) to evaluate to what extent the redistribution of soil constituents could be explained by the redistribution of soil mass.

4.3 Materials and Methods

4.3.1 Tillage Translocation Simulation

A convoluting procedure was used in this study to simulate tillage translocation. Considering the landscape to be a series of adjacent sections, a given section receives soil translocated from its preceeding sections (Figure 4.1.a). Soil in this given section is translocated into subsequent sections as well. The mass of soil in this given section after one tillage operation is the summation of all the soil translocated from its proceeding sections plus the soil in this given section that has not been translocated elsewhere. The process can be described using a continuous form function as:

$$S^a(x) = \int_0^x S^b(y)\, PD_y(x)\, dy \qquad (1)$$

where

x, y are the distances from the original point (m);

S^a (x) is the mass of soil per meter width at x after tillage operation (kg m^{-1});

S^b (y) is the mass of soil per meter width at y before tillage operation, which is a constant when tillage depth and soil bulk density are considered to be uniform across the landscape (kg m^{-1}); and

PD_y (x) is the probability density of soil translocated from y to x (kg kg^{-1} m^{-1}).

The translocation probability density, PD_y (x), was simulated using an exponential function (Lobb and Kachanoski, 1999*b*):

$$PD_y(x) = \frac{1}{d_y} \exp\left(-\frac{x-y}{d_y}\right) \qquad (0 \le x - y \le \infty) \tag{2}$$

where

d_y is the mean translocation distance at y (m).

Equation (1) and (2) were converted into discrete numeric forms as:

$$S^a(x') = \sum_{y'=0,+I}^{x'} \left(S^b(y') P_{y'}(x')\right) \tag{3}$$

$$P_{y'}(x') = \begin{cases} 1 - \exp\left(-\dfrac{I/2}{d_{y'}}\right) & (x' = y') \\ \dfrac{I}{d_{y'}} \exp\left(-\dfrac{x'-y'+I/2}{d_{y'}}\right) & (0 \le x' - y' \le D_{max}) \\ 0 & (x' - y' > D_{max}) \end{cases} \tag{4}$$

where

x', y' are the distances from the original point to the center of the sections (m);

$P_{y'}$ (x') is the probability of soil translocated from the section centralized at y' to the section centralized at x' (kg kg^{-1});

I is data interval (m);

D_{max} is the maximum translocation distance. The probability of soil being translocated beyond this range was assumed to be zero (m).

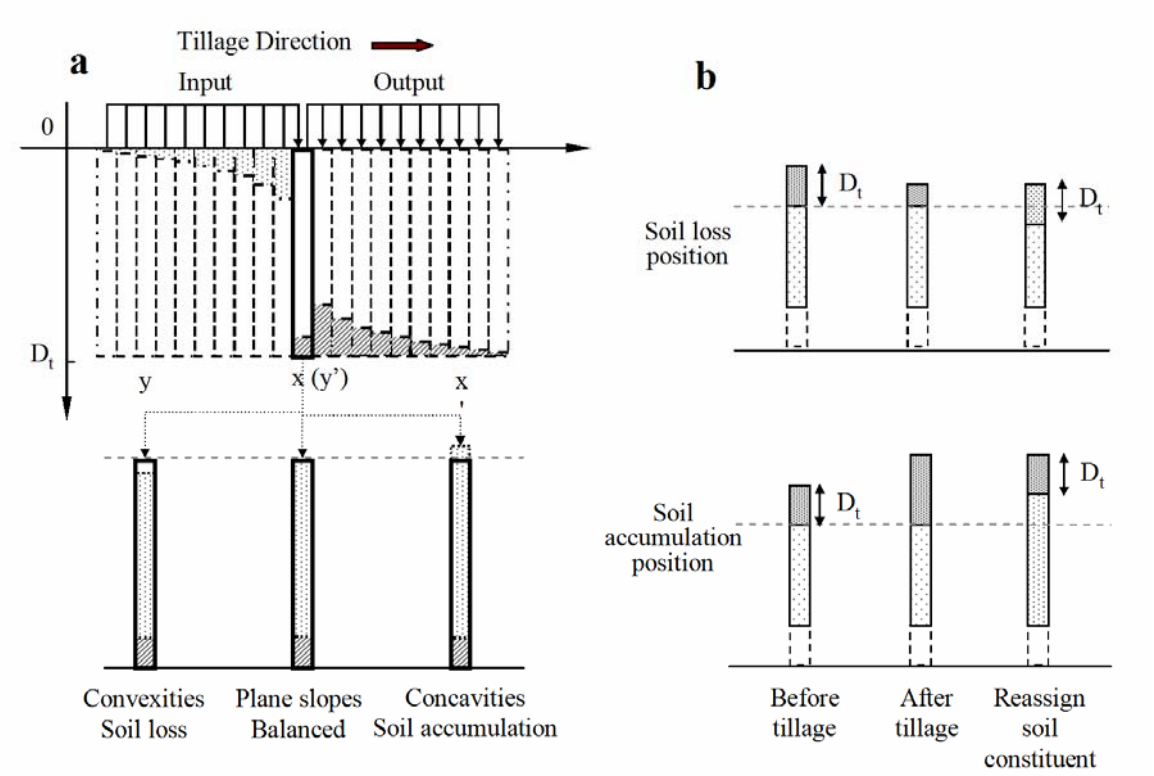

Figure 4.1 Illustrations of: a. tillage translocation process; and b. reassignment of soil constituent after tillage.

The mean translocation distance ($d_{y'}$) in Equation (4) determines the shape of the soil distribution curve, i.e. how much soil is translocated to which distance. In mathematical terms, $d_{y'}$ is the expected value (mean) of the distribution function, and indicates the average distance of the soil being translocated. The variation of the distribution function, which is an indicator of the dispersion of the translocated soil, is

$d_{y'}$[2]. The value of $d_{y'}$ varies across the landscape. Several factors contribute to this variation. Previous studies has proven that for a given tillage implement or tillage sequence, the value of $d_{y'}$ is mainly determined by topographic features, i.e. slope gradient and/or slope curvature, at location y' (e.g. Lindstrom et al., 1992; Lobb et al., 1999; Li et al., Chapter 2). A linear function was commonly used to calculate $d_{y'}$:

$$\mathbf{d}_{y'} = \mathbf{A} + \mathbf{B}\,\boldsymbol{\theta}_{y'} + \mathbf{C}\,\boldsymbol{\varphi}_{y'} \qquad (5)$$

where

A is tillage translocation distance on level land (m);

B is additional tillage translocation due to the effect of slope gradient (m $\%^{-1}$);

$\theta_{y'}$ is slope gradient at y' (%);

C is additional tillage translocation due to the effect of slope curvature ($m^2\ \%^{-1}$);

$\varphi_{y'}$ is slope curvature at y' (% m^{-1}).

The values of A, B and C characterize the dispersivity and erosivity of the tillage implements (Li et al., Chapter 2). They are determined by implement type, tillage speed, tillage depth and various soil properties (Lobb et al., 1999a). For a certain tillage implement or tillage sequence, the values of A, B and C are calibrated with field tillage translocation experiments. In this study, A, B and C were assumed to equal 1 m, 0.02 m $\%^{-1}$, 0.04 $m^2\ \%^{-1}$ for one full sequence (one year), respectively, which represents a typical conventional tillage system (with mouldboard plough) in corn production in the northern North American Great Plains (Lindstrom et al., 1992; Lobb and Kachanoski, 1999*a*; Schumacher et al., 1999).

4.3.2 Soil Mass and Soil Constituent Redistribution

Tillage erosion (soil mass loss or gain due to tillage) at a given location is calculated by the differences in the soil mass before and after a tillage operation:

$$TE(x') = (S^a(x') - S^b(x')) = S^b(x')\left[\left(\sum_{y'=0,+I}^{x'} P_{y'}(x')\right) - 1\right] \quad (6)$$

where

TE (x') is net soil mass accumulation per meter width at x' after the tillage operation, a negative value indicating net soil loss (kg m^{-1})

Since S^b was considered to be a constant across the landscape, the variation of tillage erosion (TE) is solely determined by the integration term in Equation (6). When the integration term is less than one, soil loss occurs (Figure 4.1.a, convexities); when the integration term equals to one, input and output soil is balanced and no soil loss or soil accumulation occurs (Figure 4.1.a, plane slopes); when the integration term is greater than one, soil accumulation occurs (Figure 4.1.a, concavities).

A similar procedure was used to simulate soil constituent redistribution:

$$C^a(x') = \sum_{y'=0,+I}^{x'} \left(C^b(y')\, P_{y'}(x')\right) \quad (7)$$

where

C^a (x') is the amount of a soil constituent at location x' after the tillage operation (kg m^{-1}); and

C^b (y') is the amount of a soil constituent at location y' before the tillage operation (kg m^{-1}).

In contrast to S^b, the amount of a soil constituent before the tillage operation, C^b, varies over the landscape and over time, so that both C^b and P_y (x) affect C^a.

4.3.3 TillTM

A Tillage Translocation Model (TillTM) was developed and written in Visual Basic 6.0 ® code. TillTM is a two-dimensional model (in the horizontal and vertical dimensions). The inputs for the TillTM are the topography data and soil constituent concentration as a function of depth at a series of data points along the tillage direction. Three layers are defined for the input data, the up-layer, the mid-layer and the bottom-layer (Table 4.1). The model runs in loops. Each loop represents one tillage operation or one full sequence of tillage operations (e.g. one year). In every loop, TillTM calculates the variations of elevation at every data point using Equations (3) to (6). After the first loop, the depth of up-layer is set as that of the till-layer. The output from one loop is used as the input for the next loop.

Table 4.1 Summaries of the initial TillTM inputs for the hypothetical landscapes and the transect at the Cyrus site.

	Depth	Bulk Density *	Organic carbon			Inorganic carbon		
			Content	Decay	Input	Content	Decay	Input
	m	kg m^{-3}	%	% yr^{-1}	kg m^{-2} yr^{-1}	%	% yr^{-1}	kg m^{-2} yr^{-1}
Hypothetical landscapes								
Up-layer †	0 - 0.20	1000	2.50	1.0	0.05	--	--	--
Mid-layer	0.20 - 0.50	1200	0.25	0	0	--	--	--
Bottom-layer	0.50 - ∞	1300	0.05	0	0	--	--	--
The transect at the Cyrus site								
Up-layer †	0 - 0.25	1110	2.70	0	0	1.0	0	0
Mid-layer	0.25 - 0.50	1230	0.70	0	0	2.0	0	0
Bottom-layer	0.50 - ∞	1300	0.20	0	0	3.0	0	0

* bulk density of the fine earth portion.
† set at tillage depth in this study.

The simulation of soil constituent redistribution involves two steps. Firstly, for a given data point, the resulting soil constituent content in the active-till-layer after tillage

is calculated using Equation (7). Soil constituent concentration within this active-till-layer was assumed to be uniform after every tillage operation. Secondly, Soil constituents are reassigned for the next tillage sequence according to the change of elevation (soil mass loss or gain). On soil loss positions, after tillage, there is a net output of soil mass from the active-till-layer (Figure 4.1.b. soil loss position). During the next tillage operation, tillage depth will exceed the depth of the original active-till-layer and tillage implement will cut into the mid-layer. The top of the original mid-layer becomes a part of the current-till-layer and, therefore, soil constituents in this part of the mid-layer are assigned to the current-till-layer and the depth of the mid-layer decreases accordingly. The mid-layer may eventually disappear on a soil loss position and in which case, the current-till-layer sits directly on the bottom-layer, which is assumed to be the parent material layer. In contrast, on soil accumulation positions, there is a net input of soil mass into the active-till-layer after tillage (Figure 4.1.b. soil accumulation position). During the next tillage operation, tillage implements will not be able to reach the bottom part of the original active-till-layer. Soil constituents in this untouched part of the active-till-layer are assigned to the mid-layer.

Five-meter width buffer zones were added to both ends (boundaries) of the landscapes. The curves in the buffer zone were made so that the slope gradient gradually changes to zero. This is based on the fact that in most cases, boundary areas of fields are flat. Soil mass and soil constituent loss or gain was averaged within the buffer zones after every tillage sequence to simulate tilling the headlands (usually contour tillage) in the field boundary areas. The buffer zone data were excluded from the analysis.

A simplified routine was incorporated into the TillTM to simulate the decay or

enrichments of soil constituent due to other processes. For example, OC was assumed to decompose at constant rates (decay rate) in different layers. Meanwhile, a constant amount of OC was added into the till-layer annually to simulate the input of OC from residues and manure applications (Table 4.1).

4.3.4 Hypothetical Landscapes

Hypothetical elevation data were generated to represent four landscapes: Plane Slope (PS), Symmetric Hill (SH), Asymmetric Hill (AH) and Irregular Hill (IH). The PS is a straight line with a constant slope gradient of 10 %. The SH has two symmetric side slopes with the summit in the middle (100 m). The AH has two asymmetric side slopes (i.e. one side slope is shorter and steeper than the other side slope), with the summit to the left of middle (50 m). The IH is a secondary fine-scale variation added onto the SH, representing a more complex landscape with secondary topographic features. Similar to the SH, the IH is symmetric in nature. All the four hypothetical landscapes have the same length, data density (0.1 m interval, 2001 data points), and average absolute value of slope gradient and approximately the same average slope curvature (Table 4.2). Furthermore, for the three hills (SH, AH, IH), the percentages of convex and concave portions are also the same. The differences between these four landscapes lie in the different ranges and variations of slope gradient and slope curvature. From PS to SH to AH, the ranges of slope gradient and slope curvature increase. IH has the widest range of slope curvature (-2.36 to 2.32 % m^{-1}) but its range of slope gradient (absolute value, 0.0 to 22.0 %) is narrower than that of AH (absolute value, 0.0 to 30.6 %).

Other initial input data for TillTM are summarized in Table 4.1. The amount of

OC input equals the decomposed OC if there were no tillage-induced OC redistribution. This was set so that the resulting redistribution of OC can be attributed solely to tillage translocation.

Table 4.2 Characteristics of the four hypothetical landscapes.

	Length	Data interval	Slope gradient *			Slope curvature †			
			Ave	Max	Min	Ave	Max	Min	Convex ‡
	m	m	%	%	%	% m^{-1}	% m^{-1}	% m^{-1}	%
Plan Slope (PS)	200	0.10	10.0	10.0	10.0	0.00	0.00	0.00	--
Symmetric Hill (SH)	200	0.10	10.0	15.7	0.0	0.00	0.49	-0.49	50
Asymmetric Hill (AH)	200	0.10	10.0	30.6	0.0	0.06	1.40	-1.84	50
Irregular Hill (IH)	200	0.10	10.0	22.0	0.0	0.00	2.32	-2.36	50

* absolute value of slope gradient.

† positive for convex positions and negative for concave positions.

‡ the percentage of the convex portion.

Three tillage patterns have been examined, i.e. forward, backward and alternating-direction tillage directions. In the forward and backward directions, tillage is conducted on the same direction every year, i.e. always forward or always backward. In alternating directions, tillage is conducted in opposite directions at the same frequency, i.e. one forward followed by one backward. For the two symmetric landscapes (SH and IH), forward and backward tillage are the same so only forward tillage was simulated. The model was run for 2, 10 and 50 yrs, representing the short-, medium- and long-term temporal scales, respectively.

4.3.5 Model Validation ---- The Cyrus Site

The model was validated using data collected in a field located near the town of

Cyrus, in west central Minnesota, USA. The study area (2.7 ha) is an undulating landscape and features a trough in the western part, a knoll in the middle and a slightly concave slope towards the eastern side of the field (Figure 4.2). The field has been cultivated for approximately 100 yrs and has been under conventional tillage (annual mouldboard plough and tandem disc) for more than 40 yrs. Tillage was conducted in west-east directions, alternately. Major crops grown in this field are corn, winter wheat and soybean. Most of the soils in this field site are of the Mollisol soil order in the USDA taxonomy and are fine loamy, deep, and moderately to well drained. Soil parent material is carbonate-rich Wisconsin-aged glacial till. Previous studies suggested that both water and tillage erosion contribute to soil redistribution in this field but the major pattern of soil redistribution is dominated by tillage erosion (De Alba et al., 2004; Papiernik et al., 2005; Li et al., Section 3.4.2).

Along a transect across the mid-slope in the study area, 19 soil cores were collected to a depth of 1.40 – 1.50 m at approximately 10 m density (Figure 4.2). The locations of the sample points were surveyed using a Trimble AgGPS-132 system with differential correction. Soil samples were sectioned by genetic horizons and were then air-dried and sieved through a 2-mm screen. The fine earth portion (soil particles < 2 mm in diameter) was subsampled for total carbon (TC) and inorganic carbon (IC) analysis, using a LECO 2000 CN analyzer and a pressure calcimeter, respectively. Soil organic carbon (OC) was determined by the difference between TC and IC. OC and IC contents for horizons (with various depth-ranges for different sample points) were weighted based on depth and were converted to an area (volume) basis as the mass of OC and IC within 0 – 0.25 m and 0.25 –1.00 m depth over a unit area. Samples were also taken at five

landscape positions (summit to footslope) on an adjacent grassed hillslope that had no documented history of cultivation. The same procedures as those used for the transect samples were used to determine the area-based OC and IC contents.

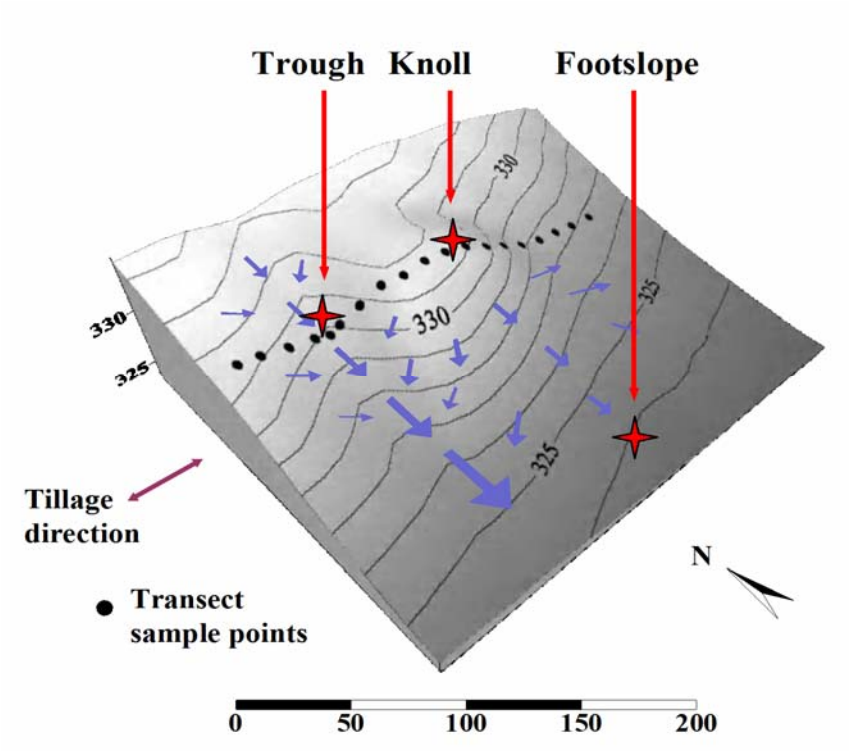

Figure 4.2 Topography at the Cyrus site and the locations of the sample points.

Tillage-induced OC and IC redistributions along the transect over the past 100 yrs were simulated using TillTM. The model inputs are summarized in Table 4.1. The surveyed current elevation data were used since the elevation data prior to the broken of the field are not available. A SPLINE function was used to interpolate the elevation data to 0.1 m density. The initial OC and IC contents were assumed to be uniform across the transect and were calculated by averaging the OC and IC contents, respectively, of the samples taken at the mid-slope positions on the grassed hillslope. Soil bulk density (fine

earth) was also assumed to be uniform across the transect and was determined for each layer by averaging those of the transect samples and the grassed hillslope samples. In addition, soil bulk density was assumed not subject to change over time. Tillage pattern in TillTM was set as alternating and the A, B and C values were set as the same as those used for the hypothetical slopes. For tillage erosion simulation, the model was run for 2 loops. The output tillage erosion rates, therefore, represent the current intensity of tillage erosion. For OC and IC simulation, the model was run for 100 loops to represent the past 100 yrs. No change was applied to the elevation as a result of ongoing tillage erosion in the OC and IC simulation, i.e. the surveyed elevation data were used for all the 100 loops. This was done because the current elevation is already smoother than it was 100 yrs ago and including the feedback of tillage erosion on elevation will make the elevation further smoothed after every loop and, therefore, more different from that of the past. Also, no decay rate and annual input of OC or IC were applied due to the lack of data. The output OC and IC content were also converted to an area (volume) basis as the mass of OC and IC within 0 – 0.25 m and 0.25 –1.00 m depth over a unit area. The performance of TillTM was evaluated using the correlation coefficients between the field measurements and the model estimates.

To examine the profile distribution of soil constituents in detail, 2-cm depth increment samples were taken at one baseline location and three locations within the field (knoll, trough and footslope, Figure 4.2). The baseline point is located on a level position in an adjacent grassed land with no documented cultivation in its history. At each of these four locations, seven cores were taken and samples from the same depth range were mixed together, air-dried and sieved (2-mm screen). ^{137}Cs radioactivity of these samples

was detected at 662 keV using Broad Energy Germanium Gamma spectrometers (Canberra BE3830, Landscape Dynamics Laboratory, University of Manitoba, Canada) with counting time ranging from 4 to 12 hrs, providing a detection error < 10 %. January 1, 2000 was used as the reference date of ^{137}Cs radioactivity. Subsamples (5 – 10 g) were taken and were digested with 6 N HCl to eliminate the IC. Carbon content in the digested samples, which is considered as OC content, was detected using a LECO CN analyzer.

4.4 Results and Discussion

The results of TillTM simulation for the four hypothetical landscapes are shown in Figure 4.3 to Figure 4.6. In these figures, the Elevation charts show the initial elevation (0 yr). For each tillage pattern there are three charts: the Tillage erosion charts show the average tillage erosion rates of 0 – 2 yr, 2 – 10 yr and 10 – 50 yr; and the Till-layer OC and Profile OC charts show the amount of OC within the depth of 0 – 0.20 m (the tillage depth) and 0 – 1.00 m, respectively, after the given years of tillage.

4.4.1 Tillage Erosion

The patterns of tillage erosion on all four hypothetical landscapes were primarily determined by topography. On the Plane Slope (PS), most of the landscape in the middle showed neither soil loss nor soil accumulation. This is because slope gradient is uniform on the PS and, therefore, at a given location, the amount of output soil is exactly the same

as the amount of the input soil (Figure 4.3). On the three hills (SH, AH and IH), soil loss corresponded to convexities and soil accumulation corresponded to concavities. The intensity of tillage erosion (negative for soil loss and positive for soil accumulation) was negatively correlated with slope curvature (negative for concavities and positive for convexities), i.e. the higher the slope curvature was, the more intensive the soil loss was. This is clearly shown when comparing the tillage erosion pattern of the SH to that of the AS or IH. On the AS (Figure 4.5), tillage erosion was isolated in a narrower spatial range and erosion rates were higher than on the SH (Figure 4.4). This is due to the higher absolute values of slope curvature on the hilltop and on the steep side slope on the AS compared to those on the SH. On the IH, tillage erosion was mainly determined by the secondary (fine-scale) topographic features, i.e. soil loss on small convexities and soil accumulation on small concavities (Figure 4.6). Excluding the boundary areas, the local-tillage-erosion rate of IH was characterized by peaks and valleys or larger amplitude than those of the SH and the AH. However, the primary (coarse-scale) topographic features also affected the basic trend of tillage erosion, e.g. the highest local-soil-loss rate was found on the small convexities on the hilltop.

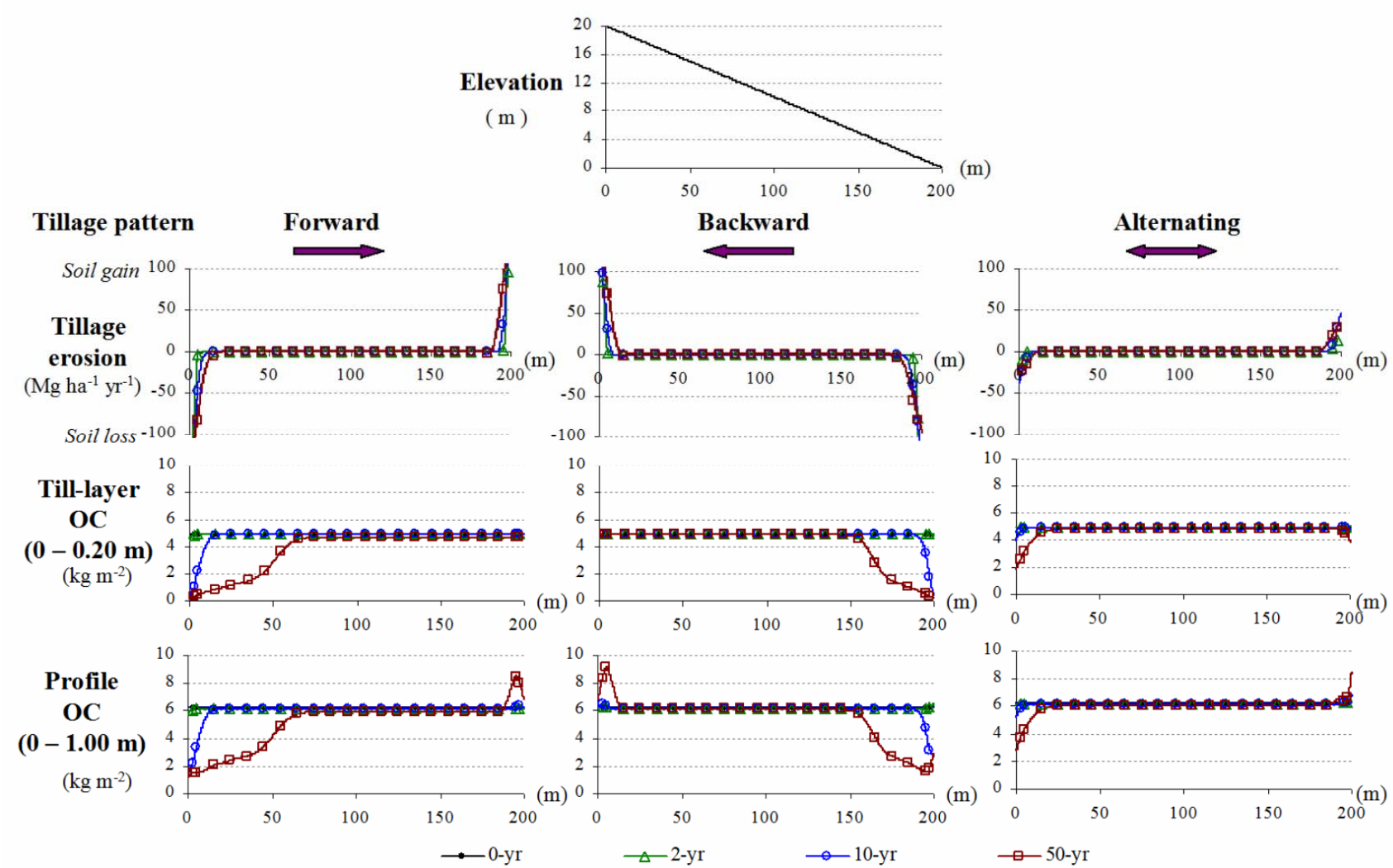

Figure 4.3 Tillage erosion and soil organic carbon (OC) redistribution on a hypothetical Plane Slope.

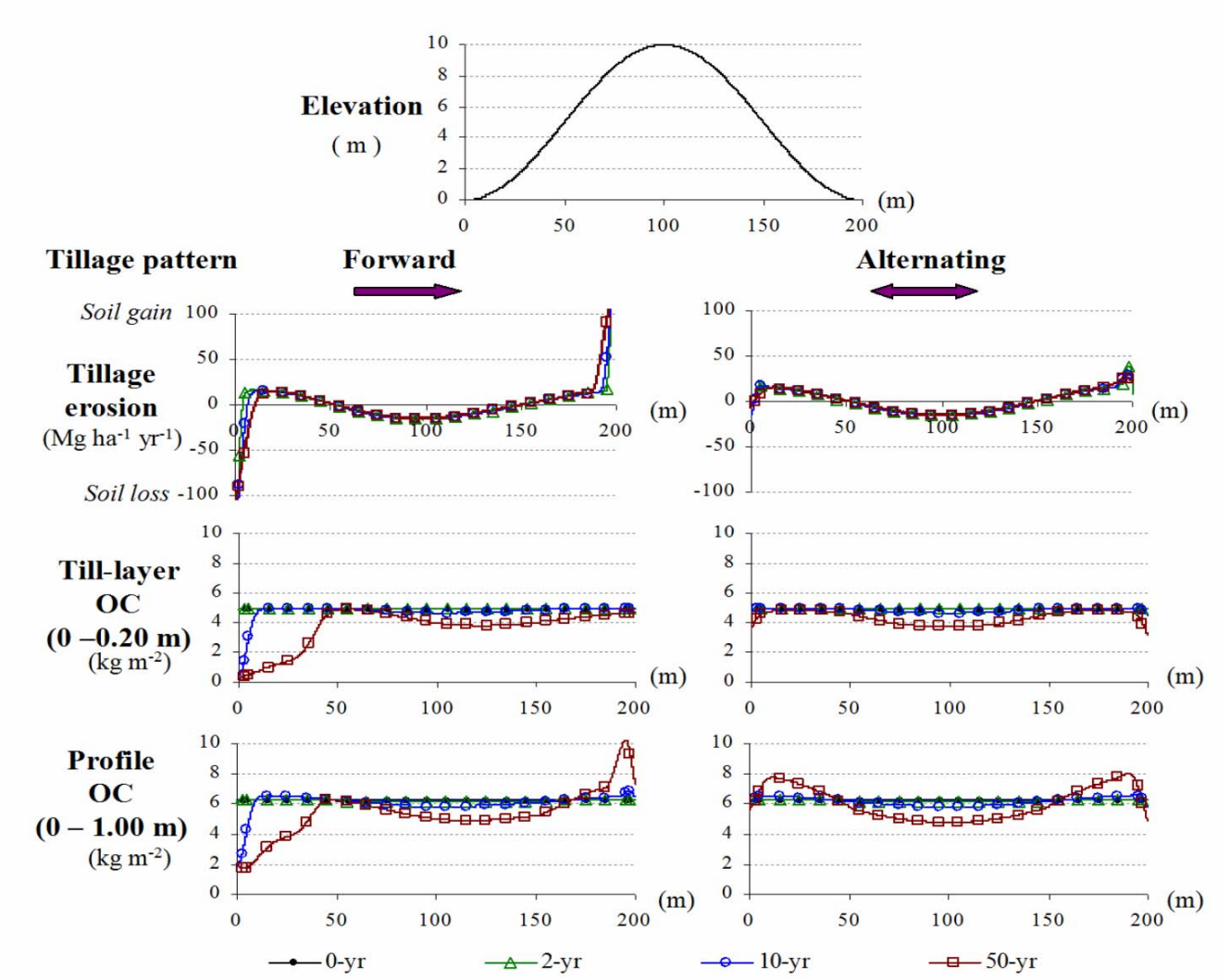

Figure 4.4 Tillage erosion and soil organic carbon (OC) redistribution on a hypothetical Symmetric Hill.

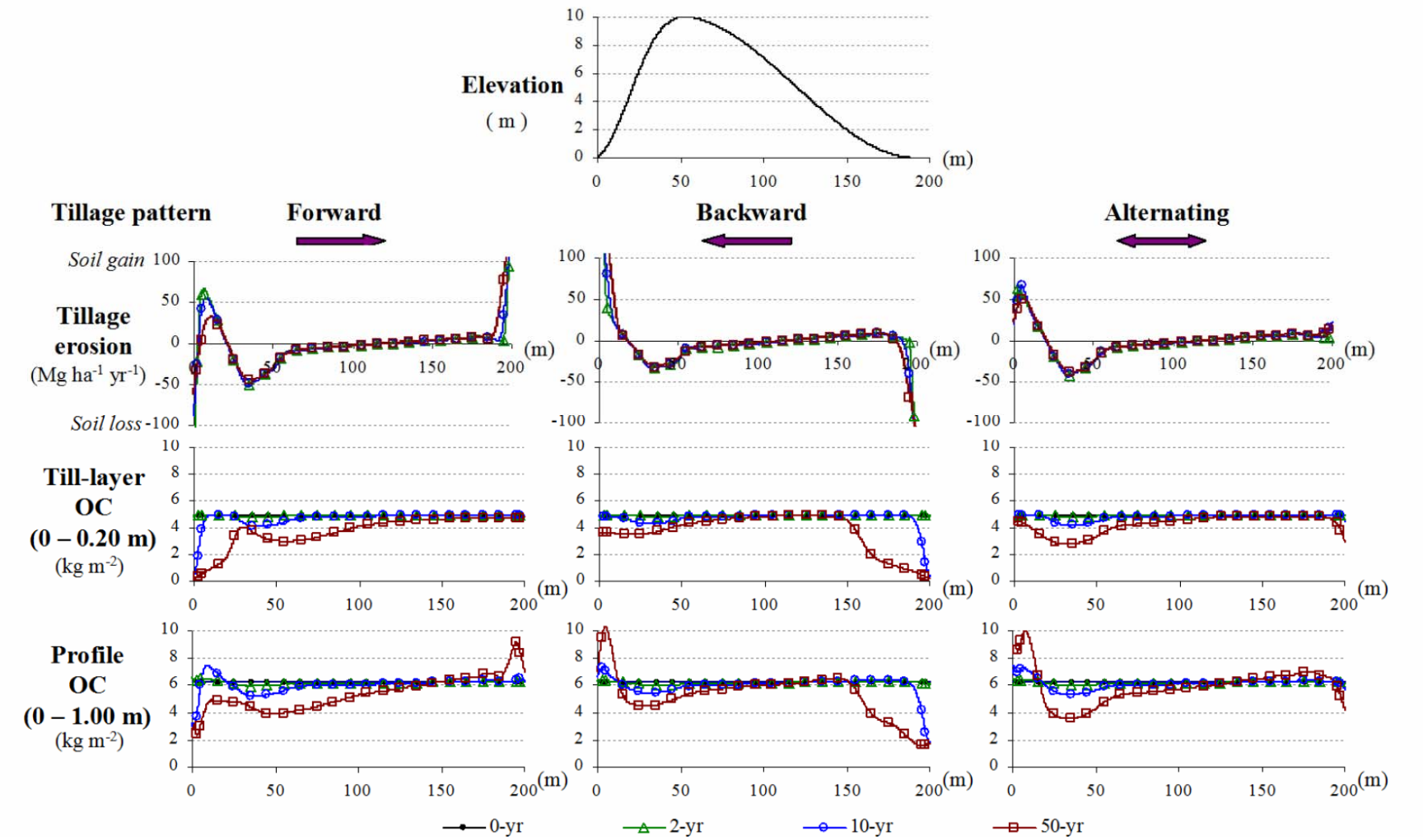

Figure 4.5 Tillage erosion and soil organic carbon (OC) redistribution on a hypothetical Asymmetric Hill.

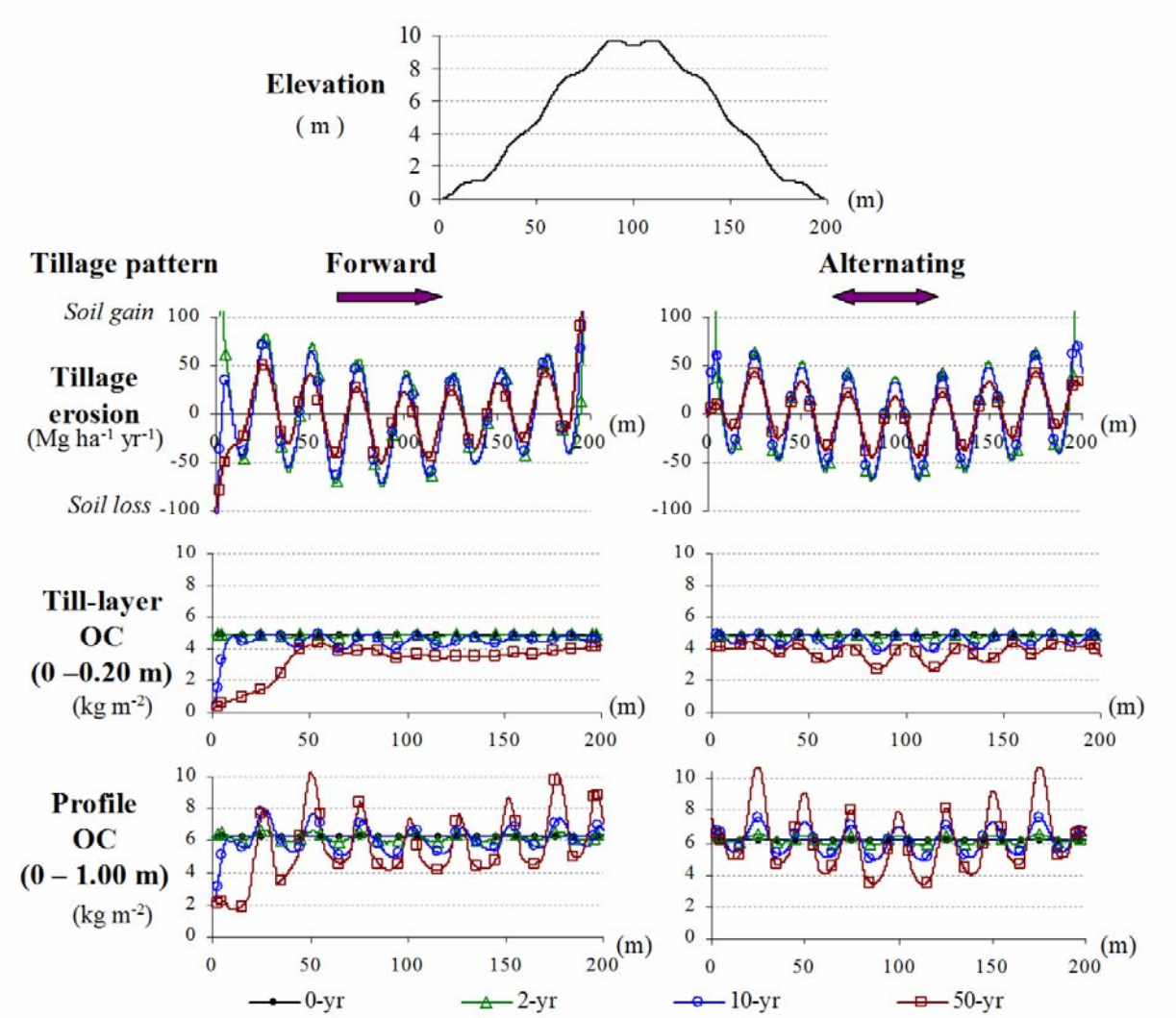

Figure 4.6 Tillage erosion and soil organic carbon (OC) redistribution on a hypothetical Irregular Hill.

Tillage pattern affected tillage erosion in the boundary areas. Under one-direction tillage (forward or backward tillage), the general pattern was characterized by soil loss near the start-boundaries and soil accumulation near the end-boundaries (referred to as boundary effect). The boundary effect was intensive under one-direction tillage but affected a limited distance, typically about 10 m from the boundary after 50 yrs of tillage (Figure 4.3 – 4.6). Under alternating-direction tillage, the boundary effect was considerably less intensive than that under one-direction tillage because the forward and backward translocation cancels each other. It is noteworthy that on the PS, even under alternating-direction tillage, noticeable soil loss occurred near the top (left boundary) and noticeable soil accumulation occurred near the bottom (right boundary, Figure 4.3). This agrees well with field evidence reported by several researchers that soil loss occurs on the downside of the field boundaries and soil accumulation occurs on the upside of the field boundaries (Govers et al., 1999).

Excluding the boundary areas, on the PS, SH and AH, tillage erosion rates were almost identical for all temporal scales, indicating that temporal scale has no noticeable effect on tillage erosion for topographically simple landscapes (Figure 4.3 – 4.5). However, on the IH, the peaks and valleys of the 2-yr curve had the highest amplitudes, those of the 50-yr curve had the lowest amplitudes and those of the 10-yr curve were in between (Figure 4.6). This is due to the feedback of tillage erosion on the topography. The ongoing tillage erosion planes off the small convexities and fills up the small concavities, i.e. the small convexities and concavities are gradually smoothed out. The smoothing of the topography, as a result of tillage erosion, causes the subsequent decrease of tillage erosion on this landscape over time.

4.4.2 Till-layer OC

Unlike tillage erosion, which was counted as a rate (the amount of soil mass loss or gain per year), Till-layer OC was counted as the total amount of OC in the till-layer. Till-layer OC content was lower than or equal to the initial OC level on all the four hypothetical landscapes after tillage, indicating that till-layer OC always decreases to some extent due to tillage translocation. The decrease of till-layer OC is a result of OC dilution due to the mixing effect, the transfer of OC-poor subsoil into the till-layer. The till-layer OC did not increase in soil accumulation locations because soil accumulation only increases the depth of the high-OC horizon, not the concentration of OC in the till-layer. The rate and spatial extent of till-layer OC loss were determined by the number and size of soil loss spots, which were the sources of transferring subsoil into the till-layer, and the extent of the tillage translocation. Topography, tillage pattern (direction) and the temporal scale all strongly affect the pattern and intensity of till-layer OC loss.

The pattern of till-layer OC loss varied dramatically over time. The general trend was that the longer the tillage period, the more profound the till-layer OC loss and the wider was the till-layer OC loss spread. In the short-term (2-yr), no noticeable till-layer OC loss was found on any landscape; in the medium-term (10-yr), till-layer OC loss occurred in the soil loss positions; and in the long-term (50-yr), more significant till-layer OC loss was observed. And, in addition, the spatial extent of till-layer OC loss went beyond the spatial extent of soil loss, in some cases across the entire landscape (e.g. on the IH, Figure 4.6).

Till-layer OC redistribution was also affected by tillage pattern. Under one-

direction tillage, intensive till-layer OC loss occurred near the start-boundaries in the medium-term (10-yr) and propagated to about 50 m in the long-term (50-yr). This is because the output of soil mass from the start-boundaries to the rest of the landscape, i.e. tillage continuously brings up subsoil and translocates it elsewhere. Under alternating-direction tillage, the till-layer OC loss in the boundary areas was much less intensive because the compensation of input and output of soil mass and, therefore, OC in forward and backward tillage.

Landscape topography, more specifically, the number of convexities and the slope curvature of these convexities, determined the pattern and rate of soil loss and, therefore, affected the pattern of till-layer OC redistribution. On PS, other than the boundary areas, there was no noticeable till-layer OC loss in the short- and medium-term (Figure 4.3). In the long-term, under both backward- (upslope) and alternating-direction tillage, no noticeable till-layer OC loss occurred in the non-boundary areas either. Under forward-(downslope) tillage, very slight till-layer OC loss was found from about 70 m to 200 m, indicating that OC-poor soil has been spread over from the start-boundary to the entire landscape through tillage translocation and has caused the slight decrease of OC in the non-boundary areas. In fact, this spreading out of the OC-poor soil also occurred under backward- (upslope) and alternating-direction tillage, but the effects were even weaker than that under forward-direction tillage so that were not expressed (Figure 4.3). The differences between forward (downslope) and backward (upslope) tillage directions lie in the different tillage translocation intensities: compared to that of upslope tillage, downslope tillage translocates soil further and, therefore, propagates the OC-poor soil from the start-boundary further and faster.

On the SH and the AH, the hilltop provides another source of OC-poor soil. Till-layer OC loss in the hilltops started to show up in the medium-term (Figure 4.4, 4.5). Compared to that on the SH, till-layer OC loss on the AS was more isolated. In the long-term, under alternating-direction tillage, till-layer OC loss extended beyond the soil loss area but the patterns of till-layer OC loss were similar to those of soil loss, e.g. maximum soil loss corresponded to maximum till-layer OC loss. In contrast, under one-direction tillage, till-layer OC loss shifted toward the tillage direction. For example, on the AH, under forward tillage for 50 yrs, maximum soil loss occurred at about 35 m, while till-layer OC content at 35 m (about 4.0 kg m^{-2}) was higher than that at 50 m (about 3.0 kg m^{-2}) (Figure 4.5). This is because along the tillage direction, a given point in the landscape only receives soil from its preceeding points and outputs soil to its subsequent points. At the point with the highest local soil loss rate, the OC content in the soil output is lower than that in the soil received because the maximum amount of subsoil is transferred into the till-layer by tillage at this point. Therefore, at subsequent points, the till-layer OC content is lower than that at the point of maximum soil oss. Under one-direction tillage, this difference compounds over time and causes a shift of maximum OC-loss-position from the maximum soil-mass-loss-position. This shifting effect has an implication in field sampling: the lowest till-layer OC might not always be found at locations with the highest soil loss rate.

Till-layer OC loss on the IH (Figure 4.6) was considerably more intensive than that on the SH or on the AH (Figures 4.4 and 4.5, respectively) because all the small convexities are sources of OC-poor soil. In the medium-term, significant till-layer OC loss occurred on the small convexities and in the long-term, the entire landscape showed

significant till-layer OC loss. This indicates that on a topographically complex landscape, till-layer OC depletion is more widespread.

4.4.3 Profile OC

The TillTM provides estimates of both OC content in the till-layer and the sub-layer. The profile OC takes into account the OC in both the till- and sub-layer (to the depth of 1.0 m). Profile OC rather than the sub-layer OC is reported because profile OC provides the overall budget of OC at a given location. Unlike the till-layer OC content, profile OC content might be greater than the initial level. However, this only occurs at some, not all, soil accumulation positions, where the OC-rich surface soil is buried under the till-layer. Whether the profile OC content increases or decreases at a soil accumulation position is determined by the balance between the decrease of OC content in the till-layer and the increase of OC content in the sub-layer.

For all the four hypothetical landscapes, under alternating-direction tillage, the patterns of profile OC agreed well with the respective patterns of tillage erosion: loss on convexities and gain on concavities. Under one-direction tillage, in addition to the topographic features, profile OC was also affected by tillage direction: loss near the start-boundaries and gain near the end-boundaries. This is also similar to the pattern of tillage erosion. Due to continuous loss (or gain) of soil mass at a given location, the loss (or gain) of profile OC generally increased over time. However, in some soil-mass-gain positions, profile OC may decrease, For example, on the AH, under forward tillage, in the range of about 5 – 10 m, tillage caused soil accumulation. In the medium-term (10-yr), profile OC content was greater than the initial level in this area, but in the long-term (50-yr), within

the same area, profile OC content was much lower than the initial level (Figure 4.5). This could be explained by that the till-layer OC concentration near the start-boundary decreases dramatically over time, so that OC concentration in the buried soil also decreases dramatically, i.e. from close to the initial till-layer (up-layer) OC level to the initial bottom-layer OC level and the overall OC budget in the profile was lower than the initial profile OC level.

On the PS, SH and AH, for most of the landscapes, the patterns of profile OC were similar to those of the till-layer OC. On the IH, under both one-direction and alternating-direction tillage, the patterns of profile OC were very different from those of the till-layer OC, but very similar to the respective tillage erosion patterns (Figure 4.6). Profile OC gain was found in the small concavities and increased over time, although soil accumulation rate in these small concavities decreased over time. This indicates that significant amounts of OC are buried under the till-layer in these small concavities.

For all four hypothetical landscapes, it appeared that the patterns of both the till-layer OC and the profile OC, more or less, were similar to the respective patterns of tillage erosion, especially under alternating-direction tillage and/or in the medium-term. This suggests that the pattern of tillage-induced OC (soil constituent) redistribution can be assessed, indirectly, through the estimation of the tillage erosion pattern. The diffusion models are much simpler than the convoluting models but diffusion models usually provide acceptable accuracy for estimating tillage erosion. These results suggest that diffusion models may be useful in assessing the pattern of soil constituent redistribution. However, caution should be taken when the tillage is conducted continuously in one direction, or more broadly, when there is a predominant tillage direction, because of the

shifting effect. In addition, in long-term simulation, the spatial extent of OC loss exceeding that of soil loss also needs to be taken into account. In these cases, a convoluting model similar to the one reported here may provide a more accurate estimate of soil constituent redistribution.

4.4.4 The Transect at the Cyrus Site

The field-measured and TillTM-estimated data along the transect at the Cyrus site are shown in Figure 4.7. TillTM-estimated tillage erosion featured two soil loss peaks (situated at about 70 m and 100 m, respectively) and two soil accumulation peaks (situated at about 40 m and 135 m, respectively). The soil loss peaks corresponded to the convex positions and the accumulation peaks corresponded to the concave positions. It is noteworthy that in the middle of the knoll (at about 90 m), the estimated local tillage erosion rate was close to zero. This is due to the relatively linear topography at this location.

For the OC, the patterns of the field measurements and the TillTM estimates were very similar. In the till-layer (0 – 0.25 m), both the field-measured and TillTM-estimated OC content was lowest at locations around the two soil loss peaks, where OC-poor subsoil is exposed. At the locations of the two soil accumulation peaks, the increase of OC content was found considerably less significant. This indicates that the pattern of the till-layer OC is primarily determined by the position and spatial extent of soil loss spots, the sources of OC-poor soil, and is not significantly influenced by soil accumulation. This agrees with the conclusion drawn from the simulations of the hypothetical landscapes. In contrast, on both the field-measured and TillTM-estimated sub-layer (0.25

– 1.00 m) OC curves, two peaks were found at the same locations as those of the two soil accumulation peaks, where OC-rich surface soil was buried under the till-layer. At the locations of the two soil loss peaks, OC content was found not to be considerably lower than that at the linear locations.

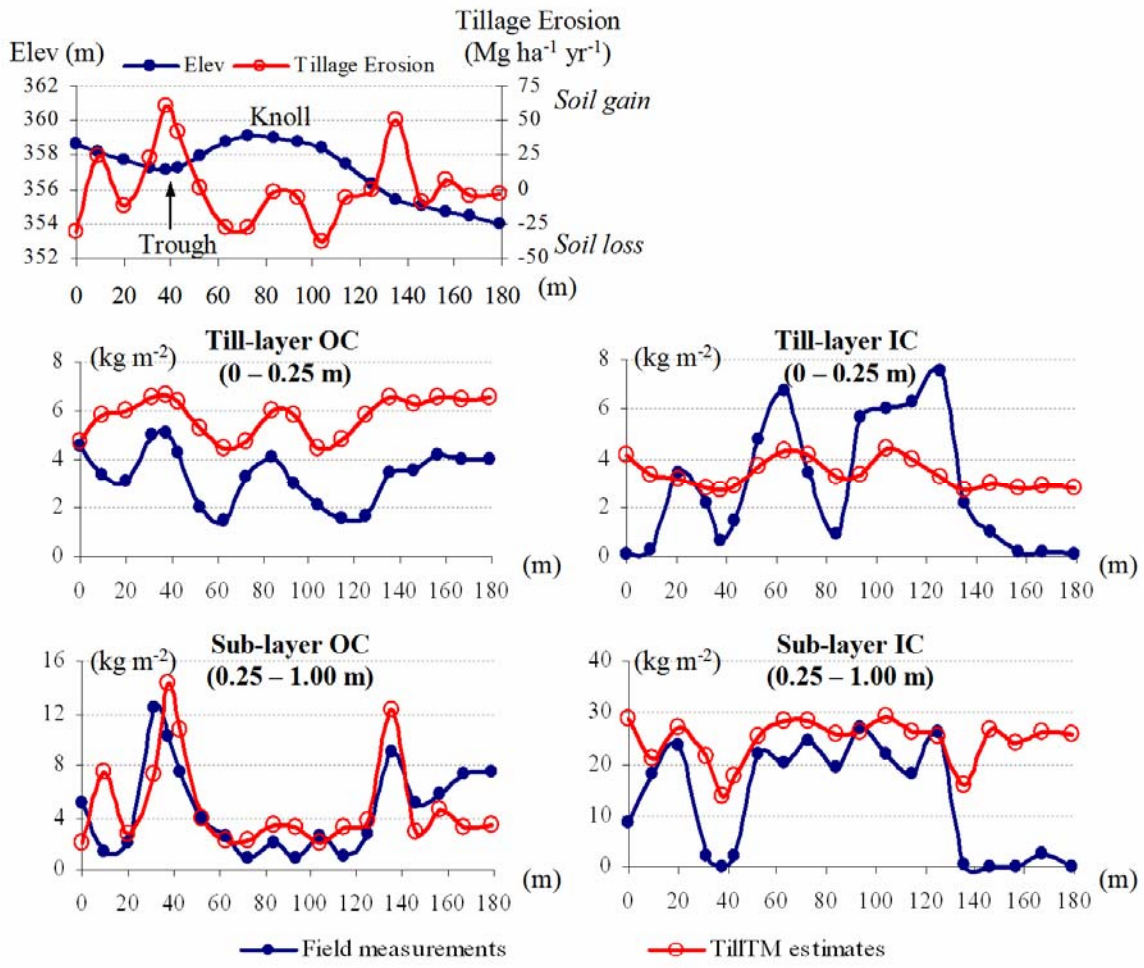

Figure 4.7 Field-measured and TillTM-estimated soil organic carbon (OC) and inorganic carbon (IC) contents along a transect at the Cyrus site.

This indicates that the pattern of the sub-layer OC is primarily determined by the position and extent of soil accumulation spots, which also agrees with the conclusion drawn from the simulations of the hypothetical landscapes.

The values of the TillTM estimated till-layer OC were considerably greater than

those of the field measurements. This suggests that the initial till-layer OC level may be greater than the input value (2.7 %) or there is a net loss of OC in the till-layer due to water erosion, decomposition and/or leaching (Papiernik et al., 2006). A test has been conducted to examine the model outputs with different settings of initial till-layer OC, decay rate, surface OC input and the translocation coefficients (i.e. A, B and C in Equation 5). The values of the estimated till-layer OC were sensitive to all these parameters but the pattern was not (data not shown). This indicates that accurate field measurements of these input data are required in order to obtain accurate OC estimates.

For the IC, the patterns of the field measurements and the TillTM estimates were also similar (Figure 4.7). Till-layer IC content was highest at the locations of the soil loss peaks and sub-layer IC content was found the lowest at the locations of the soil accumulation peaks. These are contrary to the respective patterns of OC in appearance. But the mechanisms and processes are essentially the same: the exposure of subsoil at soil loss locations and the burial of surface soil at soil accumulation locations. The differences lie in the fact that the exposed subsoil is OC-poor but IC-rich and the buried surface soil is OC-rich but IC-poor.

Correlation analysis showed that for both OC and IC, in both the till-layer and the sub-layer, the TillTM estimates were significantly correlated with the field measurements (Table 4.3). TillTM-estimated tillage erosion also significantly correlated with field-measured OC and IC in both layers. This confirms that it is possible to use a simple diffusion model to estimate the pattern of tillage-induced soil constituent redistribution. However, the correlation coefficients (absolute value) of TillTM-estimated tillage erosion against the field-measured till-layer OC and IC (0.48^{*} and $-0.38^{\dagger}$, respectively) were

significantly lower than those of the TillTM-estimated against the field-measured till-layer OC and IC (0.65** and 0.58**, respectively). This suggests the superiority of TillTM. In addition, the TillTM provides the values of OC and/or IC directly, while using a tillage erosion model, only the patterns of the OC and/or IC can be estimated.

Table 4.3 Correlation coefficients between field measurements and TillTM estimates of a transect at the Cyrus site[#].

Field measurements	TillTM estimates	TillTM-estimated tillage erosion
Till-layer OC (0 - 0.25 m)	0.65 **	0.48 *
Till-layer OC (0.25 - 1.00 m	0.64 **	0.63 **
Sub-layer IC (0 - 0.25 m)	0.58 **	-0.38 †
Sub-layer IC (0.25 - 1.00 m)	0.53 *	-0.54 *

[#] n = 19.

†, *, ** significant at the 0.10, 0.05 and 0.01 probability levels, respectively.

4.4.5 Depth Increment Profiles at the Cyrus Site

As shown in Figure 4.2, both the knoll and the trough points are in the middle of the north-south oriented slope. Local topography on the knoll is profile- and plan-convex and in the trough it is profile-linear and plan-concave. Previous studies (Li et al., Section 3.4) showed that water erosion causes soil loss at both of these locations. In the trough, water-induced soil loss is likely to be more intensive than that on the knoll given that water converges into the trough but diverges from the knoll (Figure 4.2). Field evidence also indicated that rills are well developed in the trough but not on the knoll. The local topography determines that tillage causes soil loss on the knoll but soil accumulation in the trough (Figure 4.2, 7). At the footslope location, local topography is profile-slightly-concave and plan-relatively-linear. Water erosion may cause soil loss or accumulation there. Tillage causes soil accumulation on the footslope but the intensity is likely to be lower than that in the trough given that the concavity in the trough is greater than that on

the footslope. The baseline point is on a flat uncultivated grassed land so that it is assumed that there is no water erosion or tillage erosion.

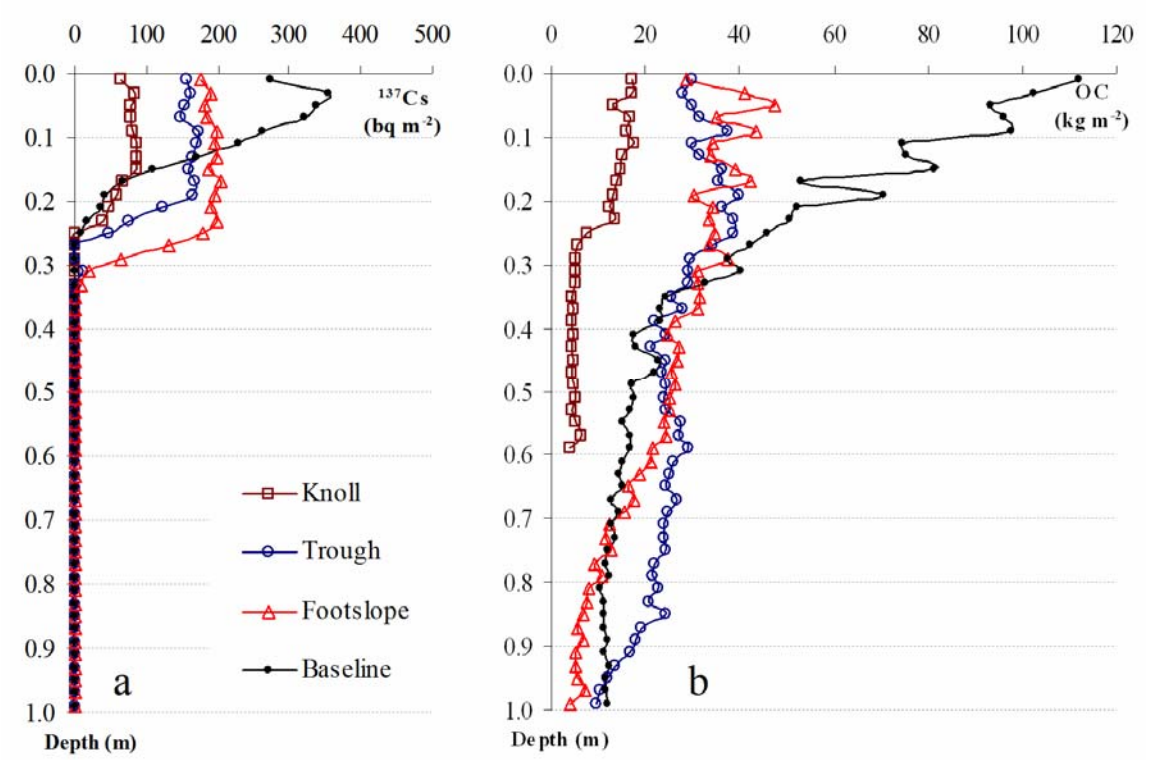

Figure 4.8 a. profile 137Cs content; and b. profile soil OC content, in 2-cm increments at four locations at the Cyrus site. The area between the curve and the two axis indicates the total 137Cs or soil OC content in the profile to a given depth.

At the baseline point, the ^{137}Cs content continuously decreased to negligible levels from the surface (except for the first point) to about 0.40 m (Figure 4.8.a). The basic pattern of ^{137}Cs at the three field points (the knoll, trough and footslope points) was relatively uniform ^{137}Cs contents within the depth of 0.20 m, decreasing sharply to negligible within the depth range of about 0.20 – 0.30 m. This indicates that tillage has mixed the ^{137}Cs within the till-layer and that the tillage depth is around 0.20 – 0.30 m. In the 0 – 0.30 m depth range, at any given depth, ^{137}Cs content of the three field points followed the order: knoll < trough < footslope. Compared to those of the baseline point,

the ^{137}Cs contents of the field points were all significantly lower at depths < 0.15 m; At depths 0.15 – 0.30 m, the ^{137}Cs contents of the knoll point were close but those of the trough and footslope points were significantly greater. The integrated profile total ^{137}Cs content (0 – 1.00 m) of the knoll (857 bq m^{-2}) was much lower, that of the trough (1878 bq m^{-2}) was also lower, and that of the footslope point (2701 bq m^{-2}) was greater than that of the baseline point (2224 bq m^{-2}). If ^{137}Cs redistribution were used as a direct measure of soil mass redistribution, the loss or gain of ^{137}Cs at the field points (compared to that at the baseline point) can be proportionally converted to gross soil erosion rate (-49.2, -12.5 and 17.2 Mg ha^{-1} yr^{-1} for the knoll, trough and footslope point, respectively).

For OC, at the baseline point, OC content decreased exponentially with depth: quickly decreasing in the top about 0.40 m and then slowly decreasing (Figure 4.8.b). The OC content remained stable at about 12 kg m^{-2} (equivalent to about 0.35 %) at depths > 0.80 m. For all three field points, the integrated profile OC content to the depth of 1.00 m (370, 1299, 1158 kg m^{-2} for the knoll, trough and footslope point, respectively, assuming at the knoll point the OC concentration in 0.60 – 1.00 m equals the average OC concentration in 0.50 – 0.60 m) were much lower than that of the baseline point (1658 kg m^{-2}). The most significant differences in OC content between the field points and the baseline point were found from the surface to about 0.30 m, indicating significant OC loss in the field within the till-layer at the field points. A reasonable explanation for this is that cultivation and cropping causes strong OC decomposition in the till-layer. At the knoll point, the OC content was significantly lower than not only that of the baseline point but also that of the trough and footslope points at any given depth, suggesting significant OC loss resulting from soil loss at the knoll point. A sharp decrease in OC

content was found at about 0.25 m. Above and below this depth, OC content remained relatively uniform. This indicates that tillage mixes the OC in the till-layer and the tillage depth is around 0.25 m, which agrees with the ^{137}Cs measurements. At the trough and footslope points, OC content also continuously decreased from soil surface. However, no sharp decreases in OC content were found at 0.25 m, instead, relatively sharp decreases in OC content were found in the range of about 0.85 – 1.00 m and of about 0.60 – 0.80 m for the trough and the footslope point, respectively. In addition, within the ranges of about 0.45 – 0.95 m and about 0.35 – 0.70 m, at the trough and footslope point, respectively, OC content was considerably greater than that at the baseline point. Both of these indicate that soil is accumulated at the trough and the footslope points: OC-rich surface soil is buried under the till-layer. Within about 0.55 – 1.00 m range, OC content at the trough point was considerably greater than that at the footslope point, indicating soil accumulation at the trough point is more intensive than that at the footslope point.

At the trough and footslope points, the depth where a sharp decrease in OC content occurs can be used as a measure of the intensity of soil accumulation. For instance, if till-layer depth is estimated as 0.25 m, soil accumulation at the trough and footslope points over the past 100 yrs can be estimated as 0.60 m (0.85 m – 0.25 m) and 0.35 m (0.60 m – 0.25 m) in total, respectively, or as the averaged rates of 76.8 and 44.8 Mg ha^{-1} yr^{-1}, respectively. These are very rough estimates given that the determination of the depths were rough and other erosion processes and OC decomposition and leaching may strongly affect the OC distribution in the profile as well. However, it does provide further evidence that at the trough point, soil is accumulated and the intensity of soil accumulation there may even be stronger than that at the footslope point. This contradicts

the ^{137}Cs estimation. We believe that the dilution effect due to tillage translocation and the change of tillage erosion rate over time due to topography change as a result of ongoing tillage erosion are the major reasons for this contradiction.

The trough point receives soil from its nearby knolls (Figure 4.2), where ^{137}Cs concentration in the soil is low (Figure 4.8.a). Soil accumulation is likely to be under estimated by using the ^{137}Cs method with a simple proportional model because proportionally less ^{137}Cs is accumulated than soil mass is. In contrast, the footslope point is further from the knoll so that the influence of the dilution effect there is minor. This is also evidenced by the fact that in the till-layer, OC content at the footslope was also slightly greater than that at the trough (Figure 4.8.b). In addition, water-induced soil loss at the trough may also cause the under-estimation of soil accumulation at the trough point because ^{137}Cs is primarily attached to fine particles and these fine particles are more susceptible to water erosion than coarse particles.

The ongoing tillage erosion causes the filling up of the trough and results in the decrease of tillage-induced soil accumulation rate over time, similar to that which occurs on the small concavities in the Irregular Hill (Figure 4.6). The highest TillTM estimated current soil accumulation rate in the trough area was about 60 Mg ha^{-1} yr^{-1} (Figure 4.7). It is reasonable to speculate that 100 yrs ago, soil accumulation rate in the trough was much greater than this current rate. Based on this point of view, the depth-estimated soil accumulation rate (76.8 Mg ha^{-1} yr^{-1}) is not surprisingly high. This also explains why at the footslope point, the depth-estimated soil accumulation rate (44.8 Mg ha^{-1} yr^{-1}) is much greater than that of the ^{137}Cs- estimated (17.2 Mg ha^{-1} yr^{-1}), which only accounts for soil erosion over approximately the past about 40 yrs.

4.5 Conclusions

On topographically simple landscapes, the pattern of tillage erosion does not change significantly over time. However, on topographically complex landscapes, the feedback of the ongoing tillage erosion on topography is significant. Soil loss rates (on the top of fine-scale convexities) and soil accumulation rates (on the bottom of those fine-scale concavities) both decrease over time. The effect of tillage pattern (direction) on tillage erosion is limited in narrow distances near the boundaries. For most part of the landscape, tillage erosion is not significantly influenced by tillage pattern.

Landscape topography, tillage pattern and temporal scale all strongly affect the pattern and intensity of soil constituent redistribution. Considering constituents that are conservative (no decay/formation), in the till-layer, soil constituent concentration decreases (e.g. for OC) or increases (e.g. for IC) on soil loss positions, i.e. convexities and/or start-boundary areas under one-direction tillage. This decrease (or increase) builds up and extends to soil accumulation areas over time. There is a net loss (or gain) of soil constituent in the till-layer from the landscape and this net loss (or gain) is more profound on topographically complex landscapes. In the sub-layer, soil constituent content increases (e.g. for OC) or decreases (e.g. for IC) on soil accumulation positions, i.e. concavities and/or end-boundary areas under one-direction tillage. This increase (or decrease) also builds up over time but does not extend to soil loss areas. The pattern of profile soil constituent content (in both till- and sub-layer) is similar to that of tillage erosion.

Tested against field measurements, the TillTM developed has been shown to estimate the pattern of the soil constituent redistribution precisely. However, in order to obtain accurate estimation of soil constituent content, detailed field measurements of the input data are required. Although it is less accurate, a simple diffusion model may also be used to assess the pattern of soil constituent redistribution through the estimation of tillage erosion, given the similarity between the redistribution patterns of tillage-induced soil mass and soil constituents.

4.6 Acknowledgements

Financial support for this study was provided by Natural Sciences and Engineering Research Council of Canada (NSERC) as part of the "Tillage erosion and its impacts on soil characteristics and pesticide fate processes at the large-scale" project. The authors would like to thank S. Tsai and H. Koiter for the assistance of the laboratory analysis. The authors particularly thank the Manitoba Soil Survey Lab for the help of carbon analysis. We would also like to thank J.A. Schumacher for providing the topographic survey data.

4.7 References

De Alba, S., Lindstrom, M.J., Schumacher, T.E., Malo, D.D., 2004. Soil landscape evolution due to soil redistribution by tillage: a new conceptual model of soil catena evolution in agricultural landscapes. Catena 58, 77-100.

Govers, G., Vandaele, K., Desmet, P.J.J., Poesen, J., Bunte, K., 1994. The role of tillage in soil redistribution on hillslopes. Eur. J. Soil Science 45, 469-478.

Govers, G., Lobb, D.A., Quine, T.A., 1999. Tillage erosion and translocation emergence of a new paradigm in soil erosion research. Soil Tillage Research 51, 167-174.

Kachanoski, R.G., de Jong, E., 1984. Predicting the temporal relationship between soil Cesium-137 and erosion rate. J. Environmental Quality 13, 301-304.

Lindstrom, M.J., Nelson, W.W., Schumacher, T.E., 1992. Quantifying tillage erosion rates due to moldboard plowing. Soil Tillage Research 24, 243-255.

Lindstrom, M.J., Nelson, W.W., Schumacher, T.E., Lemme, G.D., 1990. Soil movement by tillage as affected by slope. Soil Tillage Research 17, 255-264.

Lobb, D.A., 1997. Impact of tillage translocation and tillage erosion on the estimation of soil loss using ^{137}Cs. J. Soil Water Conservation 52, 306.

Lobb, D.A., Kachanoski, R.G., 1999*a*. Modelling tillage erosion in topographically complex landscapes of southwestern Ontario, Canada. Soil Tillage Research 51, 261–278.

Lobb, D.A., Kachanoski, R.G., 1999*b*. Modelling tillage translocation using step, linear-plateau and exponential functions. Soil Tillage Research 51, 317-330.

Lobb, D.A., Kachanoski, R.G., Miller, M.H., 1999. Tillage translocation and tillage

erosion in the complex upland landscapes of southwestern Ontario. Soil Tillage Research 51, 189-209.

Papiernik, S.K., Linstrom, M.J., Schumacher, J.A., Farenshorst, A., Stephens, K.D., Schumacher, T.E., Lobb, D.A., 2005. Variation in soil properties and crop yield across and eroded prairie landscape. J. Soil Water Conservation 60, 388-395.

Papiernik, S.K., Linstrom, M.J., Schumacher, T.E., Schumacher, J.A., Malo, D.D., Lobb, D.A., 2006 (In press). Characterization of soil profiles in a landscape affected by long-term tillage. Soil Tillage Research.

Quine, T.A, Govers, G., Walling, D.E., Zhang, X., Desmet, P.J.J., Zhang, Y., Vandaele, K., 1997. Erosion processes and landform evolution on agricultural land - new perspectives from caesium-137 measurements and topographic-based erosion modelling. Earth Surface Processes and Landforms 22, 799-816.

Schumacher, T.E., Lindstrom, M.J., Schumacher, J.A., Lemme, G.D., 1999. Modeling spatial variation in productivity due to tillage and water erosion. Soil Tillage Research 51, 331-339.

Van Oost, K., Govers, G., Van Muysen, W., Quine, T.A., 2000. Modeling translocation and dispersion of soil constituents by tillage on sloping land. Soil Science Society Am. J. 64, 1733-1739.

Van Oost, K., Govers, G., Van Muysen, W., 2003*a*. A process-based conversion model for caesium-137 derived erosion rates on agricultural land: an integrated spatial approach. Earth Surface Processes and Landforms 28, 187-207.

Van Oost, K., Van Muysen, W., Govers, G., Heckrath, G., Quine, T.A., Poesen, J., 2003*b*. Simulation of the redistribution of soil by tillage on complex topographies. Eur. J.

Soil Science 54, 63-76.

4.8 Nomenclature

A	tillage translocation distance on level land (m)
AH	Asymmetric Hill
B	additional tillage translocation due to the effect of slope gradient (m $\%^{-1}$)
C	additional tillage translocation due to the effect of slope curvature (m^2 $\%^{-1}$)
C^a (x')	the amount of a soil constituent at location x' after the tillage operation (kg m^{-1})
C^b (y')	the amount of a soil constituents at location y' before the tillage operation (kg m^{-1})
D_{max}	the maximum translocation distance. The probability of soil being translocated beyond this range was assumed to be zero (m)
D_t	tillage depth (m)
d_y	mean translocation distance at y (m)
I	data interval (m)
IC	soil inorganic carbon
IH	Irregular Hill
OC	soil organic carbon
$P_{y'}$ (x')	the probability of soil translocated from the section centralized at y' to the

	section centralized at x' (kg kg^{-1})
PD_y (x)	the probability density of soil translocated from y to x (kg kg^{-1} m^{-1})
PS	Plane Slope
S^a (x)	the mass of soil per meter width at x after tillage operation (kg m^{-1})
S^b (y)	the mass of soil per meter width at y before tillage operation, which is a constant when tillage depth and soil bulk density are considered to be uniform across the landscape (kg m^{-1})
SH	Symmetric Hill
TC	soil total carbon
TE (x')	net soil mass accumulation per meter width at x' after the tillage operation, a negative value indicating net soil loss (kg m^{-1})
TillTM	Tillage Translocation Model, a computer program written in VB code
x, y	distance from the original point (m)
x', y'	the distance from the original point to the center of the sections (m)
$\theta_{y'}$	slope gradient at y' (%)
$\varphi_{y'}$	slope curvature at y' (% m^{-1})

5. GENERAL CONCLUSION

5.1 The Context of the Research

The major aspects of tillage translocation and tillage erosion were examined in this study: from the field measurement of tillage translocation, to the modeling of tillage erosion and tillage-induced redistribution of soil constituents, to the applications and validations of the models. The field measurement of tillage translocation, which was carried out in a cereal-production system, was the basis of all of the studies. The experimental tillage translocation data were used to calibrate a diffusion/dispersion type model. Calibrated diffusion/dispersion type models were used to estimate tillage erosion in two field sites. The tillage erosion estimates, coupled with water erosion estimates, were validated by comparison to the total erosion estimates, which were determined using ^{137}Cs technique. A convolution procedure, which is a further development of the diffusion/dispersion type model, was used to simulate tillage-induced redistribution of soil constituents and soil mass.

5.2 Major Findings

Tillage erosivity in cereal-production systems was found to be considerably less intensive than that in corn-production systems. Secondary tillage and seeding could be as erosive as primary tillage in cereal-production systems providing that seeding is typically conducted shortly after its proceeding tillage operation. Slope curvature was found to have a significant effect on tillage translocation although slope gradient was the dominant factor.

In topographically complex landscapes, both water and tillage erosion contributed to total soil erosion. On the knolls of hummocky landscapes, tillage erosion dominated the pattern of total soil erosion. On the slope of undulating landscapes, neither water erosion nor tillage erosion dominated the other erosion process. Combining water and tillage erosion models generally provided better estimations of total soil erosion than the component models on their own. For a given landscape element, the patterns of water and tillage erosion were predictable so that landscape segmentation could be used as a tool to assess the patterns of water, tillage and total erosion and, therefore, variations of soil properties in topographically complex landscapes.

The tillage-induced redistribution pattern of soil constituents was found related to but to be different from the pattern of tillage erosion (soil mass redistribution). In the till-layer, soil constituent content was primarily determined by soil mass loss pattern. In the sub-layer, soil constituent content was primarily determined by soil mass accumulation pattern. In some cases, topographic feature, tillage pattern and temporal scale all strongly

affect the redistribution of soil constituents. In general, the more complex the landscape and/or the longer the time scale, the more significant were the effects of tillage on the redistribution of soil constituents. Also, under one-direction tillage, the effects of tillage on the redistribution of soil constituents were more significant than those under alternating-direction tillage. Given the similarity of tillage-induced soil mass and soil constituent redistributions, it is possible to use a simple diffusion/dispersion model to assess the pattern of soil constituent redistribution through the estimation of tillage erosion.

5.3 Suggestions for Future Studies

Future studies on tillage translocation are needed for broader ranges of cropping and tillage systems, in particular, conservation tillage and no-till systems. Tillage translocation caused by secondary and seeding implements need to be stressed. In this study, slope curvature was found to significantly affect tillage translocation, however, the effect of slope curvature was not consistent for different tillage implements. A more specified experiment design is suggested to examine how tillage translocation is affected by slope curvature.

Studies are needed on the integration of water, wind and tillage erosion models and the use of this integrated model to estimate total soil erosion and to examine the overall effects of soil erosion processes on soil properties in topographically complex

landscapes,. The linkage and the interactions between different erosion processes need further investigation for the purpose of integrating water, wind and tillage erosion models. It is also suggested to explore the use of landscape segmentation procedure(s) as a simple tool to assess the pattern of soil erosion on topographically complex landscapes.

The developed TillTM model in this study could be used to estimate the redistribution of all soil constituents that move with soil mass. Future studies are suggested to couple TillTM with water and/or wind erosion models to examine the effects of soil erosion on other biophysical process such as nutrients movement, pesticide fate and greenhouse gas emission. Further development of the TillTM model is suggested to be carried out to include the lateral dispersion of soil mass and soil constituents.

APPENDIX A

Appendix A.1. Field measured tillage depth and summation curve estimated errors by averaging the data of the first two samples.

		DT		SH		LC		AS		LC/AS
	Plot	D_T m	ε %	D_T m	ε %	D_T m	ε %	D_T m	ε %	ε %
Long Slope Area	1	0.09	0.0	0.02	1.3		2.9	0.03	0.0	2.3
	2		3.1	0.01	0.7	0.06	8.2		0.8	1.2
	3	0.07	1.6		0.1		3.3		0.7	3.7
	4	0.14	4.9		0.0	0.10	0.8		1.0	0.3
	5		2.6		0.3	0.10	1.3	0.06	1.1	2.5
	6	0.12	2.8		0.1		1.2	0.03	0.9	1.4
	7		3.8		0.3	0.08	3.7	0.04	11.7	4.3
	8		3.1		0.5			0.05	1.5	1.9
	9	0.09	1.6						1.8	0.3
	10	0.08	2.1					0.04	3.3	0.8
	11								1.4	1.0
	12								0.3	5.2
	13									1.8
	14									1.5
	15									0.0
Bowl Area	1	0.09	1.6	0.01	0.8					1.3
	2	0.10	3.9		0.4					1.5
	3		4.0		0.0					1.4
	4		1.9		0.0					0.6
	5	0.12	1.3		0.4					0.5
	6		2.5		0.1					1.6
	7		4.2		0.3					0.1
	8	0.08	4.4		0.2					0.8
	9									0.1
Average		0.10	2.7	0.01	0.3	0.09	3.1	0.04	2.0	1.5
S.D.		0.02	1.3	0.01	0.3	0.02	2.5	0.01	3.2	1.3

Appendix A.2. Summary of simple regression analyses of TM against slope curvature.

Implement		Model			Intercept	Slope Curvature	
		n	Pr > F	R^2	α	γ	Pr > | t |
DT	Long Slope Area	10	0.20	0.19	12.62	3.04	0.20
DT	Bowl Area	8	0.73	0.02	17.61	-1.36	0.73
DT	Both Area	18	0.56	0.02	15.25	1.18	0.56
SH	Long Slope Area	8	0.52	0.07	0.53	-0.55	0.52
SH	Bowl Area	8	0.30	0.18	0.37	0.25	0.30
SH	Both Area	16	0.51	0.03	0.53	-0.25	0.51
LC	Long Slope Area	7	0.50	0.09	20.10	2.21	0.50
AS	Long Slope Area	12	0.57	0.03	4.34	0.55	0.57
LC/AS	Long Slope Area	15	0.24	0.10	32.47	8.86	0.24
LC/AS	Bowl Area	9	0.47	0.08	27.38	-5.44	0.47
LC/AS	Both Area	24	0.17	0.08	30.37	7.83	0.17

APPENDIX B

Appendix B.1. Correlation coefficients of ^{137}Cs estimates with model estimates along transects at the Cyrus site.

Transects parallel to tillage direction							Transects perpendicular to tillage direction						
ID	n	E_{Wepp}	E_{Usle}	E_{Ti}	$E_{Wepp+Ti}$	$E_{Usle+Ti}$	ID	n	E_{Wepp}	E_{Usle}	E_{Ti}	$E_{Wepp+Ti}$	$E_{Usle+Ti}$
0	18	0.47 *	0.51 *	-0.27	0.22	0.23	0	16	0.34	0.41	-0.19	0.40	0.45 *
1	18	0.36	0.09	0.57 *	0.61 **	0.46 *	1	16	0.17	0.33	0.03	0.29	0.44 *
2	18	0.41 *	0.39	0.37	0.51 *	0.59 **	2	16	0.11	0.27	-0.13	0.02	0.32
3	12	0.29	-0.41	0.71 **	0.70 *	0.20	3	15	0.46 *	-0.06	-0.46 *	-0.01	-0.14
4	18	0.38	-0.09	0.74 ***	0.76 ***	0.41 *	4	15	0.51 *	0.05	0.34	0.57 *	0.11
5	18	0.52 *	-0.06	0.59 **	0.75 ***	0.35	5	16	0.32	0.24	0.68 **	0.52 *	0.57 *
6	18	-0.21	-0.16	0.22	0.09	-0.09	6	16	0.22	0.11	0.47 *	0.43 *	0.48 *
7	18	0.36	0.08	0.09	0.20	0.26	7	15	0.52 *	0.49 *	0.27	0.63 *	0.64 **
8	18	0.48 *	-0.34	0.45 *	0.51 *	0.01	8	15	0.69 **	0.63 *	0.08	0.67 **	0.66 **
9	18	0.35	-0.37	0.44 *	0.45 *	-0.21	9	15	0.41	0.31	0.15	0.43	0.43
10	17	0.51 *	0.10	0.30	0.59 *	0.30	10	15	0.16	0.13	0.35	0.36	0.47 *
11	18	0.70 **	0.43 *	0.38	0.69 **	0.63 **	11	15	0.41	0.28	0.61 *	0.68 **	0.77 ***
12	18	0.25	0.37	-0.09	0.18	0.37	12	15	0.45 *	0.59 *	0.15	0.54 *	0.70 **
13	18	0.26	-0.19	-0.37	0.14	-0.24	13	16	0.04	0.24	0.06	0.11	0.27
14	18	0.10	-0.42 *	0.10	0.14	-0.42 *	14	16	-0.05	0.16	0.51 *	0.59 *	0.30
15	17	0.45 *	0.15	0.04	0.42 *	0.16	15	16	0.24	0.58 *	0.36	0.63 **	0.61 *
							16	16	0.42	0.48 *	-0.19	0.13	0.44 *
							17	16	0.33	0.48 *	0.74 **	0.66 **	0.55 *

*,**,*** significant at the 0.05, 0.01 and 0.001 probability levels, respectively.

Appendix B.2. Correlation coefficients of ^{137}Cs estimates with model estimates along transects at the Deerwood site.

Transects parallel to tillage direction							Transects perpendicular to tillage direction						
ID	n	E_{Wepp}	E_{Usle}	E_{Ti}	$E_{Wepp+Ti}$	$E_{Usle+Ti}$	ID	n	E_{Wepp}	E_{Usle}	E_{Ti}	$E_{Wepp+Ti}$	$E_{Usle+Ti}$
0	7	-0.92 **	-0.76 *	0.82 *	0.46	0.10	0	8	-0.51	-0.65 *	0.33	0.26	-0.09
1	7	0.65	0.41	0.65	0.86 *	0.71 *	1	8	-0.61	-0.51	0.22	0.11	0.11
2	8	0.45	-0.48	0.25	0.32	0.15	2	9	0.61 *	-0.10	0.72 *	0.75 *	0.77 *
3	8	0.56	-0.15	0.66 *	0.68 *	0.65 *	3	7	0.65	-0.17	0.66	0.80 *	0.49
4	9	0.59 *	0.29	0.42	0.58	0.49	4	9	0.18	0.49	-0.02	0.09	0.41
5	8	0.33	0.20	0.49	0.64 *	0.61	5	8	-0.37	-0.55	0.72 *	0.66 *	0.29
6	7	0.43	0.31	0.46	0.52	0.48	6	8	-0.48	-0.61	0.81 *	0.89 **	0.80 *
7	6	0.36	0.09	0.12	0.19	0.14	7	4	-0.54	-0.98 *	0.65	0.68	0.50
8	3	-0.83	-0.44	0.85	0.85	0.92	8	2	---	---	---	---	---

*,**,*** significant at the 0.05, 0.01 and 0.001 probability levels, respectively.